

# Numerical and Experimental Investigation of AMBs Supported Rotor System with Auxiliary Bearings

Vom Fachbereich Maschinenbau  
an der Technischen Universität Darmstadt

zur

Erlangung des Grades eines Doktor-Ingenieurs (Dr.-Ing.)  
genehmigte

Dissertation

vorgelegt von

M.Sc. Lei Xie

aus Henan, VR. China

Brichterstatter: Prof. Dr.-Ing. R. Nordmann

Mitbrichterstatter: Prof. Dr. h. c. Dr.-Ing. H. Birkhofer

Tag der Einreichung: 26.02.2009

Tag der mündlichen Prüfung: 10.06.2009

Darmstadt 2009

D17

# Acknowledgment

I would like to sincerely thank all the people who contributed invaluable help during my Ph.D studies:

In particular, I am grateful to my supervisor, professor Dr.-Ing. Rainer Nordmann for giving me such a precious opportunity to work in his research group and for his guidance, encouragement, trust and valuable advice.

I am grateful to professor Dr.-Ing. Herbert Birkhofer for his interest in my work and for being co-supervisor of my thesis.

I would next like to thank Mr. N. Butzek for his help in Maschinendynamik; Mr. A. Spieß for his help in data recovery and computer problems; Ms. M. Helfert for her recommendation of a very good book about nonlinear dynamics; Mr. S. Kern for his help in Matlab and system identification; Mr. M. Ernst his help in FEM analyses and software NASTRAN; Mr. F. Fomi Wamba, B. Hasch, M. Marszolek and G. Schuck for their help and explanation in lab and test rig; Mr. E. Mpouah Ngondi for his corrections and constructive comments and advices on my thesis.

I am also appreciated our secretaries Frau U. Willner, Frau P. Chen, Frau S. Backhaus and Frau B. Lampertand for their assistance in official and my personal live in Germany.

I gracefully acknowledge Dr B. Aeschlimann of Mecos AG for his valuable help in test rig and Mr. Carlos Eguti of ITA, Brazil, for his help in optical sensor.

A very special thank to my friends, Hongtao Sun, Bitan Su, for the memorable PhD study in TU darmstadt.

Thanks to my parents, and my husband Xi Dou for their endless support and love!

Mainz, Feb. 2009

Lei Xie

# Zusammenfassung

Beim Stromausfall oder kurzzeitiger hoher Überbelastung in den die aktiven magnetischen Lager kommt der schnell drehende Rotor mit dem Fanglagern in Kontakt. Dabei ist eine kritische Bewegung, nämlich der Rückwärtswirbel, möglich. Der Rückwärtswirbel kann zur hohen Belastung für Rotor und Lager und somit zur Zerstörung der Maschine führen. Aus diesem Grund ist es wichtig, numerische und experimentelle Untersuchungen über das durch die aktiven magnetischen Lager unterstützte Rotorsystem durchzuführen.

In dieser Arbeit wird das mathematische Modell für den durch die aktiven magnetischen Lager unterstützten Rotor mit Fanglagern vorgestellt. Eine theoretische Methode zur Abschätzung der äquivalenten Steifigkeit und Dämpfung des aktiven magnetischen Lagers wird entwickelt. Die dynamische äquivalente Steifigkeit und Dämpfung des Systems werden aus dem Frequenzgang des digital gesteuerten aktiven magnetischen Lagers berechnet.

Um die entscheidenden Faktoren und Parameter zu identifizieren, werden viele Experimente in dieser Arbeit durchgeführt. Modifikationen bzw. Erweiterungen in Hardware und Software werden am Prüfstand in dieser Arbeit durchgeführt. Damit werden neuartige Messungen ermöglicht. Wichtige Parameter wie z.B. Eigenfrequenzen und Dämpfungsgrade werden durch Analyse der experimentellen Daten mit Frequenzbereichs- und Zeitbereichsmethoden identifiziert. Diese Parameter werden in der numerischen Simulation verwendet.

Detaillierte Modelle für den durch AMB unterstützten Rotor mit Fanglagern werden vorgestellt. In den Modellen werden die diskontinuierliche Steifigkeit auf Grund des Lagerspiels, der nichtlineare Hertz-Kontakt und die Coulombsche Reibungskraft berücksichtigt. Das Fanglager im Prüfstand kann fixiert bzw. flexibel montiert werden. Dementsprechend wird es auch in der Simulation modelliert.

Der Rotor wird als Starrkörper oder starrer Balken unter Berücksichtigung des Pa-

parameterbereichs modelliert. Differentialgleichungen werden formuliert. Die numerische Methode wird für die nichtlinearen zeitvarianten gewöhnlichen Differentialgleichungen in der Simulation mit Hilfe der Event-Funktion in MATLAB entwickelt. Zur Untersuchung des dynamischen Verhaltens des Systems werden ihre zeitliche Entwicklung, Orbit-Diagramm, Poincaré-Section-Diagramm und Waterfall-Spektrum-Diagramm als Simulation durchgeführt.

Ergebnisse von der Bifurcation-Analyse werden präsentiert. Die Bifurcation-Analyse ist geeignet zur Feststellung der wichtigen Faktoren und Parameter für das Verhalten des Systems und damit zur Verbesserung der Konstruktion. Mit der Bifurcation-Analyse werden Parameterstudien über die Rotordrehzahl und die Steifigkeit des aktiven magnetischen Lagers und des Fanglagers durchgeführt. Die komplexe Bewegung des Rotors wird bei der Veränderung der Parameter beobachtet.

# Abstract

In case of active magnetic bearing power failures or high transient overloads, the fast spinning rotor interacts with the auxiliary bearing. A critical motion is possible, called backward whirl. It can produce very high loads on rotor and bearings, which can lead to the destruction of the machine. Therefore, it is important to make numerical and experimental investigations of active magnetic bearings (AMBs) supported rotor system with auxiliary bearings.

The models for the AMBs supported rotor with auxiliary bearing system are introduced. The theoretical method for estimation equivalent stiffness and damping of the AMB is developed in this work. The dynamic equivalent stiffness and damping of the AMB-rotor system is calculated from the knowledge of frequency response of the digitally controlled AMB.

In this work, plenty experiments have been made to explore which factors or parameters are essential for the system performance. Some modifications and extensions of the hardware and software of the test rig have been done. Several important parameters of system such as stiffness and damping have been estimated through frequency domain and time domain methods by analyzing the experimental results. These parameters were used in numerical simulations. Under some specific designed cases, it is found that the rotor undergoes a complicated motion behavior, the backward whirl. The experiment results have been presented and analyzed.

The detailed models of the AMBs supported rotor interacting with the auxiliary bearing system are introduced, which considered discontinuous stiffness caused by bearing clearance effect, nonlinear Hertzian contact and Coulomb friction forces. Furthermore, according to the real test rig, the auxiliary bearings could be modeled as fixed and compliant mounted. The rotor is modeled as rigid mass or rigid beam by paying regard to its operation range. Several groups of differential equations are presented and the numerical simulation method is developed for the nonlinear

time variant ODEs based on event functions in MATLAB. Numerical investigations as time history, orbit diagram, Poincaré section diagram and waterfall spectrum diagram are proposed to study the complex dynamic response of the system. It is found that the AMB-rotor-auxiliary bearing system undergoes complicated motion behaviors including chaotic motion.

The bifurcation analysis results are presented, to explore which factors or parameters are essential to system performance then find an appropriate optimized design to prevent it. The important parameters studies on the rotor driving frequency, the support and contact stiffness are carried out through bifurcation analysis. The complicated motions of rotor are observed by changing the control parameters.

# List of Symbols

$\alpha$	contact stiffness ratio
$\alpha_d$	damping parameter of nonlinear Hertzian contact
$\varphi_i$	$i$ th eigenvector
$\mathbf{K}_i$	current stiffness parameter of AMB
$\mathbf{K}_s$	displacement stiffness parameter of AMB
$\delta$	non-negative radial penetration between rotor and auxiliary bearing
$\hat{\square}$	nondimensionalized variable
$\kappa$	local stiffness parameter of nonlinear Hertzian contact
$\lambda_i$	$i$ th eigenvalue
$\mu$	coefficient of friction
$\mu_0$	permeability of air
$\sigma_i$	$i$ th Hankel singular value
$\sum F$	net force or resultant force
$\tau, \eta$	dimensionless time, driving frequency
$\Theta$	transverse moment of inertia
$\xi$	non-dimensional distance along the element
$\zeta$	damping ratio
$A$	cross-section area of flux path; step function amplitude
$A, B, C, D$	state space matrix of AMB-rotor-auxiliary bearing system

$a, b, c, d$	state space matrix of AMB digital controller
$A(z)$	cross section area on the Euler-Bernoulli beam element at point $z$
$Cs$	clearance between rotor and auxiliary bearing
$D, \mathbf{D}$	damping matrix
$d_1$	equivalent damping provided by AMB
$E$	Young's modulus
$f$	friction force
$F_{\text{amb}}$	electromagnetic force provided by active magnetic bearing
$F_{\text{b}}$	force provided by auxiliary bearing
$F_{\text{ex}}$	other excitation forces
$F_{\text{m}}$	magnetic force
$F_{\text{u}}$	unbalance force
$g$	air gap
$G_F(S)$	transfer function of filter
$G_s(s)$	transfer function of sensor
$G_w(s)$	transfer function of over all control part
$G_{AD}(s)$	transfer function of AD converter
$G_c(s)$	transfer function of controller
$G_{DA}(s)$	transfer function of DA converter
$H_1, H_2, H_3, H_4$	four Hermite element shape functions
$I$	moment of inertia of the cross section
$i$	current
$i_{x+}, i_{x-}, i_{y+}, i_{y-}$	actual coil currents in magnetic actuators
$i_{x0}, i_{y0}, i_x, i_y$	bias currents and perturbation currents in magnetic actuators

$K, \mathbf{K}, K_e$	stiffness matrix
$k_1$	equivalent stiffness provided by AMB
$k_2$	mounting stiffness of auxiliary bearing
$k_c$	contact stiffness of auxiliary bearing
$K_{tr}$	spring constant per tolerance ring wave
$k_b$	stiffness of auxiliary bearing
$K_{st}$	static overall controller gain
$l_e$	length of the Euler-Bernoulli beam element
$m$	mass of rotor
$M, \mathbf{M}, M_e$	mass matrix
$n$	numbers of wire loops in the electromagnet
$N$	normal contact force
$p$	wave pitch of tolerance ring
$q$	general displacement vector
$t$	thickness of tolerance ring
$T_e, U_e$	kinetic and potential energies of the beam element
$W$	width of tolerance ring
$w_d$	damped natural frequency
$w_n$	natural frequency of AMB-rotor system
$x, y$	center of rotor
$x_b, y_b$	center of auxiliary bearing

# Contents

<b>Acknowledgment</b>	<b>i</b>
<b>Zusammenfassung</b>	<b>ii</b>
<b>Abstract</b>	<b>iv</b>
<b>1 Introduction</b>	<b>1</b>
1.1 Active magnetic bearing-rotor system . . . . .	1
1.2 Motivation and objectives . . . . .	3
1.3 Structure and overview of the thesis . . . . .	5
<b>2 Review of the State of the Art</b>	<b>7</b>
<b>3 Model of AMB Supported Rotor with Auxiliary Bearing System</b>	<b>10</b>
3.1 Rotor . . . . .	10
3.1.1 Rigid rotor . . . . .	11
3.1.2 Flexible rotor . . . . .	12
3.1.3 Model reduction . . . . .	18
3.2 Active magnetic bearing . . . . .	20
3.2.1 Principle of active magnetic bearings . . . . .	20
3.2.2 The equivalent stiffness and damping of AMB supported rotor system . . . . .	23
3.3 Auxiliary bearing and tolerance ring . . . . .	28
3.3.1 Auxiliary bearing . . . . .	28
3.3.2 Tolerance ring . . . . .	29
3.3.3 Model of auxiliary bearing . . . . .	31
3.4 Excitations of the rotor system . . . . .	32
3.4.1 Unbalance . . . . .	32
3.4.2 Contact and friction force between rotor and auxiliary bearings	33

3.4.3	Other excitations . . . . .	36
<b>4</b>	<b>Test Rig and Experimental Investigation</b>	<b>37</b>
4.1	Description of the build-up test rig . . . . .	37
4.1.1	Rotor and active magnetic bearing . . . . .	39
4.1.2	Auxiliary bearing settings . . . . .	43
4.1.3	Sensors and data acquisition system . . . . .	45
4.1.4	Digital control system . . . . .	48
4.2	Identification of important system parameters . . . . .	49
4.2.1	Time domain method . . . . .	50
4.2.2	Frequency domain method . . . . .	52
4.3	Experiments and Results Analysis . . . . .	58
4.3.1	Parameter identification experiments . . . . .	59
4.3.2	Parameter study experiments . . . . .	59
4.3.3	Experimental results analysis and rotor motion behaviors . . . . .	60
<b>5</b>	<b>Numerical Simulation of Interaction between Rotor and Auxiliary Bearing</b>	<b>64</b>
5.1	Basic model of the system . . . . .	65
5.1.1	The Equations of motion . . . . .	66
5.1.2	Nondimensionlised equations . . . . .	67
5.1.3	Steady state harmonic response analysis . . . . .	68
5.1.4	Stability discussion . . . . .	71
5.2	Extended models of the system . . . . .	72
5.2.1	Rigid beam rotor with rigid mounting auxiliary bearing model . . . . .	73
5.2.2	Rigid rotor with flexible mounting auxiliary bearing model . . . . .	76
5.3	Numerical computing method . . . . .	78
5.3.1	State space representation . . . . .	79
5.3.2	Numerical simulation of a nonlinear time variant system . . . . .	80
5.4	Simulation results and analysis . . . . .	82
5.4.1	Case 1: variant of driving frequency with linear contact model . . . . .	82
5.4.2	Case 2: variant driving frequency with Hertzian nonlinear contact model . . . . .	86
5.4.3	Case 3: contact force with different contact model . . . . .	89
5.4.4	Case 4: waterfall spectrum analysis . . . . .	91

<b>6</b>	<b>Bifurcation Analysis of Rotor System Parameters</b>	<b>93</b>
6.1	Theory introduction . . . . .	93
6.1.1	Dynamic system . . . . .	93
6.1.2	Poincaré section diagram . . . . .	94
6.1.3	Bifurcation diagram . . . . .	95
6.2	Parameter study of the dynamic system . . . . .	95
6.2.1	Driving frequency . . . . .	96
6.2.2	Support stiffness . . . . .	97
6.2.3	Contact stiffness . . . . .	98
<b>7</b>	<b>Conclusion and Outlook</b>	<b>100</b>
	<b>Bibliography</b>	<b>102</b>

# 1 Introduction

## 1.1 Active magnetic bearing-rotor system

In various technical areas rotating machinery systems are in operation, like turbines, pumps, compressors, motors and generators etc. With development of mechatronic technology, nowadays, one of innovative bearing technologies, active magnetic bearings are being used in increasing numbers in rotating machinery systems in order to increase efficiency reliability, performance of rotary machine.

Active magnetic bearings (AMBs) operate by applying an electromagnetic field to ferromagnetic materials used in both the rotor and stator, creating a magnetic flux path that includes the rotor, stator, and air gap. AMB-rotor systems are open loop unstable systems. In order to keep the rotor system stable, they require continuous power input and an active control system to make a suitable electromagnetic force on the rotor. AMB-rotor systems have obvious advantages comparing with conventional bearing rotor system. They can provide high rotating speeds, non-contacting, friction-free motion in rotary applications, do not require lubrication, and are virtually maintenance-free. Furthermore, there are more potential advantages in AMB-rotor systems with respect to smart behaviors. Tuning possibilities for stiffness and damping of AMBs, the active vibration damping, possible unbalance compensation and novel features like identification, diagnosis and correction can be realized with modern control technology in AMB-rotor system. In this way it is possible to design new machines with higher performance, higher reliability and longer lifetime[1].

Since the first active magnetic bearing application in a satellite fly wheel in the early 1970's [19], active magnetic bearings have become increasingly popular for the use in industry. An application area actually already well established and developed rapidly further is turbo machinery. Products range from small turbo molecular

pumps to large compressors for pipeline gas, and to turbo generators for power plants. Besides these main applications, magnetic bearings can also be found in blood pumps, centrifuges, x-ray devices and more recently in gas turbines for transport applications. A recent research project of international interest is the turbo generator in AMB for the high temperature helium reactor technology [20].

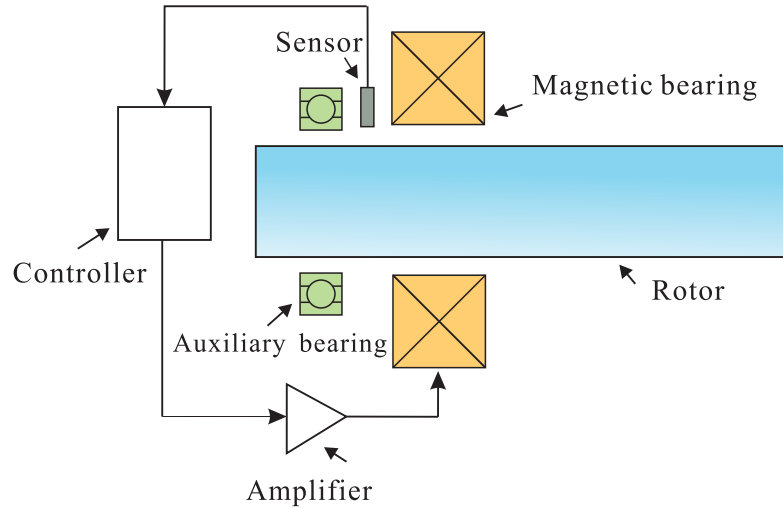


Figure 1.1: Principle of AMB-rotor-auxiliary bearing system

AMB-rotor systems are comprised of these distinct parts: magnetic bearing itself, controller, position sensor, power amplifier, rotor, and auxiliary bearings [18]. A basic set-up of the AMB-rotor system is presented in figure 1.1. For operation, the sensor measures the position of the shaft and the measured signal is sent to the controller where it is processed and then, the signal is amplified and fed as a current into the coils of the magnet, generating an electromagnetic field that keeps the shaft in a desired position. The strength of the magnetic field depends on the air gap between the shaft and the magnet bearing and the dynamics of the system including the design of the controller. In normal working conditions, rotor is flying in the bearings, it does not contact with any part. But in case active magnetic bearings have power failures or transient overload adds on the rotor, auxiliary bearings support high speed rotating rotor and avoid it to destroy the rotor itself and surrounding components such as seals, impellers and sensors etc.. Therefore, the auxiliary bearings play an important role for the active magnetic bearing supported rotor systems. Magnetic bearings usually require some forms of

auxiliary bearings in application to commercial rotating machinery.

## 1.2 Motivation and objectives

In application to commercial rotating machinery, auxiliary bearings play an indispensable role in active magnetic bearings supported rotor systems. The block diagram is shown in figure 1.2 which considers AMB-rotor-auxiliary bearing system from general dynamic system aspects.

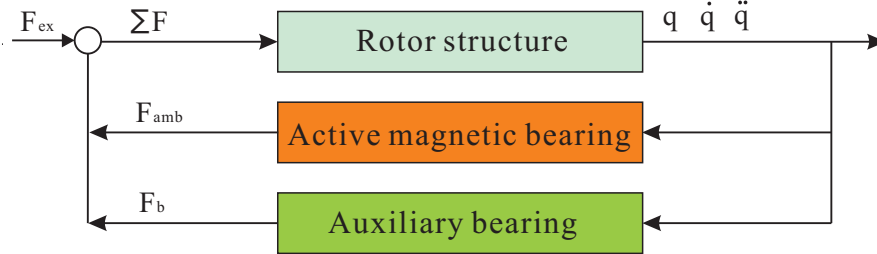


Figure 1.2: Block diagram of AMB-rotor-auxiliary bearing system

Here, rotor can be considered as a structure plant. AMBs as actuator provide suitable controlled forces  $F_{amb}$  on rotor, which is determined by dynamic response of rotor  $q$ , basic parameters of magnetic actuator and controller strategy.  $F_{ex}$  are general external excitation forces, which include unbalance force cause by unavoidable initial rotor unbalance, and the other uncertain circumstances excitation forces.  $F_b$  is dynamic interaction force provided by auxiliary bearings when rotor interacts with auxiliary bearing in case AMBs have power failure or undesirable transient overload adds on rotor, which includes contact force and friction force.  $\Sigma F$  is an external net force adding on the rotor plant. Hence, AMB-rotor-auxiliary system can be considered as a close loop dynamic system. From aspect of rotor, forces are inputs and dynamic responses are outputs. From aspect magnetic bearing and auxiliary bearing, they are on the contrary.

In normal working conditions, the controlled electromagnetic forces support the high speed rotor and keep it flying in the active magnetic bearings without interaction with auxiliary bearing. In this situation the rotor plant only has  $F_{amb}$  and  $F_{ex}$  as inputs. AMB-rotor system is stable through a proper controller design. In the

event of AMBs failure, or transient load conditions, the high speed spinning rotor interacts with the stationary auxiliary bearings. Complex dynamic interaction force  $F_b$  acts on the high speed spinning rotor as an extra inputs of the rotor plant. It is worth to mention that a fatal unstable state of rotor motion, backward whirl, can occur. During backward whirl, rotor reaches very high frequencies and thus can produce very high loads on rotor and bearings, which can lead to the destruction of machine [3]. The economical impact of destruction of rotary machine must not be underestimated. Therefore, it will have theoretical and practical significance on the investigation of AMB-rotor-auxiliary bearing system, exploration which factors or parameters are essential to this kind destructive unstable motion and then finding an appropriate design to prevent it by means of both numerical and experimental methods.

The main objective of the research work presented here is to make numerical and experimental investigation of the active magnetic bearing supported rotor system with auxiliary bearing and to study AMB-rotor-auxiliary bearing system parameters and then provide reliable information about the harmful unstable motion of system, backwards whirl, try to find a possible optimized system design. Several intermediate objectives lead to the achievement of the main objective. These are:

- To build some detailed mathematical models of the AMB-rotor-auxiliary bearing system with consideration of nonlinear factors such as nonlinear Hertzian contact, friction, clearance effect.
- To study the system parameters, which influence the whole dynamic by means of time history, orbit diagram, bifurcation diagram, Poincaré section diagram and spectrum analysis.
- To develop experimental strategy to deal with modeling of rotating structural dynamics and system identification.
- To design experiments to study and analysis the system parameters such as rotor unbalance, rotor driving frequency, eigenfrequency of rotor, transient overload disturbance, misalignment etc..
- To verify the different kinds of the system model and parameters on the modified build-up test rig, then to evaluate, compare and analyze both numerical results and experimental results.

### 1.3 Structure and overview of the thesis

This thesis presents numerical and experimental investigations of the active magnetic bearing supported rotor system with auxiliary bearing. The detailed models of AMB-rotor-auxiliary bearing system are build based on the test rig, and different kinds of experiment setting verify the numerical studies. The thesis is organized in the following way:

Chapter 2 summarizes the state of the art. The research work about AMB-rotor system with auxiliary bearing and the interaction between rotor and a stationary object such as seal or auxiliary bearing is of interest to scientists and engineers on account of the importance of the correlated phenomena, backwards whirl of rotor.

A good mathematical model of the real system is the basis for any successful controller design and therefore much attention is drawn towards this step. Chapter 3 introduces the theoretical background used to derive a completely new simulation model of the existing test rig. It starts with a description of models of the real AMB-rotor-auxiliary bearing system that are used in the thesis. These models are important and the basis for the following numerical investigation. Different kinds of rotor models including rigid and flexible model are presented. The models of active magnetic bearing model and several auxiliary bearing settings are also introduced. The inevitable unbalance of rotor provides harmonic excitation. Interaction forces between rotor and auxiliary bearing in case of AMB power failure and transient overload, are discussed in this chapter.

In chapter 4 the test rig which is build for the experimental investigation of the system will be described. The main components of the test rig such as rotor, active magnetic bearing and its control system and various kinds of auxiliary bearing setting will be shown. The pulse sensor build for rotor speed measurement and data acquisition system will be described. Through curve fitting, some important system parameters are identified through experiment results. The experiment procedure for the parameter study with different test settings will be explained. The experimental results is presented and analyzed.

In chapter 5, the models which are introduced in chapter 3 will be used for numerical

investigations. The equations of motion which are built for the basic model of system are introduced. Steady state harmonic response and stability of system will be discussed. Several kinds of extend system models are presented, which include rigid beam rotor interaction with rigid mounting auxiliary bearing model, rigid rotor interaction with flexible mounting auxiliary bearing model and general FE rotor model. Numerical computing method and time variant system simulation method are briefly described. Numerical simulations results will be presented and analyzed. Then the experimental data will be compared with the corresponding numerical simulation results.

Bifurcation analysis of rotor system parameters will be presented in chapter 6. The theoretical fundamental of bifurcation analysis will be introduced in brief. A parameter study will be presented in this chapter. Some possible crucial system parameters such as driving frequency, support stiffness, contact stiffness will be used as control parameters in the bifurcation analysis respectively.

Conclusion will be drawn in chapter 7, which summaries the achievement of the present work, and then makes an outlook for future research.

## 2 Review of the State of the Art

The research work about AMB-rotor system with auxiliary bearing and the interaction between rotor and stationary object such as seal or auxiliary bearing is of interest to scientist and engineer, and this topic has been analyzed and studied by several authors on account of the importance of the correlated phenomena, backwards whirl of rotor.

The work of Ehrich in publication [4] has clearly demonstrated a physical model with two degrees of freedom. The calculated analytical vibration response reveals and quantifies that the interaction phenomena are a function of the level of bearing clearance, rotor unbalance level, and of the relative values of rotor and stator natural frequencies. The physical model is based on strong simplifications. Friction between rotor and stator is not considered by author. In [5], Ehrich mentioned that the high orders of subharmonic vibration of high speed rotor in bearing clearance are found to be possible for system with low damping and extreme nonlinearity. Black in [22] examined the resonance vibrations in an elastic rotor surrounded by an annular clearance. In his model the friction at the clearance space is taken into account. The rotor and stator represent two degrees of freedom. For different frequencies a coupled motion between rotor and stator may occur in a variety of forms and circumstance. Choy and Padovan in [8] investigated dry-friction whip and whirl through the numerical integration of the nonlinear equations of motion. They neglected the mass of the stator and modeled the contact using a linear stiffness; however, they produced simulations that showed the inclusion of bounce modes, contact initiation, and steady state behavior.

In [14], the authors give a good survey of the work published on auxiliary bearings that include different kinds of system model which have been studied. In [27, 28, 29], Muszynaska gave a mathematical model and demonstrated the synchronous and asynchronous motions of the rotor. The experimental results, mainly the appear-

ance of subharmonic vibrations are reported. Full annular rubbing interaction between rotor and seal, including synchronous or reverse (backward) precessions, has been experimentally and analytically discussed by Bently and Yu [6] [7]. These research works are on the basic model of rotor and stator contact and the experiment phenomena.

In recent years many studies have been carried out about the nonlinear model of interaction between AMBs-rotor with auxiliary bearings. Jiang and Ulrich outlined the analytical study of the stability of a more realistic rotor-to-stator contact model in [23], which considered the stator as an elastic body having finite mass and being elastically supported. In this study, the analytical solution corresponding to the synchronous full annular rub motion, is solved, and then the stability condition of it is derived. Analytical methods are presented and measurements performed with full-size machinery are evaluated. Extensive theoretical and experimental studies on the various types of rotor motion in the contact case were also carried out by Wegener and Markert in [25, 24]. Their test facility consists of a flexible rotor with one disk, which contacts a flexibly mounted different retainer bearing-setups. Recent publications in this area are the thesis of Fumagalli and Bartha in [16][21], who performed extensive measurements to improve the understanding of the nonlinear contact dynamics, and in thesis of Bartha, he examined the special and potentially very damaging case of dry friction backward whirl in some detail. Orth developed a modeling tool called ANEAS to simulate AMBs rotor system and study the effect of the initial start point of rotor and behavior of rotor after drop down [2, 13, 17]. Chu and Lu [10] performed experiments to observe the chaotic motion in a rubbing rotor system, the experiments showed that the system motion generally contained the multiple and fractional harmonic components and if the rub-impact became more serious, the chaotic motion could be observed in experiments. The dynamical behavior of a parametrically excited simple rigid disk-rotor supported by active magnetic bearings was investigated by Amer [30]. The steady-state response and the stability of the solutions for various parameters were studied numerically, using the frequency response function method. The numerical results showed that the system behavior included multiple solutions, jump phenomenon, and sensitive dependence on initial conditions. It is also shown that the system parameters have different effects on the nonlinear response of the rotor. The dynamics during a rotor drop into auxiliary bearings after a complete failure of the magnetic bearings was

subject of paper [11] from Kirk. In this paper, Kirk gave a very detail review of the analysis method of transient rotor drop down to auxiliary bearing for AMBs rotor system. Keogh, and Cole developed experimental procedures to study the contact dynamic response with consideration of misalignment [12]. In [31], authors presented the study to enable an assessment of the transient thermal response of an auxiliary bearing to be made from the contact rotor dynamics that may arise in a rotor/magnetic/ auxiliary bearing system. Chaotic and regular vibration of the rotor due to bearing clearance has been extensively investigated in publication [9] by Karpenko.

The interest in this topic has increased, and there are numerous results in this researching field. However, since this rotor dynamic behavior is very complex and dependent upon the precise conditions at the moment of loss of support as well as the details of the friction at the interface between rotor and auxiliary bearing inner race and auxiliary bearing dynamic compliance and other uncertain factors, it is very difficult to draw general conclusions from either transient simulations or actual drop tests. Therefore, investigations of AMB-rotor-auxiliary bearing system through experimental and numerical methods are still desirable.

## 3 Model of AMB Supported Rotor with Auxiliary Bearing System

This chapter aims at providing an overview of the AMB supported rotor with auxiliary bearing system and presenting the basic mathematical models for the system important components. The whole AMB-rotor-auxiliary bearing system is divided into four parts: rotor, active magnetic bearing, auxiliary bearing and excitations. A comprehensive study of AMB-rotor-auxiliary dynamic system is multidisciplinary, because the dynamic rotor behavior depends on the behavior of active magnetic bearings, controller design, mechanics, tribology and knowledge from the other fields.

### 3.1 Rotor

Rotordynamics has been studied extensively and deeply by scientists in [14, 32, 33] largely due to the interplay between its theory and its practice. The most common rotor model that can describe the dynamic behavior of rotors clearly and effectively is so called Jeffcott rotor model. It consists only one massive unbalanced disk attached to massless flexible shaft which is supported by rigid bearings.

Rotor can be modeled as rigid rotor or flexible rotor on accounts of different practical fields. If the deformation of the rotating shaft is negligible in the operating speed range, it is called a *rigid rotor*. If the shaft deforms appreciably at some rotational speed range, it is called a *flexible rotor*. Therefore, the range of the operating speed relative to these critical speeds determines whether the rotor is rigid or flexible [33]. In general, depending on the stiffness of the support and the type of mode to be discussed, the same system may be considered as a rigid rotor or a flexible rotor.

As shown in figure 3.1, this type of plot is called a critical speed map [40]. The first three critical speeds typically vary with bearing support stiffness. In this case, the higher critical speeds are insensitive to support bearing stiffness and in the high support bearing stiffness range nearly all critical speeds are insensitive to it. As the results, the range of the operating speed relative to these critical speeds determines whether the rotor is rigid or flexible.

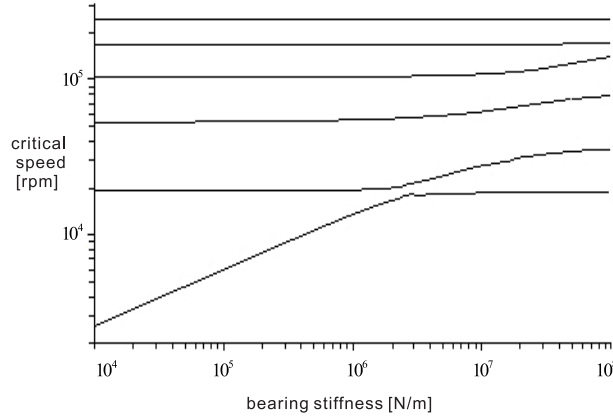


Figure 3.1: Critical speed map

#### 3.1.1 Rigid rotor

A diagram of the considered rotor is shown in figure 3.2 which is modeled as a rigid rotor. The rotor is supported in two active magnetic bearings which provide equivalent radial stiffness  $k_1$ , and radial damping  $d_1$ .  $m$  is the mass of rotor.

It can be assumed that the magnetic force is the sum of damping and spring force. The equation of motion of the rigid mass rotor is given by the well-known equation for mass-spring-damping system:

$$M\ddot{q} + D\dot{q} + Kq = 0, \quad (3.1)$$

where  $M$  is mass matrix  $M = \begin{bmatrix} m & 0 \\ 0 & m \end{bmatrix}$ ;  $D$  is damping matrix  $D = \begin{bmatrix} 2d_1 & 0 \\ 0 & 2d_1 \end{bmatrix}$ ;

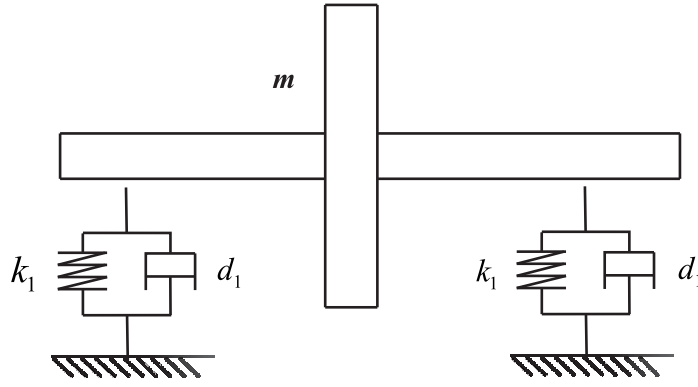


Figure 3.2: Rigid rotor model

$K$  is stiffness matrix  $K = \begin{bmatrix} 2k_1 & 0 \\ 0 & 2k_1 \end{bmatrix}$ ;  $q$  is the rotor displacement  $q = \begin{bmatrix} x \\ y \end{bmatrix}$ ;  $\dot{q}$  and  $\ddot{q}$  are respectively the first and second derivative of  $q$  with respect to time. It is worth noting that the equation of motion of the rotor system does not consider the excitations in equation 3.1. The equivalent stiffness and damping provided by active magnetic bearing  $k_1, d_1$  are dependent on the rotor position (the air gap between the rotor and the bearing) and the coil currents controller design parameters. About the equivalent static and dynamic stiffness and damping calculation will be discussed in next section of this chapter.

#### 3.1.2 Flexible rotor

If the shaft deforms appreciably at some rotational speed ranges, the rotor is not considered as a rigid rotor but an elastic structure. Therefore the rotor can be described as an elastic continuum, which is called a flexible rotor. Such a continuous system has infinite degrees of freedom. Because there is no general approach to the dynamics of an elastic body, in practice, the only feasible approach is the discretization of the continuum and the application of the methods for discrete system [35]. Many discretization techniques have been developed. It is very difficult to make a satisfactory classification of the discretization techniques. One approach is the so called *assumed modes methods*. These methods are based on assumptions that the deforms of system is a linear combination of  $N$  known functions of the space coordinates. The other approach is the so called *lumped mass method*. The

### 3 Model of AMB Supported Rotor with Auxiliary Bearing System

modeling of a flexible rotor can be accomplished by using this method, which was introduced in [38]. It is kind of an extension of the rigid-rotor model. The mass is subdivided into multiple point masses along the structure where the point masses are connected by spring-damper configurations abstracting the elastic properties. A further refinement method is the *finite element method*. It is a general discretization method for the solution of partial derivative differential equations and consequently, it finds its application in many other fields beyond structural dynamics. Using a finite element method, the discretization of the continuous system like flexible rotor is fulfilled.

The Finite Element Method is extensively introduced in [36]. As we know, with computer technology development, there are some commercial or open-source softwares with various element types for the structure Finite Element(FE) modeling. The choice of the element type is a crucial step of the FE modeling.

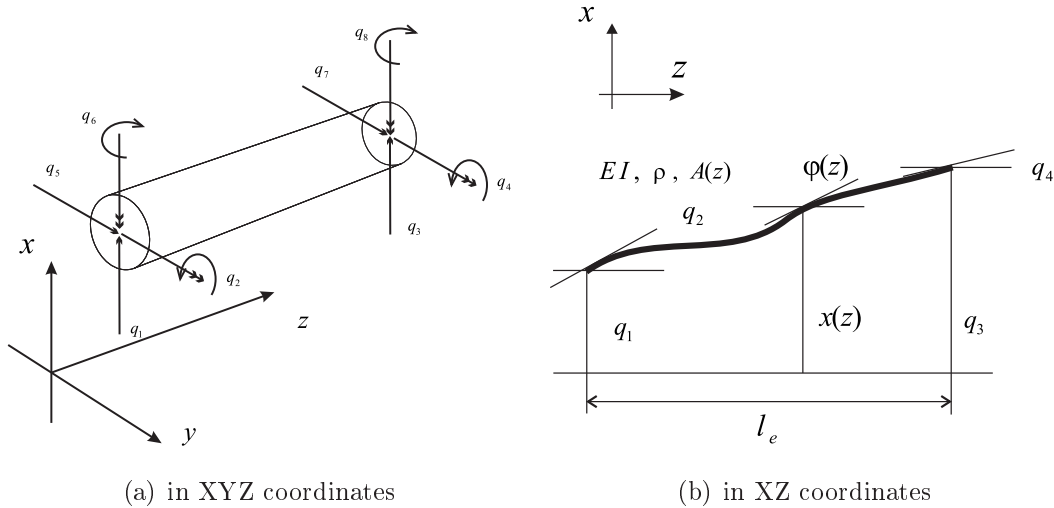


Figure 3.3: Bernoulli beam element

The experimental rotor is supported by two active magnetic bearings in normal working condition. In this study, the lateral vibration is concerned in AMB-rotor-auxiliary bearing system. Therefore, the deformation of the rotor in axial direction and torsional vibrations could be neglected in this flexible model. In term of computing efficiency and model representation performance, the experimental rotor can also be modeled as a flexible rotor by using Euler-Bernoulli beam elements [34] [37]

in this study.

Figure 3.3(a) shows an Euler-Bernoulli beam element in  $XYZ$  coordinates. It is free to bend in the  $xz$  and  $yz$  plane and it does not consider the shear deformation. The two translational and two rotational displacements at nodal coordinates for this beam can be expressed as a vector:  $q_e = \left[ q_1 \ q_2 \ q_3 \ q_4 \ q_5 \ q_6 \ q_7 \ q_8 \right]^T$ .

Figure 3.3(b) shows beam element in  $XZ$ -plane,  $z$  is the any distance along the element from the left end. The length of the beam is  $l_e$ . Young's modulus is  $E$ . The second moment of area of the cross section, constant over the length, is  $I$ .  $A(z)$  is the cross section area at any point  $z$  on the element. The mass per unit length,  $\rho A(z)$  is assumed as constant value  $\rho A$  over the length. Being the static displacements  $x(z)$  and  $y(z)$  of the beam in  $XZ$ -plane and  $YZ$ -plane respectively, with concentrated loads and moments, the displacement shapes are cubic polynomials of  $z$ . As a result, all the displacement functions must be of the general form:

$$x(z) = a_0 + a_1z + a_2z^2 + a_3z^3 \quad (3.2)$$

$$y(z) = b_0 + b_1z + b_2z^2 + b_3z^3 \quad (3.3)$$

The slope,  $\phi(z)$ , at any point  $z$  in figure 3.3(b), is given by differentiating equation 3.2 with respect to  $z$ .

$$\phi(z) = \frac{dx}{dz} = a_1 + 2a_2z + 3a_3z^2 \quad (3.4)$$

Since the beam element is assumed as symmetrical, it is convenient to use Hermite element shape functions as cubic polynomials which represent unity displacement for the accordant coordinate only in  $YZ$  plane, while they are zero at all other coordinates. Figure 3.4 shows the four static displacement functions, which are also used as assumed vibration modes for the element. These are defined by applying unit values of the end displacements,  $q_1$ ,  $q_2$ ,  $q_3$  and  $q_4$ , one at a time, with the other three fixed.  $\xi = \frac{z}{l_e}$ , is the non-dimensional distance along the element,  $\xi$  is in the unit interval  $[0, 1]$ ,  $\xi \in [0, 1]$ . The four shape functions are given by:

$$\begin{aligned} H_1 &= 1 - 3\xi^2 + 2\xi^3, & H_2 &= l_e\xi(1 - \xi)^2, \\ H_3 &= 3\xi^2 - 2\xi^3, & H_4 &= l_e\xi^2(1 - \xi). \end{aligned} \quad (3.5)$$

### 3 Model of AMB Supported Rotor with Auxiliary Bearing System

The displacement  $x(\xi)$  and the rotations  $\phi(\xi)$  at any point on the element, in terms of end displacements, can be expressed by using the four element shape functions in equations 3.5:

$$x(\xi) = H_1q_1 + H_2q_2 + H_3q_3 + H_4q_4 = \sum_{k=1}^4 H_kq_k, \quad (3.6)$$

$$\phi(\xi) = H'_1q_1 + H'_2q_2 + H'_3q_3 + H'_4q_4 = \sum_{k=1}^4 H'_kq_k. \quad (3.7)$$

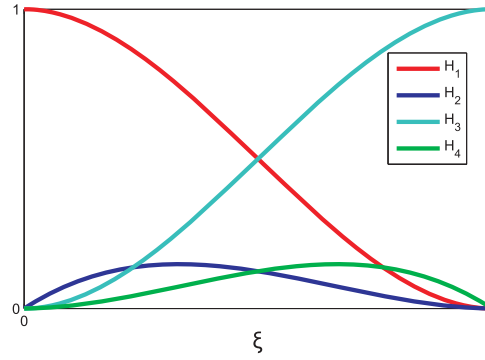


Figure 3.4: Hermite Interpolation Shape Functions

The kinetic and potential energies of the beam element,  $T_e$  and  $U_e$ , are respectively found as follows:

$$T_e = \frac{1}{2} \int_0^{l_e} \rho A(z) (\dot{x}(z))^2 dz = \frac{\rho A}{2} \int_0^{l_e} (\dot{x}(z))^2 dz, \quad (3.8)$$

$$U_e = \frac{EI}{2} \int_0^{l_e} \left( \frac{d^2x(z)}{dz^2} \right)^2 dz, \quad (3.9)$$

where,  $\dot{x}(z)$  means the first derivative of displacement  $x(z)$  with respect to time. Since  $z = l_e\xi$ ,  $dz = l_e d\xi$ ,  $d^2z = l_e^2 d^2\xi$ , equation 3.8 and equation 3.9 become:

$$T_e = \frac{\rho A l_e}{2} \int_0^1 (\dot{x}(\xi))^2 d\xi, \quad (3.10)$$

$$U_e = \frac{EI}{2l_e^3} \int_0^1 \left( \frac{d^2x(\xi)}{d\xi^2} \right)^2 d\xi. \quad (3.11)$$

### 3 Model of AMB Supported Rotor with Auxiliary Bearing System

---

Applying Hamilton's Principle to this unified beam element,  $L_e = T_e - U_e$

$$\delta \int_{t_1}^{t_2} L_e dt = \delta \int_{t_1}^{t_2} T_e - U_e dt = 0. \quad (3.12)$$

That leads to expressions for the components of the mass matrix  $M_e$  and stiffness matrix  $K_e$  of the Euler-Bernoulli beam element in the  $XZ$ -plane:

$$M_e = \frac{A\rho l_e}{420} \begin{bmatrix} 156 & 22l_e & 54 & -13l_e \\ 22l_e & 4l_e^2 & 13l_e & -3l_e^2 \\ 54 & 13l_e & 156 & -22l_e \\ -13l_e & -3l_e^2 & -22l_e & 4l_e^2 \end{bmatrix}, \quad (3.13)$$

$$K_e = \frac{EJ}{l_e^3} \begin{bmatrix} 12 & 6l_e & -12 & 6l_e \\ 6l_e & 4l_e^2 & -6l_e & 2l_e^2 \\ -12 & -6l_e & 12 & -6l_e \\ 6l_e & 2l_e^2 & -6l_e & 4l_e^2 \end{bmatrix}. \quad (3.14)$$

As mentioned above, the according stiffness and mass matrices for the beam element in the  $XY$ -plane can be derived in the same manner. The only difference is the relationship between lateral and rotational displacement. The matrix of mass  $\mathbf{M}$  and stiffness  $\mathbf{K}$  for the rotor are assembled by suitable superposition. That is a sum up of the components of all element matrices belonging to the same node and the same degree of freedom. For the FE rotor model which is discrete to  $N - 1$  beam elements by  $N$  nodes, the size of stiffness matrix and mass matrix is  $2N \times 2N$ .  $\mathbf{D}$  is damping matrix. It can be modeled as a linear combination of the mass and stiffness matrices in some case, which is known as proportional damping [34]:

$$\mathbf{D} = \alpha \mathbf{K} + \beta \mathbf{M}.$$

The equation of motion for flexible rotor model in  $XZ$  and  $YZ$ -plane can be expressed as:

$$\mathbf{M}\ddot{\mathbf{q}} + \mathbf{D}\dot{\mathbf{q}} + \mathbf{K}\mathbf{q} = 0, \quad (3.15)$$

### 3 Model of AMB Supported Rotor with Auxiliary Bearing System

where,  $\mathbf{M}$  is mass matrix  $\mathbf{M} = \begin{bmatrix} M_x & 0 \\ 0 & M_y \end{bmatrix}_{4N \times 4N}$ .  $\mathbf{D}$  is damping matrix  $\mathbf{D} = \begin{bmatrix} D_x & 0 \\ 0 & D_y \end{bmatrix}_{4N \times 4N}$ .  $\mathbf{K}$  is stiffness matrix  $\mathbf{K} = \begin{bmatrix} K_x & 0 \\ 0 & K_y \end{bmatrix}_{4N \times 4N}$ .  $q$  is the rotor displacement  $q = \begin{bmatrix} q_x \\ q_y \end{bmatrix}_{4N \times 1}$ .  $\dot{q}$  and  $\ddot{q}$  are respectively the first and second derivative of  $q$  with respect to time.

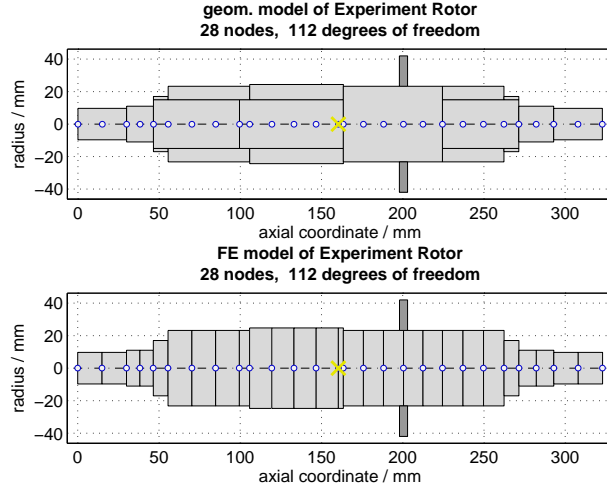


Figure 3.5: FE model of free - free experimental rotor

Figure 3.5 presents an example of FE model of experimental rotor in this study. The experimental rotor can be subdivided to 27 beam elements by 28 nodes, and each node has four degrees of freedom. When the motion of rotor in  $x$  and  $y$  lateral direction are in study, the mass matrix become a  $224 \times 224$  matrix. Furthermore, the most flexible structures are subdivided by great quantity elements much more than this one in reality. The matrix of mass, stiffness and damping could be very high-order matrix. The equation of motion composed of these kind of large matrices can be solved by using a standard time integration scheme. However, time domain analysis may be time consuming since the number of equations used to describe the flexible body is the same as the number of degrees of freedom and the equations are highly coupled [39]. As a result, this multi-degree of freedom FE rotor model usually cannot be used in simulation and structure control design directly, but this problem can be solved by model reduction. There are many reduction methods such

as the static reduction method, the component mode synthesis method [44].

#### 3.1.3 Model reduction

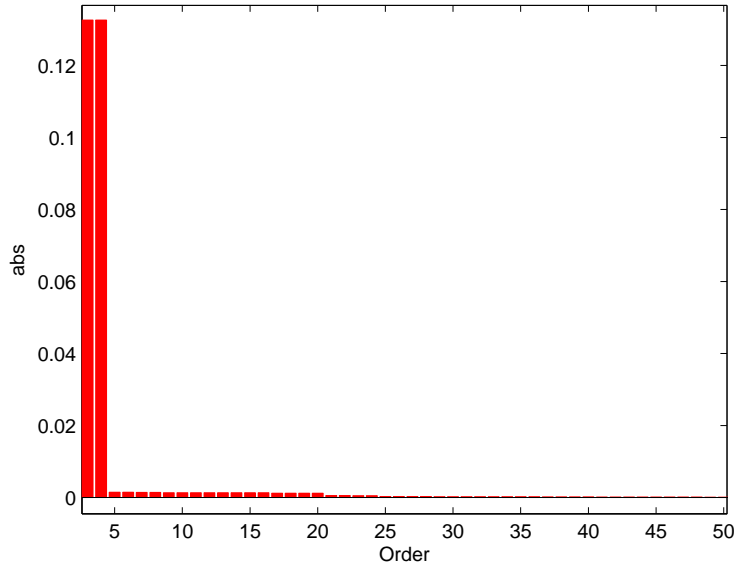


Figure 3.6: The Hankel singular values of the AMB-rotor FE model

In many instances, a reduced model of dynamic system, which captures the main features of the original complex model, is necessary due to limited computational accuracy or storage capabilities. The reduced model may then be used in place of the original complex model, either for simulation or control. Especially, for simulating large elastic systems, which are mostly modeled by the Finite Element Method (FEM), model reduction is a necessary procedure. In order to reduce the systems of large dimensions, various techniques have been developed during the last decades, many of which share some common characteristics (Guyan, Dynamic, CMS, IRS, SEREP) [42].

In control theory, Hankel singular values, named after Hermann Hankel, provide a measurement of energy for each state in a system. They are the basis for balanced model reduction, in which high energy states are retained while low energy states

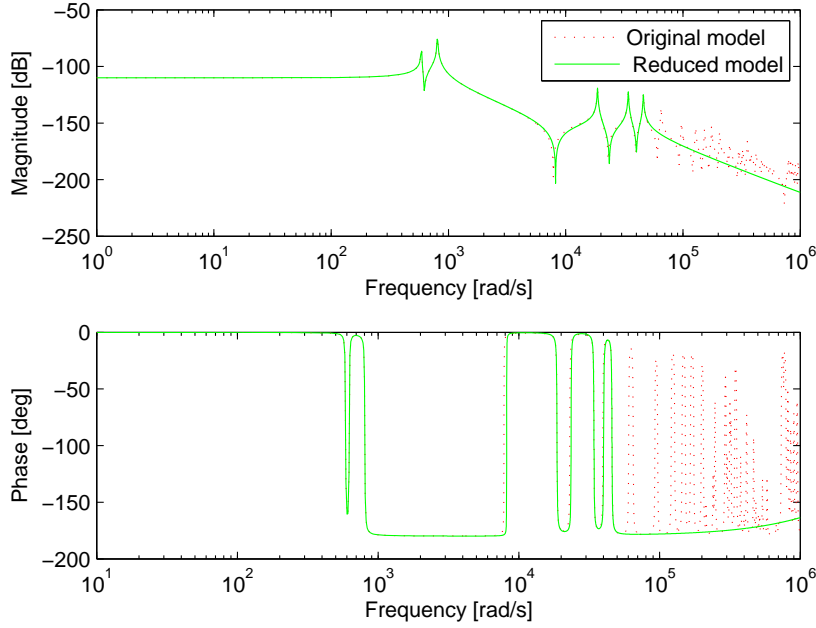


Figure 3.7: Comparison of transfer functions of the original and reduced models.

are discarded. The reduced model retains the important features of the original model[43].

Hankel singular values are calculated as the square roots  $\sigma_i, i \geq 0, i = 1, \dots, n$ , of the eigenvalues,  $\lambda_i, i \geq 0, i = 1, \dots, n$ . For the FEM model of rotor, the eigenvalues can be calculated as following,

$$[\mathbf{K} - \lambda_i \mathbf{M}] \varphi_i = 0,$$

where  $\lambda_i$  is the  $i$ th eigenvalue and  $\varphi_i$  is the  $i$ th eigenvector.

As an example, the Hankel singular values are computed for reduction of the AMB supported rotor FE model. The Hankel singular values of the FEM is shown in figure 3.6 with drawing a bar graph. The order of original FE model is 116. The desired reduced model keeps the 20 largest orders. Figure 3.7 shows the comparison of transfer functions of the original and reduced models. In practice, only the lowest frequency modes contribute significantly to the response of the system. High frequencies complicate the time integration procedure, burden the numerical performance of the model. Therefore, high frequency modes can be neglected without a

significant loss of accuracy [41].

In conclusion, a rigid rotor model and a finite element model of a flexible rotor is introduced and studied in this work. It is important to choose a suitable rotor model based on the experimental test rig and to meet different study goals.

## 3.2 Active magnetic bearing

In this part, basic mathematical models of magnetic bearings and related actuators are presented. An analysis is carried out to calculate the inductance, flux densities, stored magnetic energy and magnetic forces. Typical structures for the radial magnetic bearing and related actuators are described. The principles of a feedback control strategy for magnetic bearings are introduced. As a result of the analysis, a simple representation of the magnetic bearing is introduced. The equations of motion for rotor supported by active magnetic bearings system are developed and how the process of a controller affects the equivalent stiffness and damping parameters of the AMB-rotor system is discussed. The references [45] [46] [18] provide a detailed overview about this topic.

### 3.2.1 Principle of active magnetic bearings

The principle of active magnetic bearing is to use the electromagnetic force for rotor suspension. The simplest horseshoe shape electromagnetic actuator which levitates the I-shaped core by counteracting the force of gravity is shown as in figure 3.8.

The primary objective of analyzing the behavior of this kind of magnetic actuator is to determine the forces generated by the actuator in response to the current applied to its coils and the motion of the actuated device. Once this analysis is well established, it can be used in the design of actuators both in that it provides insight into the effects of the various design parameters and in that the analysis can be used to evaluate design choices. It is worth mentioning that it is common to assume that the magnetic flux is confined to the iron and the gap volumes (no leakage) for high permeability magnetic structures with a small air gap. This gives rise to some errors, but the results are mostly satisfactory [18]. If the magnetizing characteristic curve

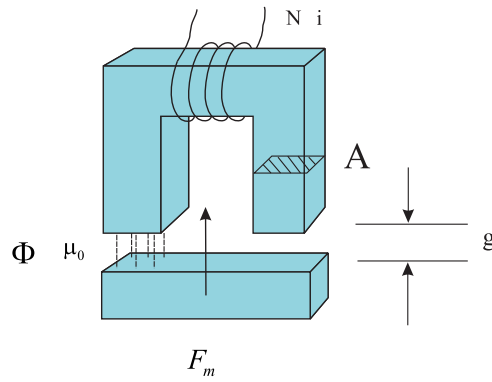


Figure 3.8: Horseshoe shape electromagnetic actuator

is linear (i.e., no saturation), the magnetic force  $F_m$  can be derived from the energy stored in the air gap between electromagnetic actuator and the I-shaped core. The force is given by

$$F_m = \frac{n^2 A \mu_0 i^2}{4g^2}, \quad (3.16)$$

where,  $n$  refers to the numbers of wire loops in the electromagnet,  $A$  is the cross-section area of flux path,  $\mu_0$  is the permeability of air,  $\mu_0 = 4\pi \times 10^{-7} \text{N/Ampere}^2$ ,  $i$  is the instantaneous current value in the coil,  $g$  is the air gap between the actuator and the I shape core.

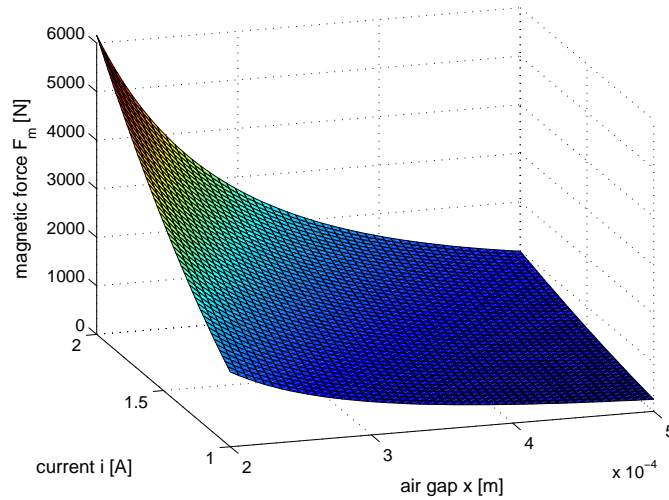


Figure 3.9: The relationship of current, air gap and magnetic force

### 3 Model of AMB Supported Rotor with Auxiliary Bearing System

---

Figure 3.9 gives us a straightforward insight into the relationship between the magnetic force  $F_m$ , current  $i$  and air gap  $g$  by a calculate example. It has been calculated under the assumption that coil carries 350 turns of wire,  $n = 350$ , the cross-section area of flux path  $A = 0.0016\text{m}^2$ , the current varies from 1 to 2 Ampere, air gap length varies from 0.0002 to 0.0005 meter. It can be said that the magnetic force  $F_m$  is proportional to  $i^2$  and  $g^{-2}$ .

The system which uses a single horseshoe shape magnetic actuator to suspend core like above example is susceptible to small disturbances and is highly unstable. For this reason, radial active magnetic bearings use electromagnets as opposed to permanent magnets as shown in figure 3.10. By positioning several magnets radially around the rotor, it achieves greater stability.

The real configuration of magnetic bearing used in test rig is also shown in figure 3.10. Each axis of the bearing actuator consists of two opposing magnets, and each magnet produces an attractive force. The magnetic bearing controller is designed such that the actual coil current  $i_{x+}, i_{x-}, i_{y+}, i_{y-}$  is composed of a set bias currents  $i_{x0}, i_{y0}$ , which define the working point around and perturbation currents  $i_x, i_y$  that are varying the suspend force to counter shaft displacements.

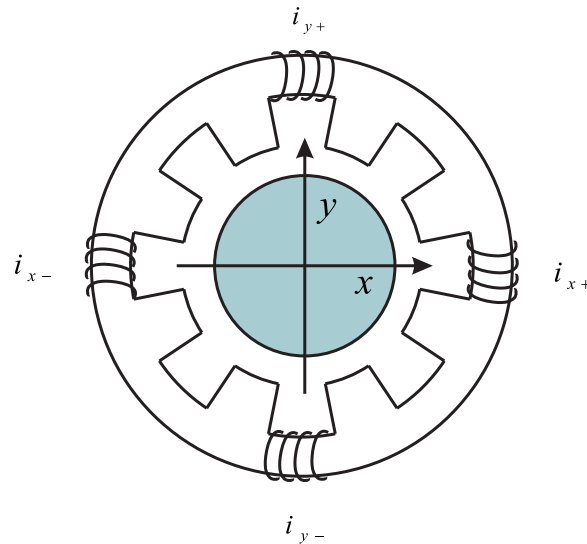


Figure 3.10: Configuration of radial magnetic bearing

$$\begin{aligned} i_{x+} &= i_{x0} + i_x & i_{x-} &= i_{x0} - i_x \\ i_{y+} &= i_{y0} + i_y & i_{y-} &= i_{y0} - i_y \end{aligned} \quad (3.17)$$

The forces on the rotor  $F_m^x$  and  $F_m^y$  are respectively the difference between the two directions in axis  $x$  and  $y$ . Using equation 3.16, we can calculate the net force on the rotor by the following equations:

$$\begin{aligned} F_m^x &= \frac{N^2 A \mu_0}{4} \left[ \left( \frac{i_{x0} + i_x}{s_0 - x} \right)^2 - \left( \frac{i_{x0} - i_x}{s_0 + x} \right)^2 \right], \\ F_m^y &= \frac{N^2 A \mu_0}{4} \left[ \left( \frac{i_{y0} + i_y}{s_0 - y} \right)^2 - \left( \frac{i_{y0} - i_y}{s_0 + y} \right)^2 \right]. \end{aligned} \quad (3.18)$$

where,  $s_0$  is the initial air gap between rotor and magnetic bearing.

In the operating range of the magnetic bearing, the hysteresis effects and saturation effects are neglected. By applying a Taylor series expansion of equation 3.18, the magnetic force equation can be linearized about the working point and the equation 3.18 becomes

$$F_m^x = \mathbf{K}_i i_x + \mathbf{K}_s x, \quad F_m^y = \mathbf{K}_i i_y + \mathbf{K}_s y, \quad (3.19)$$

$$\mathbf{K}_i = \frac{N^2 \mu_0 A i_0}{s_0^2}, \quad \mathbf{K}_s = \frac{N^2 \mu_0 A i_0^2}{s_0^3}. \quad (3.20)$$

The current stiffness parameter  $\mathbf{K}_i$  and displacement stiffness parameter  $\mathbf{K}_s$  are the so called *actuator gain* and *open loop stiffness* in [18]. They depend on the initial air gap between magnet and rotor  $s_0$  and the bias current  $i_0$ . They can also be determined by experimental method.

#### 3.2.2 The equivalent stiffness and damping of AMB supported rotor system

In order to analytically estimate the stiffness and damping parameter of AMB-rotor system, it can be assumed that the magnetic force is the sum of damping and

spring force and rotor is rigid mass. The simple rotor model composed by a rigid rotor and two radial active magnetic bearings has been developed in the previous section. The equation of motion of this kind of model is given by equation 3.1. Since the controlled magnetic forces in  $x$  and  $y$  directions have the same manner and it is assumed that they are uncoupled with each other, the following analysis about the equivalent stiffness and damping of AMB-rotor system is only presented in  $x$  direction for simplification. But all equations are valid for the  $y$  direction.

It is worth mentioning that the analysis about the close loop active magnetic bearing rotor system is under the following assumptions:

- All the control components such as sensor, filter, AD converter, DA converter have relatively wide linear working range;
- The magnetic bearing is around working point, the magnetic force is linearized. No magnetic leakage and saturation are considered;
- Rotor can be model as a rigid rotor supported by spring and damping elements.

As figure 3.11 shows, the displacement sensor detects the position of the suspended rotor. The sensor output voltage is filtered and fed to AD converter. Then the digital signal is as the input to a controller. The controller algorithm yields the command for the current. The power amplifier converts the signal of DA converter to current, which generates a controlled magnetic force through magnetic actuator so that the generated magnetic force follows the force command.

From equation of motion  $m\ddot{x} + d_1\dot{x} + k_1x = F_{ex}$  and equation 3.19, what can be derived by:

$$\begin{aligned} F_m^x &= -d_1\dot{x} - k_1x = \mathbf{K}_i i_x + \mathbf{K}_s x, \\ m\ddot{x} - \mathbf{K}_s x - \mathbf{K}_i i_x &= F_{ex}. \end{aligned} \quad (3.21)$$

The magnetic force  $F_m^x$  is generated by active magnetic bearing to stably suspend the rotor in  $x$  direction. It can be assumed as the sum of damping and spring force.  $k_1$  and  $d_1$  are respectively the equivalent stiffness and damping parameters. The damping force  $-d_1\dot{x}$  is proportional to the speed of the suspended rotor. The spring force  $-k_1x$  is proportional to the displacement of the suspended rotor. They are both negative in term of they in the opposite direction to the speed and displacement

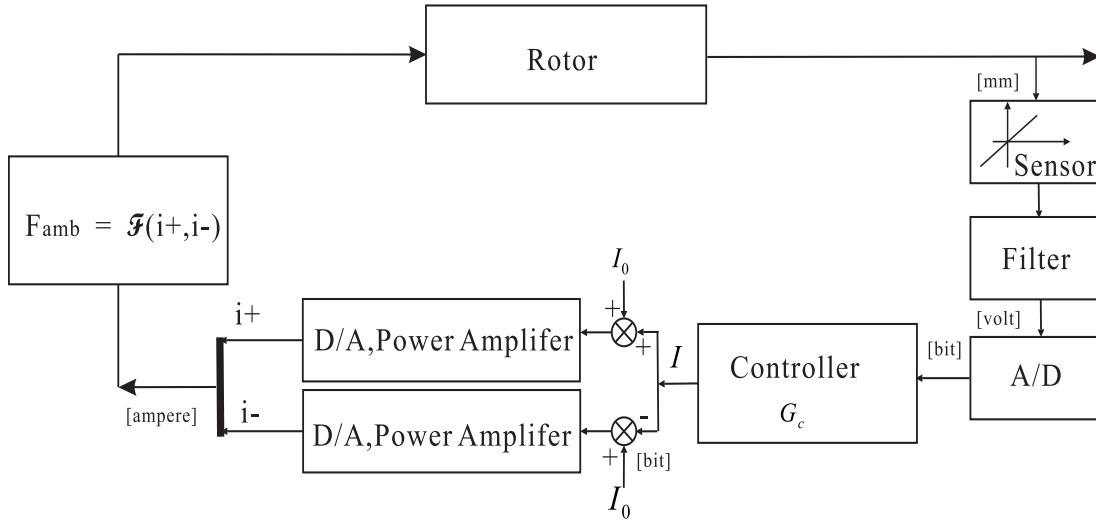


Figure 3.11: A close loop active magnetic bearing rotor suspension system

of the suspend rotor. In equation 3.21, the so called *negative stiffness*  $-\mathbf{K}_s$  can be found. That means, the  $\mathbf{K}_i i_x$  must be well designed and controlled to keep the system stable.

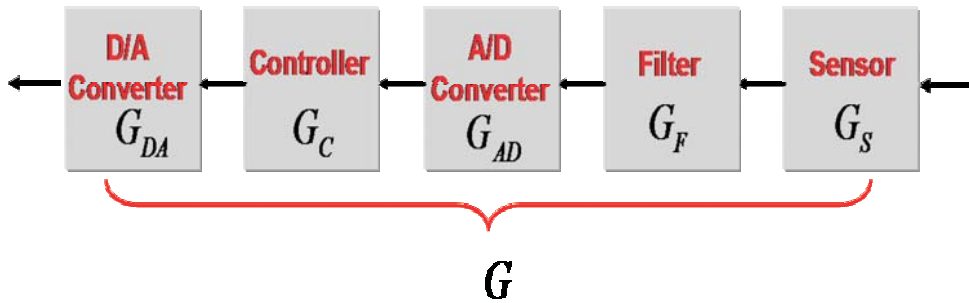


Figure 3.12: The block diagram of the controller part

The block diagram of the AMB controller part is shown in figure 3.12. It is seen that the whole controller part determines the appropriate currents for each electromagnet based on shaft position. The whole feedback controller part transfer function from the displacement of rotor to the controlled current of magnetic bearing can be defined as:

$$G(s) = -\frac{I_x(s)}{X(s)}. \quad (3.22)$$

The whole controller transfer function is a series connection of sensor transfer function,  $G_s(s)$ , the transfer function of filter  $G_F(S)$ , the transfer function of AD converter  $G_{AD}(s)$ , transfer function of controller  $G_c(s)$  and transfer function of DA converter  $G_{DA}(s)$ . Therefore, the whole feedback controller part transfer function can be expressed by:

$$G(s) = G_s(s)G_F(S)G_{AD}(s)G_c(s)G_{DA}(s). \quad (3.23)$$

Equations can be obtained from applying the Laplace transform to the equations 3.21 then substituting equation 3.22 in it and with the assumption  $\dot{x}(0) = 0$ ,  $x(0) = 0$ ):

$$\begin{aligned} s^2mX(s) + d_1sX(s) + k_1X(s) &= F_{\text{ex}}(s), \\ s^2mX(s) - \mathbf{K}_sX(s) - \mathbf{K}_iG(s)X(s) &= F_{\text{ex}}(s). \end{aligned} \quad (3.24)$$

The transfer function for the whole close loop AMB-rotor system  $G_w(s)$  will represent the relation between the input and the output. Here they are excitation force  $F_{\text{ex}}$  and displacement  $x$  respectively. The transfer function of the whole AMB supported rotor system  $G_w(s)$  can be derived from equation 3.24:

$$\begin{aligned} G_w(s) &= \frac{X(s)}{F_{\text{ex}}(s)} = \frac{1}{ms^2 + d_1s + k_1}, \\ G_w(s) &= \frac{X(s)}{F_{\text{ex}}(s)} = \frac{1}{ms^2 - \mathbf{K}_s - \mathbf{K}_iG(s)}. \end{aligned} \quad (3.25)$$

Assume that  $G(s)$  has been well designed to overcome the negative stiffness and provide damping to the system to make the whole AMB rotor system stable. As a result, the whole feedback controller part transfer function can be obtained from equations 3.22 and 3.24 as

$$G(s) = \frac{k_1 + \mathbf{K}_s + d_1s}{\mathbf{K}_i}. \quad (3.26)$$

Hence, from equation 3.26, the conclusion can be drawn that the equivalent stiffness  $k_1$  and damping  $d_1$  depend on  $G(s)$ , and the dynamic value of  $k_1$  and  $d_1$  can be calculated by the frequency response of  $G(s)$ .

Assume that  $s = jw$ , by evaluating transfer function  $G(jw)$  and  $\frac{k_1 + \mathbf{K}_s + d_1 w j}{\mathbf{K}_i}$  at the specified frequency points  $w$ , the information about the magnitude and phase of the response at the frequency  $w$  are obtained, then by comparing the magnitude and phase of the frequency responses of the two sides of the equation 3.26, the equivalent stiffness  $k_1$  and damping  $d_1$  can be calculated.

Defining  $K_{st}$  as the static overall controller gain of  $G(s)$  under the condition  $s = jw$ ,  $w = 0$ ,

$$K_{st} = \|G(jw)\|_{w=0} = \|G_s(jw)\| \cdot \|G_{AD}(jw)\| \cdot \|G_C(jw)\| \cdot \|G_{DA}(jw)\|_{w=0}. \quad (3.27)$$

The static equivalent stiffness of rotor  $k_1$  is calculated as:

$$k_1 = K_{st} \mathbf{K}_i - \mathbf{K}_s. \quad (3.28)$$

Here, a calculation example is presented based on real build up test rig. The current stiffness parameter  $\mathbf{K}_i$  and displacement stiffness parameter  $\mathbf{K}_s$  of the magnetic bearing used in the test rig are known. The  $K_{st}$  as the static overall controller gain of  $G(s)$  can be obtained by dynamic properties characteristics of each components of the control part such as displacement sensor, filter, AD converter and controller and DA converter, which will be introduced in next chapter. By substituting all the parameters into equation 3.28, the value of static equivalent stiffness  $k_1$  can be calculated. Table 3.1 lists the parameters and results.

Table 3.1: Parameters and the static equivalent stiffness of rotor system

The displacement stiffness parameter	$\mathbf{K}_s$	39.7	[N/mm]
The current stiffness parameter	$\mathbf{K}_i$	19	[N/A]
The static overall controller gain	$K_{st}$	67.0102	[A/mm]
The static equivalent stiffness of rotor system	$k_1$	$5.96 \times 10^5$	[N/m]

If the transfer function of overall feedback control part  $G(s)$  can be represented as  $-(\mathbf{k}_p + \mathbf{k}_d s)$  as a PD controller, and it is assumed that the whole controller part including displacement sensor, filter, etc. is already known and it makes the system stable, the parameters  $\mathbf{k}_p$  and  $\mathbf{k}_d$  can be obtained. Then, for calculating the equivalent stiffness  $k_1$  and damping  $d_1$ , the following equations can be derived by equation 3.26,

$$k_1 = \mathbf{k}_p \mathbf{K}_i - \mathbf{K}_s, \quad (3.29)$$

$$d_1 = \mathbf{k}_d \mathbf{K}_i. \quad (3.30)$$

Through the introduction of the basic mathematical model of magnetic bearing and the principle of a feedback control strategy, the analytical estimation method for the equivalent stiffness  $k_1$  and damping  $d_1$  parameters of AMB-rotor system is developed. As a result of the analysis, a simple representation of the magnetic bearing is obtained. The equivalent stiffness and damping of AMB-rotor system are a mixture of the magnetic actuator properties and the whole control components properties. In this work, they can be estimated by experimental methods as well.

## 3.3 Auxiliary bearing and tolerance ring

### 3.3.1 Auxiliary bearing

Auxiliary bearings play an indispensable role in active magnetic bearings (AMBs) supported rotor systems. In normal working conditions, rotor is suspended in the bearings, it does not contact with any part. But in case active magnetic bearings have a power failure or the transient overload adds on the rotor, auxiliary bearings support high speed rotating rotor and avoid it to destroy the other parts of machine [53]. It is also called a catcher bearing, retainer bearing or a back-up bearing in some publications. The clearance between the auxiliary bearings and rotor is smaller than that of the magnetic bearing so that they can protect the magnetic bearing. Typically, fifty percent of the clearance between the magnetic bearing and rotor is used for the auxiliary bearing clearance [51].

The diversity in both requirements and applications has led to the development of several auxiliary bearing concepts, each having its own advantages and disadvantages. Generally, the auxiliary bearing concepts in use today fall into three categories. These are plain bearings, rolling element bearings, and special design bearings. Plain bearings can be made of a variety of materials including bronze, graphite, solid polymer and ceramic [54]. However, as auxiliary bearings, they are operating without lubrication system, plain bearings may wear faster and have

higher friction than rolling element bearings. To overcome the drawbacks of plain bearing, rolling element bearings are used as auxiliary bearings due to their low rolling friction. There are many types of rolling element bearings, each tuned for a specific kind of load and with specific advantages and disadvantages [55]. But, the rapid deterioration of auxiliary bearing can result from rotor impacts and high-speed touchdowns through experiment investigation. The third type of auxiliary bearing is special design bearings as mentioned above such as the zero clearance bearings [56]. They have been carried out in order to improve the auxiliary bearings performance. In addition, an active retainer bearing being attached to the foundation through unidirectional electromagnetic actuators is presented in the literature [57]. However these special design bearings are complex and expensive, therefore they are not widely used as auxiliary bearing in AMB-rotor system.

In this work, ball bearing has been chosen as auxiliary bearing in the test rig and the tolerance ring could be used to get softer mounting stiffness.

#### 3.3.2 Tolerance ring

The tolerance ring is expected to provide soft mounting stiffness of auxiliary bearing. In some cases, the radial overload adding on the shaft, the soft mounted auxiliary bearing could protect rotor from impacting the stators and the soft mounting stiffness may also avoid one of unstable rotor motions, backward whirl. In addition, the tolerance ring could maintain the auxiliary bearing at the right position after interaction between rotor and auxiliary bearing. That means, the auxiliary bearing could be re-centered by tolerance ring. According to all of these potential advantages of tolerance ring, it has been used in the test rig.

The tolerance rings (HV42x12) used in test rig are produced by one of the manufactures, Rencol. It is a precision spring steel device comprising a thin strip into which corrugations, or waves, are formed, each of which will act as a spring as shown in figure 3.13. This strip is then rolled into a ring. The mounting stiffness  $k_2$  provided by tolerance ring is interesting for this study. The author introduced a method for the spring stiffness calculation in publication [50].

The factors influencing  $K_{tr}$  include:



Figure 3.13: Tolernace ring [48]

- Material thickness
- Wave pitch
- Wave shoulder shape
- Plannish width
- Wave root radii
- Elastic Modulus for the material
- Wave width
- Wave thinning
- Plannish thickness
- Wave crest radii.

Of these factors, for a given wave shape, the two major factors are thickness and wave pitch. So the Spring Constant  $K_{tr}[N/mm^{-1}]$  is given by:

$$K_{tr} = 4.8 \times E \times W \times \left(\frac{t}{p}\right)^3, \quad (3.31)$$

where,  $K_{tr}$  is the spring constant  $[N/mm^{-1}]$ ,  $E$  is the Elastic Modulus for the material  $[kNmm^{-2}]$ ,  $W$  is the width,  $t$  is the thickness and  $p$  is the wave pitch  $[mm]$ . The cubic power relationship allows for the possibility to engineer a very wide range of spring stiffness. The complex wave geometry with a formed wave and closed ends gives rise to a rigid structure, which can allow very high forces to be achieved with corresponding high spring stiffness. From finite element analysis of the tolerance ring models in [50], it can be seen that the wave shoulders make the main contribution to the stiffness. This is a basic guide, the actual performance of tolerance ring will be affected by the components in the system. Empirical research shows that the wave compression range for the elastic properties varies depending on the wave geometry.

Table 3.2 shows the tolerance ring (HV42x12) configurations used in test rig with

### 3 Model of AMB Supported Rotor with Auxiliary Bearing System

corresponding spring constants. It is important to note that the wide range of spring constant can be designed for a given ring size:  $k_2 = (1 - 1/3)K_{tr}$

Table 3.2: Parameter of tolerance ring(HV42x12)

Diameter	42	[mm]	Thickness $t$	0.4	[mm]
Wave pitch $p$	5	[mm]	Width	12	[mm]
No. Waves	26		Wave Height	1.02	[mm]
Spring Constant per Wave	$5.90 \times 10^6$	[N/m]	Spring Constant of Ring	$1.97 \times 10^6$	[N/m]

#### 3.3.3 Model of auxiliary bearing

It is necessary to build a model of auxiliary bearing in order to analyze the dynamic behavior AMB-rotor-auxiliary bearing during interaction between rotor and auxiliary bearings.

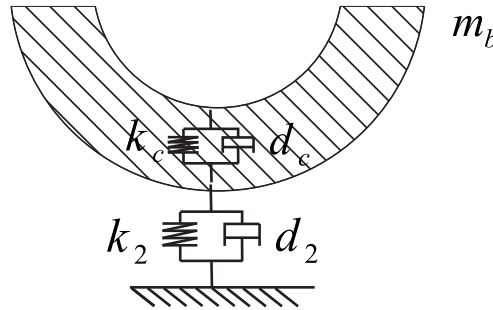


Figure 3.14: Model of auxiliary bearing with tolerance ring

Figure 3.14 shows a model of auxiliary bearing. Here stiffness  $k_2$  and damping  $d_2$  are used to model the mounting forces of auxiliary bearing, which are usually provided by housing or support components. When rotor interacts with auxiliary bearing, the additional interaction force  $F_b$  composed of contact force and friction force are generated.  $m_b$  is the mass of auxiliary bearing. Here, the contact force is also modeled as a spring and damping force.  $k_c$  and  $d_c$  are contact stiffness and damping parameters respectively. When ball bearings are taken as auxiliary bearings, there exist three contact zones: between rotor and inner ring, between

inner ring and ball, between ball and outer ring. In order to get the simplified auxiliary bearing model, the contact stiffness  $k_c$  is the whole contact stiffness of the three contact zones. In [16], the author introduced the measurement concept to obtain the parameters and variables before and after rotor impacts different stators, thus the contact stiffness can be estimated. If only considering the spring effect, the contact spring and mounting spring are in series connection, the following equation can be derived by:

$$\frac{1}{k_b} = \frac{1}{k_c} + \frac{1}{k_2}, \quad (3.32)$$

where,  $k_b$  is auxiliary bearing stiffness. If the auxiliary bearings are mounted directly with the machine housing, it could be assumed as fixed mounted auxiliary bearings; so the supporting stiffness  $k_2$  is much higher than the contact stiffness  $k_c$ , therefore, the supporting stiffness and damping could be ignored. The auxiliary bearing is fixed and the interaction force  $F_b$  is only an excitation source for AMB-rotor system. Otherwise, when the auxiliary bearings are compliantly mounted on the machine housing, the supporting stiffness and damping must be taken into account in the AMB-rotor-auxiliary bearing system. The interaction force  $F_b$  is an excitation both for AMB-rotor system and auxiliary bearing.

## 3.4 Excitations of the rotor system

### 3.4.1 Unbalance

Unbalance is the most common excitation forces acting on rotating machinery. Initial unbalance in the rotating machine is a condition of unequal mass distribution at each section of the rotor, which is unavoidable. During rotor rotating, rotor unbalance generates centrifugal force. Unbalance force, for example, is calculated by:

$$F_u = me\Omega^2, \quad (3.33)$$

where,  $me$  is unbalance of rotor,  $\Omega$  is rotor driving frequency. Usually it is assumed as a constant value, but in actual condition, it can not be simplified as a constant, but a variable depending on many factors. In [58], authors introduced experimental

formulas for the deceleration of the driving speed due to the aerodynamic torque in the case of motor power failure. In this work, the rotor driving frequency could be modeled as a time variable parameter.  $F_u$  is unbalance force, which is synchronous with rotor rotating and provides lateral harmonic excitation for rotor.

#### 3.4.2 Contact and friction force between rotor and auxiliary bearings

When active magnetic bearings have power failure or transient overload adds on the rotor, high speed rotating rotor impact auxiliary bearings and friction force is generated at the physical interface between the two surfaces in contact. This kind of excitation is very harmful to AMB-rotor system and it may cause a very serious instable motion, named backwards whirl. So it is important to study the detailed model of contact and friction.

##### Linear elastic contact force

For a simplified model, the contact force  $N$  between rotor and auxiliary bearing can be considered as an ideal elastic force, which is linear with the non-negative radial penetration  $\delta$ .

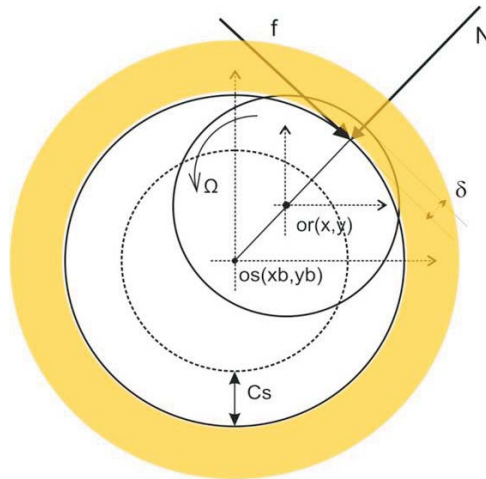


Figure 3.15: Geometry of rotor contact

As shown in figure 3.15, the absolute coordinate system is  $OXY$ . The displacement of the rotor center  $Or$  in horizontal direction and vertical direction are denoted as  $x$  and  $y$ . The center of the auxiliary bearing  $Os$  is at position  $[xb,yb]$ , which are not equal to zero when the auxiliary bearing is misaligned with absolute coordinate system. The clearance between rotor and auxiliary bearing is  $C_s$ .

The contact force  $N$  between rotor and auxiliary bearing is linear with the non-negative radial penetration  $\delta$  and the contact stiffness  $k_c$ , so contact force is expressed as follows:

$$N = k_c \cdot \delta, \quad (3.34)$$

$$\delta = \sqrt{(x - x_s)^2 + (y - y_s)^2} - C_s. \quad (3.35)$$

If we consider the metallic material's damping property  $d_c$ , which is a constant coefficient of viscous damping, the contact force is described as:

$$N = k_c \cdot \delta + d_c \cdot \dot{\delta}, \quad (3.36)$$

where,  $\dot{\delta}$  is the derivative of the radial penetration  $\delta$  with respect of time. However, this model can not correspond to the real behavior during the impact. A more exact modeling of contact, nonlinear Hertzian contact will be discussed and simulated in the following.

#### Nonlinear Hertzian contact force

In order to get more actual physical contact model, we also studied Hertzian nonlinear contact model. During rotor contacts with auxiliary bearing, the normal contact force between rotor and auxiliary bearing can be written as [15]:

$$N = \kappa \delta^{3/2} + \frac{3}{2} \alpha_d \kappa \delta^{3/2} \dot{\delta}, \quad (3.37)$$

where,  $\delta$  is radial penetration,  $\dot{\delta}$  is the derivative of  $\delta$  with respect of time,  $\kappa$  is the local stiffness parameter,  $\alpha_d$  is the damping parameter. The exponent of  $\delta$  is dependent on the type of the contact. When the two contact is sphere, it can be assumed as  $\frac{3}{2}$  [15]. When contact is between two perfectly flat surfaces, the area of contact zone does not change during the time of contact, so the ideal linear

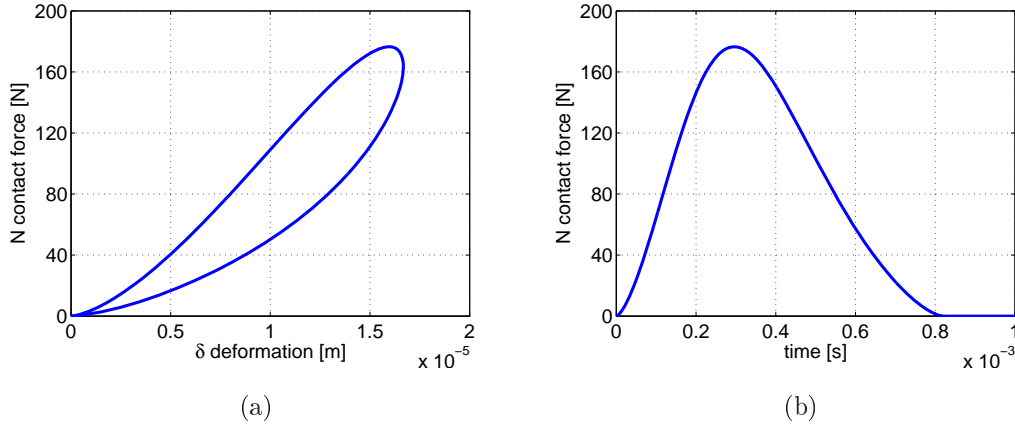


Figure 3.16: Hertzian nonlinear contact force

elastic contact law probably applies. However, in [16] the author did not provide information for cylinders in longitudinal contact and that is the contacting type in which rotor contacts with auxiliary bearing. Therefore, the author assumed that the contact could be two sphere contacts for practical purpose, exponent of  $\delta$  is equal to  $\frac{3}{2}$ . With the result of measured contact force, the detail estimation method of the contact force by using Hertzian nonlinear contact theory is also introduced.

Figure 3.16 shows the simulation results of an example of Hertzian nonlinear contact. Local stiffness parameter  $\kappa$  is about  $2.4 \times 10^9 \text{N/m}^{2/3}$  and damping parameter may be determined for small impact velocities from the linearized relation between coefficient of restitution and impact velocity [15]. Figure 3.16(a) shows the hysteresis relation between normal contact force  $N$  and penetration  $\delta$ . The stiffness varies from  $2.86 \times 10^5 \text{N/m}$  to  $1.16 \times 10^7 \text{N/m}$ . In figure 3.16(b), it can be seen that the nonlinear contact force is continually changing with time, which is different with linear contact.

#### Friction force

When the high speed rotating rotor impacts the auxiliary bearings, the friction force is generated at the physical interface between the two surfaces in contact. As figure 3.15 shows, the direction of the friction force  $f$  is opposite to the relative velocity between rotor and auxiliary bearing.

It is well known that friction in mechanical contacts is influenced by many parameters, including the geometry of the contact surfaces, their properties, the running conditions of the two surfaces, and lubricant condition, etc.. Thus, there are many friction models which have been studied. All of them attempt to capture the essence of the complicated friction phenomena with reasonable complexity representations. In [59], a number of friction models are described. Their advantages and disadvantage are also pointed out.

The Coulomb friction model has often been used because of its simplicity. The Coulomb approximation is an adequate representation of friction for the analysis of many physical systems. It is described by:

$$f = \mu N, \quad (3.38)$$

where,  $\mu$  is the coefficient of friction, which is an empirical property of the contacting materials, and  $N$  is the normal force exerted between the surfaces. In this study, for simplification, the Coulomb friction force between rotor and auxiliary bearing is not coupled with rotor driving frequency  $\Omega$ . The friction coefficient  $\mu$  is a constant in the studied model which does not change with thermal condition, sliding velocity on the two contact surfaces. But, in fact, during the high speed rotating rotor interacting with auxiliary bearings, the friction coefficient  $\mu$  is influenced by these factors considerably.

#### 3.4.3 Other excitations

It is worth mentioning that the other external forces such as gravity and aerodynamic viscous damping forces, transmission of vibration by foundation etc., can be neglected.

## 4 Test Rig and Experimental Investigation

In this chapter, the test rig used in this work is described. The test rig is designed to study the rotordynamics with nonlinear effects such as impact and friction. It can provide experimental verifications of the AMB supported rotor with auxiliary bearing system models which have been introduced in the last chapter. Several important parameters of system are estimated through different methods to analyze experimental results. These parameters will be used in numerical simulation later. In order to explore which factors or parameters are essential to system performance, some modifications and extensions of the hardware and software of the test rig have been conducted. Different experimental investigations have been carried out. Under some specific designed cases, it is found that the AMB-rotor-auxiliary bearing system undergoes complicated motion behaviors. The experiment results will be presented and analyzed.

### 4.1 Description of the build-up test rig

The test rig used in this work is shown in figure 4.1. It has been built and used as a drop down test in [16]. After some modifications and extensions of the hardware and software, the test rig is not only a drop down test rig; it has more facilities to undertake experimental research of AMB-rotor-auxiliary bearing system characteristics. All parts such as the rotor, motor and auxiliary bearings housing and bearings, displacement sensors and pulse sensor are integrated into aluminum housing.

The rotor is approximately 320mm long, the center of gravity point is at about 160mm from left side of rotor, the maximum rotor diameter is 49mm, and it weighs 3.443kg. It is supported in the radial direction by two radial magnetic bearings. A

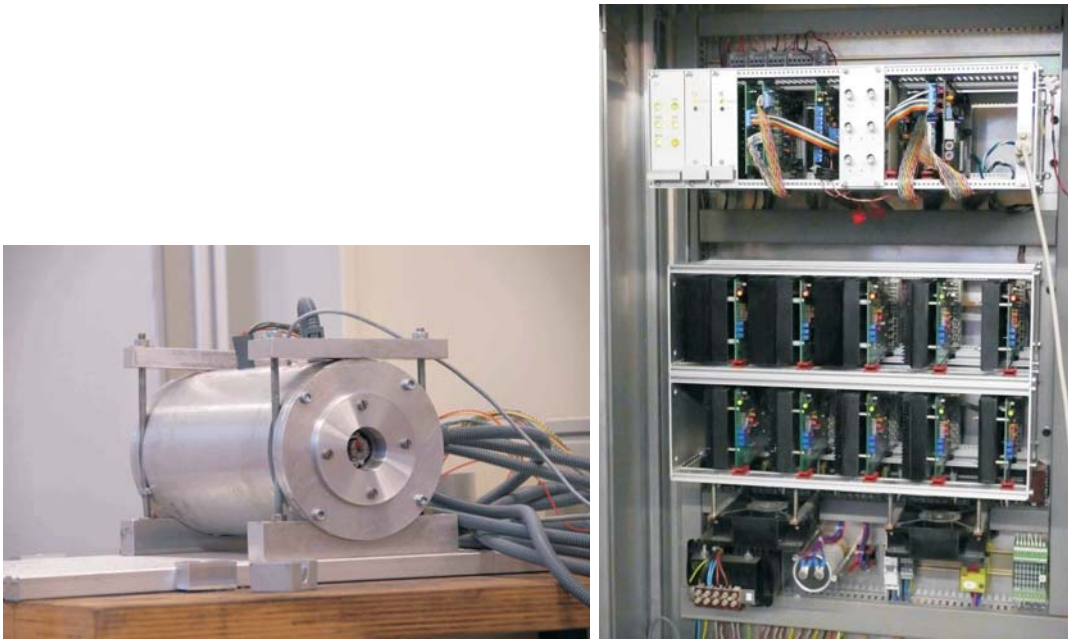


Figure 4.1: The test rig

disc which shrinks fitted onto the rotor is used to implement the axial control with the axial magnetic bearing. Different auxiliary bearing settings provide support in case of power failure or overload. A motor provides the drive power to rotor, the maximal driving frequency reaches 500Hz(30000rpm). By using optical sensor and stripes printed on the rotor, the driving frequency can be obtained. Two pairs of inductive sensors are mounted to the test rig to measure the radial displacements of the rotor, which have to be known for the controlling of AMBs. For a safety precaution, two bronze rings are placed next to the position sensors and act as second retainer bearing. To reduce the wear between the rotor and the bearings, a special case hardening was carried out at the end of the rotor. To ensure a high level of safety, the test rig has a high clearance between the rotor and stator. The air gap between the rotor and the radial active magnetic bearing is 0.75mm and between the rotor and motor it is 0.8mm[16]. The clearance between the rotor and auxiliary bearings is 0.3mm and it can be changed. Figure 4.2 is the cross section of the test rig without auxiliary bearing settings. In order to realize different experimental conditions, three kinds of auxiliary bearing settings have been applied in the test rig.

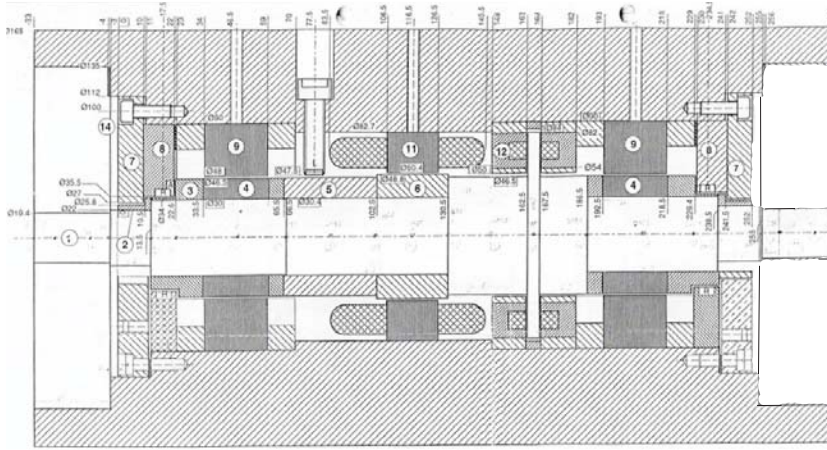


Figure 4.2: The cross section of test rig [47]

In order to explore which factors or parameters are essential to system performance, some modifications and extensions of the hardware and software of the test rig have been conducted. Parameters of the AMB-rotor-auxiliary bearing system, such as the equivalent stiffness and damping provided by active magnetic bearing, contact stiffness and damping provided by auxiliary bearing, supporting stiffness and damping provided by housing or support component components, diving frequency, the excitation forces including unbalance harmonic force and impact force and friction force, the clearance between rotor and auxiliary bearings, are studied and checked in the test rig. In a word, the test rig has more facilities to make experimental investigation.

### 4.1.1 Rotor and active magnetic bearing

As we know, through controlling the active magnetic bearing by different controller algorithms, different support stiffness and damping can be obtained, which is a big advantage comparing with conventional bearing. The equivalent stiffness and damping are a mixture of the magnetic actuator properties and the transfer function presentation of the whole control components of the system. As a result of the analysis, a simple representation of the AMB-rigid rotor is obtained in last chapter. An example of the natural frequency of the AMB-rigid rotor system can be calculated

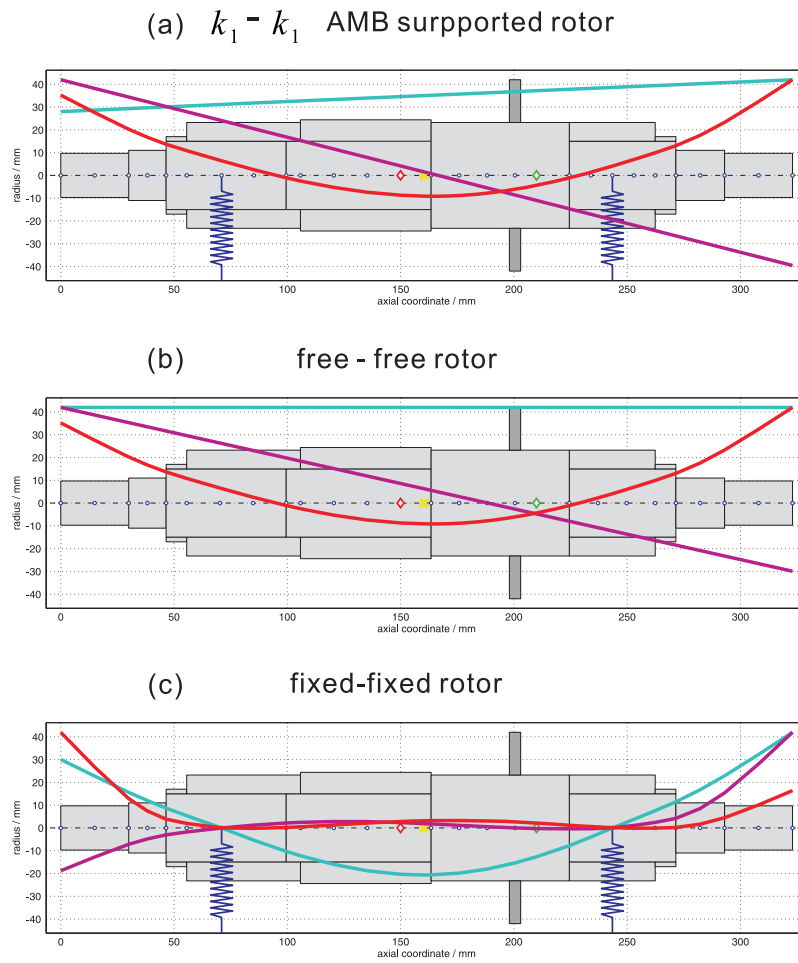


Figure 4.3: The first three mode shapes of AMB supported rotor, free-free rotor and fixed-fixed supported rotor

	mode 1	mode 2	mode 3
$k_1-k_1$ AMB rotor	94 Hz	128 Hz	2973 Hz
free free rotor	0 Hz	0 Hz	2971 Hz
fixed- fixed rotor	2557 Hz	4819 Hz	5763 Hz

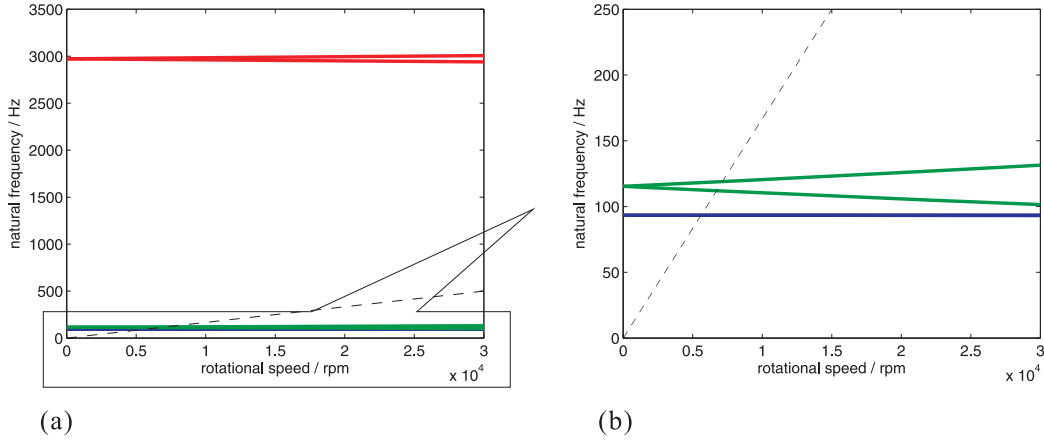


Figure 4.4: The Campbell diagram of the AMB supported experiment rotor

by:

$$w_n = \frac{1}{2\pi} \sqrt{\frac{2k_1}{m}} = 93.6\text{Hz}. \quad (4.1)$$

For more realistic calculations, a finite element model was used to determine the natural frequencies of the system. By using the FE-program package ROTORBUILD, which was developed specially for rotor dynamic problems in Matlab, the finite element model is obtained. The equation of motion of FE model can be expressed as:

$$\mathbf{M}\ddot{q} + (\mathbf{D} + \mathbf{G})\dot{q} + \mathbf{K}q = 0, \quad (4.2)$$

where,  $\mathbf{M}$  is mass matrix.  $\mathbf{D}$  is damping matrix.  $\mathbf{G}$  is skew-symmetric gyroscopic matrix.  $\mathbf{K}$  is stiffness matrix.  $q$  is the rotor displacement.  $\dot{q}$  and  $\ddot{q}$  are respectively the first and second derivative of  $q$  with respect to time.

Figure 4.3 depicts the first three mode shapes of AMB supported rotor, free-free rotor and fixed-fixed supported rotor respectively. As Figure 4.3 shows, the first bending natural frequency for the free-free experiment rotor is approximately 2971 Hz; the rigid cylindrical mode and the rigid conical mode of free-free rotor is 0 Hz. The first bending natural frequency for  $k_1$ - $k_1$  supported rotor is 2973 Hz; but the rigid cylindrical mode of  $k_1$ - $k_1$  supported rotor is 94 Hz, which is in close agreement with the calculated result by using equation 4.1 as above mentioned and the rigid conical mode of  $k_1$ - $k_1$  supported rotor is 128 Hz. The first bending natural frequency for the fixed-fixed rotor is approximately 2557 Hz. The stiffness  $k_1$  provided

by active magnetic bearing connecting the rotor is relatively small, therefore, this stiffness has no significant influence on the rotor behavior. The first three mode shapes of the  $k_1$ - $k_1$  supported rotor are similar with free-free experiment rotor. It is worth mentioning that the mode shapes and corresponding natural frequencies of the different supported rotor are calculated with high precision by FE model and they are depending upon the quality of the modeling. For a more precise determination of the quantities, an experimental analysis for the magnetic bearing supported rotor has been carried out.

Campbell diagrams are very common in the analysis of rotating machines. They show the variation of natural frequencies as a function of rotor driving frequency. Typically, the natural frequencies of the rotor change with driving frequency because of gyroscopic effects and bearing characteristics [40]. Figure 4.4 shows the Campbell diagram of the AMB supported experiment rotor with equivalent stiffness  $k_1$ . With different rotor driving frequency  $\Omega$  from 0 to 30000 rpm, the Campbell diagram shows the evolution of the natural frequencies. This diagram shows the variation of natural frequency with respect to rotor driving frequency may not be readily apparent. Its first two natural frequency curves do not tend to split obviously. In this case, the gyroscopic effect of the AMB supported experiment rotor is not significant on the first two modes, and the influence of gyroscopic effect is neglected.

The maximal driving frequency can reach 500 Hz (30000 rpm). The first bending natural frequency for  $k_1$ - $k_1$  supported rotor is 2973 Hz, only the first two modes frequencies lie in the operation range: a cylindrical and a conical rigid body mode. Additional parts such as disc, laminated rings are shrink fitted onto the rotor. The stress in high-speed rotors including disk depends on rotational speed, size, the shape of the rotor and its material properties. The complete construction of rotor is therefore a result of stress analysis. The maximal driving frequency 500 Hz is well below the limit velocity and allows for a sufficient safety margin. Table 4.1 lists the important parameters of rotor and AMB in the test rig.

The features of experiment rotor satisfied the following requirements:

- High rotor speed: The maximum speed of the rotor is set to be 500Hz (30000 rpm).
- High bending stiffness: The first bending natural frequency lies above its ro-

Table 4.1: The parameters of rotor and AMB in test rig

<b>Rotor</b>	
Mass of the rotor	3.36kg
Length of the rotor	0.323m
center of gravity	160.4mm
Polar moment of inertia of rotor	0.001kgm <sup>2</sup>
Transverse moment of inertia of rotor	0.017kgm <sup>2</sup>
Maximum driving frequency	500Hz
<b>Active magnetic bearing</b>	
Stiffness parameter of coil current	19N/A
Stiffness parameter of displacement	39.7N/mm
Clearance between rotor and active magnetic bearing	0.75mm
Maximum current	5A
Maximum voltage	120V
Number of coil windings	170
Cross section area	225mm <sup>2</sup>
Force angle acting on the rotor	22.5°

tational frequency, i.e. above 500 Hz.

- Low gyroscopic effect: In the operation driving frequency range, the variation of natural frequency with respect to rotor driving frequency can be neglected.

The experiment rotor supported by AMB can be looked as a rigid rotor without gyroscopic effect. The model of the AMB supported rotor can be simplified. The experimental investigations can be concentrated on studies of the essential parameters such as stiffness, damping provided by active magnetic bearing, contact stiffness, damping and the excitation forces, etc..

### 4.1.2 Auxiliary bearing settings

Primarily the task of auxiliary bearings is to avoid contact between the rotor and the magnetic bearing, in case active magnetic bearings have a power failure or the transient overload add on the rotor. They must prevent the destruction of the

system after a possible active magnetic bearing failure, as well as the damage during maintenance. The auxiliary bearings should withstand several failures of the system. Wear on the materials is therefore an important factor in the design. The clearance between the auxiliary bearings and rotor is smaller than that of the magnetic bearing in order to protect it. Typically, fifty percent of the clearance between the magnetic bearing and rotor is used for the auxiliary bearing clearance [18].



Figure 4.5: changeable auxiliary bearing setting

As figure 4.5 shows, single row deep groove ball bearing made by SKF (SKF 6004) is assembled to the test rig as auxiliary bearing. The manufacture gives the bearing information in detail. Some very interesting fundamental work on ball bearings has been carried out by Harris [55]. It is assumed that it is helpful, by damping the impact vibration, to place tolerance ring or o-ring between the outer ring of the bearing and the housing, which helps dissipate the impact energy of the rotor rapidly. After bearing wear has occurred, when it is designed to test different types of auxiliary bearings, they should be easily replaceable. For the design of auxiliary bearing housing, its maintainability, versatility and simplicity are considered. The adjustable ring between bearing or tolerance ring and housing is made of aluminum, which is designed for adjusting the alignment of the auxiliary bearing.

In this experimental investigations, auxiliary bearings made of rigid rings, new ball bearings and worn ball bearings have been tested in different experimental conditions, and most of our analysis on rotor dynamics concentrates on the understanding of their performance. Desired quantities such as low contact friction, high damping, good heat conduction and low wear influence the choice of material for these bearings.

### 4.1.3 Sensors and data acquisition system

#### Displacement sensor

The requirement on displacement sensors for magnetic bearing depends on its application. To measure the radial displacements of the rotor, four inductive sensors are used in the test rig for displacement measurement. The principal requirements are sensitivity, resolution, measuring range, temperature range, frequency range.

#### Pulse sensor

Black and white stripes painted on the rotor are detected by an optical sensor. The output signal of the optical sensor is thus an impulse once per revolution. When the peaks occur in the pulse signal, the white stripes are detected by optical sensor. Figure 4.6 shows the pulse signal over time.

By detecting rise-up edge of the pulse signal, thus knowing the time between two detected peaks, the rotor rotating speed can be calculated. Figure 4.7 shows the rotating speed of rotor varying over time. The initial rotating speed is 50 Hz, 60 Hz, 70 Hz respectively. The rotor was decelerated after it dropped down due to the friction torque caused by auxiliary bearing, and backward whirl of rotor motion did not occur in these cases.

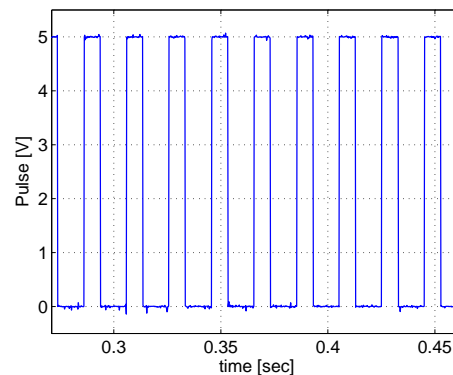


Figure 4.6: The Pulse signal for rotating speed measurement

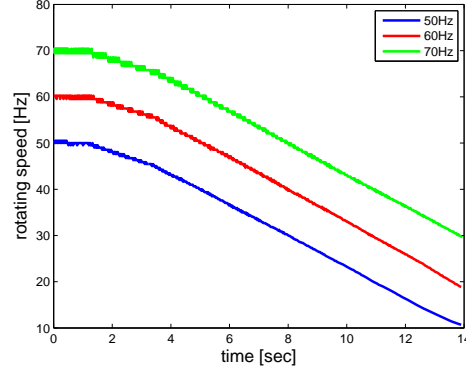


Figure 4.7: The rotating speed decay after rotor drop down

In many applications, the aerodynamic friction torque plays a vital role in the deceleration of the rotor. In [58], the authors have introduced a model to describe the deceleration of the rotor as follows:

$$\Omega = \frac{\Omega_0}{1 + at}, \quad (4.3)$$

where  $\Omega$  is the rotating speed of the rotor at time  $t$ ,  $\Omega_0$  is the initial rotating speed before deceleration of rotor, and  $a$  is the deceleration factor which depends on the load as well as on the geometry of the rotor and can be defined experimentally.

Schmitt trigger is used in pulse signal conditioning circuit for its benefit of pulse width stability. The optical sensor detected pulse signal is stored consecutively in PC.

### Data acquisition

All sensor signals are conditioned then to be connected to the data acquisition boards. For the data acquisition systems, boards AT-MIO-16F-5 and USB-6009 data acquisition (DAQ) modules from National Instruments are used in test rig. The boards are plugged into a computer, and the data are stored in the computer hard disk. One of the boards, USB-6009 has been chosen for the pulse signal acquisition as shown in figure 4.8. It has the following characteristics [49]:

- Small and portable, easier and more cost-effective connectivity



Figure 4.8: Data acquisition device NI USB-6009

- Maximum AI sample rate( Single Channel ) 48 kS/s
- eight analog input channels
- 14-bit input resolution

The software package LabVIEW is a platform and development environment for a visual programming language from National Instruments. It has been used to develop customized data acquisition applications. It includes libraries for performing a number of very useful analysis techniques. And its graphic capabilities are exploited to design virtual instruments. The developed program has been extended to be able to carry out long time measurements.

MATLAB supports NI USB 6009 and many other types of data acquisition hardware from National Instruments when the Data Acquisition Toolbox is available. This support enables hardware to use MATLAB as an environment for data acquisition, data analysis, and application development. As an example of measurement applications, it can apply USB 6009 for measurements on four channels, each with 5 kHz sampling rate (one pulse signal and three signals for the displacement sensor). Another board for five channels with 5 kHz sampling rate. The data are converted into ASCII-Code and stored directly on the hard disc of computer. A subsequent analysis of the data has been carried out with MATLAB software later. Another important Graphical User Interface (GUI) concept, which has been added to this application, is used to organize the measurements, and trigger the data acquisition.

### 4.1.4 Digital control system

A digital controller performs same control task as the continuous controller. The basic difference between these controllers is that the digital system operates on discrete signals (or samples of the sensed signal) rather than on continuous signals [61]. The magnetic bearings and the digital control units have been built by MECOS Traxler AG, Switzerland. The digital controller is based on digital signal processor(DSP) [16].

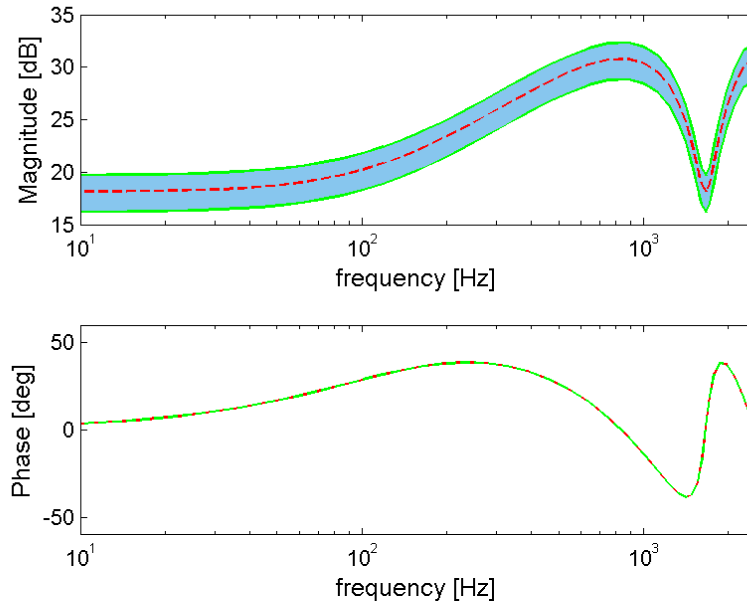


Figure 4.9: The bode diagram of digital controller

The discrete time state space equations of the digital controller can be written as:

$$\begin{aligned} W_{k+1} &= aW_k + bX_k, \\ Y_k &= cW_k + dX_k, \end{aligned} \quad (4.4)$$

where,  $W$  is called the state vector,  $Y$  is called the output vector,  $X$  is called the input (or control) vector. With software package developed by MECOS, the system state space matrix  $a$ ,  $b$ ,  $c$ ,  $d$  of the digital controller can be defined and modified.

Figure 4.9 is the bode diagram of one of the implemented digital controllers in the test rig without integrator. As an example, the magnitude of the controller can be adjudged in the shadow range in figure 4.9 by defining different suitable parameters of the state space digital controllers.

In the test rig controller, an integrator is also necessary to the system in order to drive the steady-state response. The integrator is connected with digital controller in parallel. This discrete-time integration can be written as:

$$Y_k = Y_{k-1} + DI \cdot X_{k-1}, \quad (4.5)$$

where, parameter  $DI$  is set to be 50 as default value in the digital controller.

### 4.2 Identification of important system parameters

Through the introduction and analysis of the model of AMB-rotor system in last chapter, the analytical estimation method for the equivalent stiffness  $k_1$  and damping  $d_1$  parameters of system has been developed. The estimated equivalent stiffness and damping are closely related to the magnetic actuator properties and the whole control components properties of the system. They are theoretically derived based on the equation of motion AMB-rotor system and frequency-dependent transfer function of controller.

The actual stiffness and damping coefficients of AMB-rotor system can be identified by experimental methods as well. There are two methods developed in this work for the important system parameters identification. One is proposed in time domain which is based on the early part of the step response of system. The other is by means of experimental measurement the frequency response function of system in frequency domain.

### 4.2.1 Time domain method

The equation of motion of the rotor has been derived by the well-known equation for mass-spring-damping system:

$$M\ddot{q} + D\dot{q} + Kq = 0, \quad (4.6)$$

where,  $q$  is displacement of rotor including  $x, y$ .

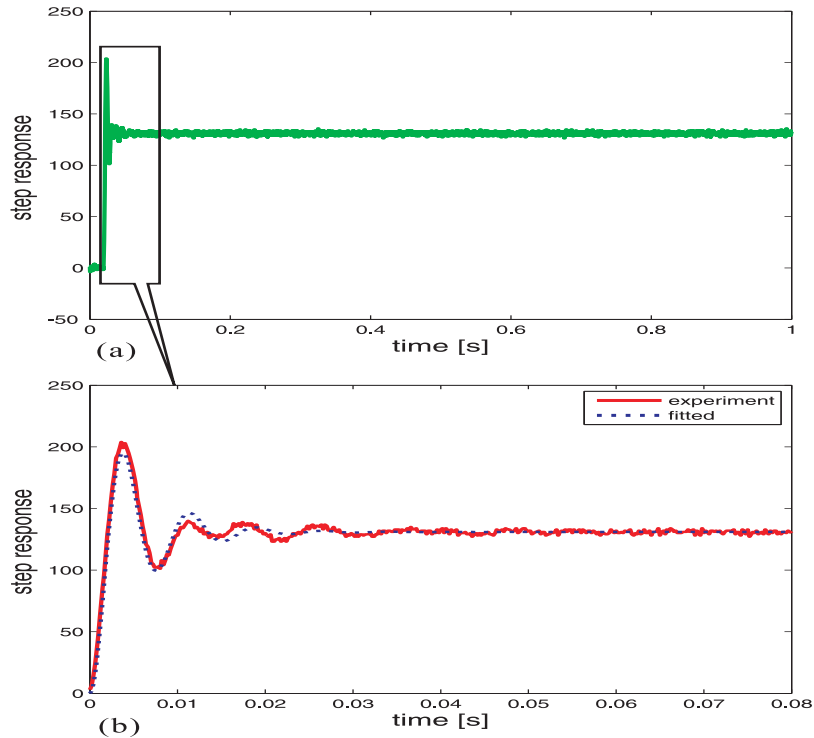


Figure 4.10: step response and fitting

By defining the offset of the controller output, a step magnetic force can be applied on the rotor and then the step response can be analyzed. Figure 4.10 gives an example of step response of rotor. From figure 4.10, it can be seen that it is an under-damped response and the corresponding system is at least a second order system.

For an under-damped second order system, the damping ratio can be calculated from the percent overshoot. This method for determining damping ratio is named

*Logarithmic decrement* [60]. It is through detecting the first two peaks in the response (or the  $n$ th peak) to determine the damping ratio and damped natural frequency, through the steady-state of the step response to find the effective spring stiffness constant, and then to estimate the stiffness and damping parameter of the system.

A novel method of characterizing the time-domain step response of a system by dynamic parameter estimation is presented in this work. The method uses samples of the experimental signal and does not require a priori information about step function amplitude, damping ratio, and natural frequency. Mathematical development of the algorithm is presented and its accuracy is fairly good.

As an example, the fundamental equation describing the response of a second order system to a step function with damping ratio less than 1 is given by:

$$q(t) = A \left[ 1 - \frac{e^{-\zeta w_n t}}{\sqrt{1 - \zeta^2}} \sin(w_d t + \arctan \left( \frac{\sqrt{1 - \zeta^2}}{\zeta} \right)) \right], \quad (4.7)$$

where,  $w_n$  is the natural frequency,  $w_n = \sqrt{\frac{K}{M}}$ .  $\zeta$  is the damping ratio,  $\zeta = \frac{D}{2\sqrt{KM}}$ .  $w_d$  is the damped natural frequency,  $w_d = w_n \sqrt{1 - \zeta^2}$ .  $A$  is step function amplitude.

The step response essentially depends on the damping ratio and natural frequency, whereas the step function amplitude operates only as a scale factor. Equation for the common step response of a system can be expressed as a function of the system parameters  $w_n$ ,  $\zeta$ ,  $A$ , and time  $t$ :

$$q(t) = q(A, w_n, \zeta, t). \quad (4.8)$$

Figure 4.10(a) shows the response of the AMB-rotor system to a step function force is sampled at a selected rate  $T_s = 0.002s$ . For a better estimation, the samples inside the box region are plotted in figure 4.10(b).

The principle of operation of the estimation method is based on the comparison between the real sampled values of the response and the estimation values of the model. Thus the problem consists in determining the system parameters  $w_n$ ,  $\zeta$ ,  $A$  to minimize the error between real sampled values and the estimation values.

The error at time  $t_i$ , is expressed as:

$$e(t_i) = q(t_i) - \hat{q}(t_i) \quad (4.9)$$

where,  $q(t_i)$  and  $\hat{q}(t_i)$  represent the sampled outputs of the model reference and the real response at time  $t_i$  respectively. The summed square of errors is given by:

$$S = \sum_{i=1}^N [e(t_i)]^2 = \sum_{i=1}^N [q(t_i) - \hat{q}(t_i)]^2, \quad (4.10)$$

where,  $N$  is the number of data points included in the fit and  $S$  is the sum of squares error estimate.

The model function has the form, where the adjustable parameters are held. To obtain the estimation of the parameters, fitting methods and algorithms are selected to minimize the summed square of residual  $S$ . These parameter values make the model best fit the data. As figure 4.10 shows, the red dashed line is the fitted curve and the blue solid line is the experiment result. In this case, the algorithm named Nelder-Mead simplex direct search is chosen as algorithms for minimization. The natural frequency  $w_n$  of the AMB-rotor system is about 852.8rad/s (135.7266Hz) and the damping ratio is  $\zeta = 0.22$ .

This novel method for estimating parameters of AMB-rotor system is proposed in time domain based only on the step response. It only needs the desired system model form and initial values of the parameters. For a LTI system the form of the step response is provided by MATLAB, therefore, regardless of whether the system is over-damped, under-damped, or critically damped, the system parameters can be estimated by using this method with relatively high precision.

### 4.2.2 Frequency domain method

The test rig makes the use of the active magnetic bearing as an actuator component as well as of the devices inherent measuring capabilities. The electromagnetic actuator generates extra dynamic forces through the air gap on the rotor as an excitation source. For this reason it is possible to identify the systems properties while the rotor is running at high speed and even during machining operations using non-contact excitation.

The results of the system identification can be used to optimize the controller design, to prevent unintentional vibrations during operating, and to make model-based fault diagnosis [62]. But this is not the focus of this work. In this work the results of the system identification are focused on validating different preconditions for a model based controller design to parameter study the AMB-rotor system because the system dynamics depend on many factors like rotor driving frequency or equivalent stiffness of AMB. The results of the system identification will be applied to the system model for numerical simulations.

In frequency domain, the frequency response is a characteristic of a system that has a measured response resulting from a known applied input. To measure the frequency response of the AMB-rotor system, one must measure the spectra of both the input force to the system and the vibration response, and this is most easily done with a dual-channel FFT analyzer. In the test rig, the defined excitation force applying on the rotor is done by the desired values for the offset of the controller output. A sine sweep is applied to the desired value. In [63], authors reviewed and gave the theoretical background of the swept sine excitation for frequency response measurement. Excitation force can be impulse or periodic chirp etc.. As shown in figure 4.11, the blue solid line demonstrates FRF measurement that can be achieved with sine sweep excitation.

After the FRF measurement and selecting the frequency range of interest, in order to find the natural frequency and damping ratio of the AMB-rotor system, the Grey-box identification process might include the following steps. The first step is to specify the mathematical structure of the model explicitly based the understanding of the physics system, and secondly through a curve fitting to estimate the unknown parameters.

The frequency response function for the whole close loop AMB-rotor system  $G_w(s)$  will represent the relation between the input, defined excitation force  $F_{ex}$ , and output, the displacement  $x$ . It can be written in rational fraction form as following:

$$G_w(s) = \frac{X(s)}{F_{ex}(s)} = \frac{a_0 + a_1s + \dots + a_ms^m}{b_0 + b_1s + \dots + b_ns^n} \quad (4.11)$$

The rational fraction form is merely the ratio of two polynomials, where in general the orders of the numerator and denominator polynomials are independent of

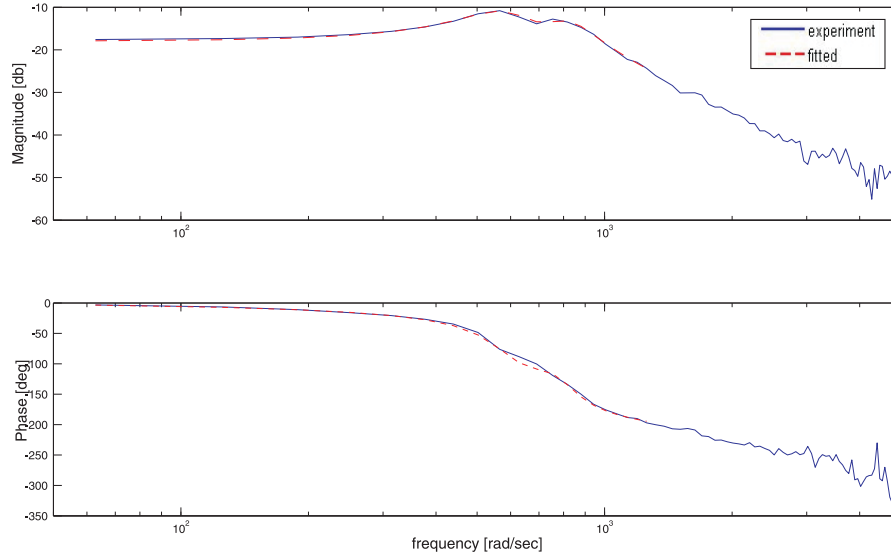


Figure 4.11: frequency response function and fitting

one another. The denominator polynomial is also referred to as the characteristic polynomial of the system.

FRF data are evaluated by the transfer function along the frequency axis. Hence, by curve fitting the analytical form in equation 4.11 to FRF data, finding the coefficients of the numerator and denominator polynomials, and then solving for the roots of both the numerator and characteristic polynomials, the poles and zeros of the transfer function can be determined. From information of poles, the natural frequency and damping ratio can be calculated.

As shown in figure 4.11, there are two peaks which can be observed in the interest frequency range. By counting resonance peaks in the measured FRF, the number of modes can be normally determined. The dashed red line demonstrates reasonably good curve fit with both the magnitude and phase of the measured FRF through a curve fitting algorithm. The first natural frequency  $f_{n1}$  is 94.3130Hz, the second natural frequency  $f_{n2}$  is 129.2121Hz. From the FE analysis of the AMB-rotor in above, the natural frequency corresponding to rigid cylindrical mode of  $k_1$ - $k_1$  supported rotor is 94 Hz, the rigid conical mode is 128 Hz. The measurement results closely coincide with FEM calculated results.

## Stiffness varying

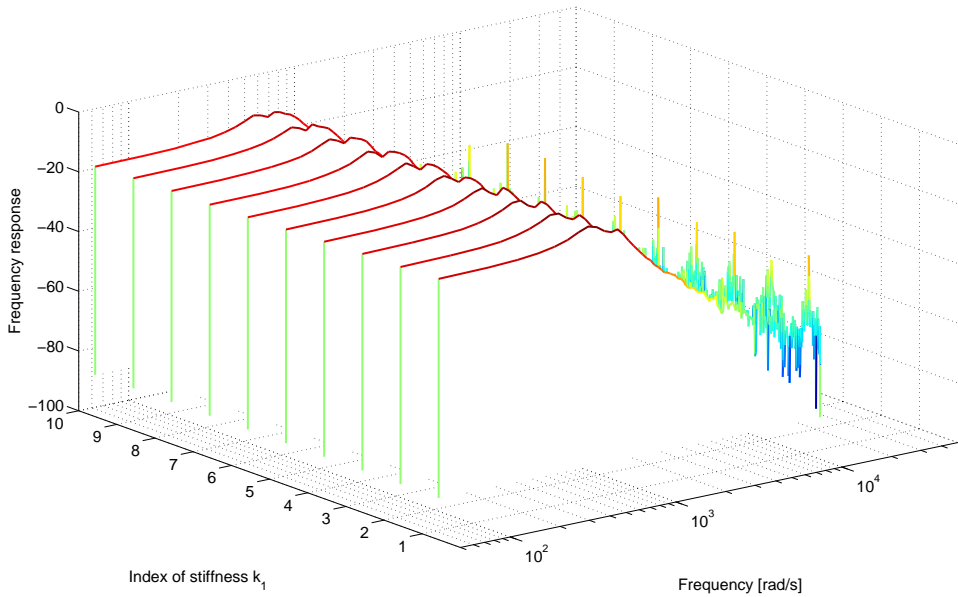


Figure 4.12: The experiment frequency response at different  $k_1$

In order to validate AMB-rotor FE model and check the influence caused by the diverse stiffnesses  $k_1$ , a series of FRF measurements have been carried out. As mentioned above, the magnitude of the controller can be adjudged in the shadow range in figure 4.9 by defining different suitable parameters of the state space digital controllers. As a result, the equivalent stiffness  $k_1$  provided by AMB can be varied in the suitable designed range [ $5 \times 10^5 \text{N/m} - 1 \times 10^6 \text{N/m}$ ]. Figure 4.12 presents the measured frequency response at different  $k_1$ . Figure 4.13 presents the fitted frequency response at different  $k_1$ .

Table 4.2 lists the calculated first two natural frequencies of AMB-rotor FE model and their corresponding equivalent stiffness  $k_1$  and the identification natural frequencies with corresponding AMB controller settings. To present the results of an experimental identification and theoretical calculation with ten different stiffness  $k_1$ , figure 4.14 is plotted. It can be clearly seen that the two kinds of results coincide with each other.

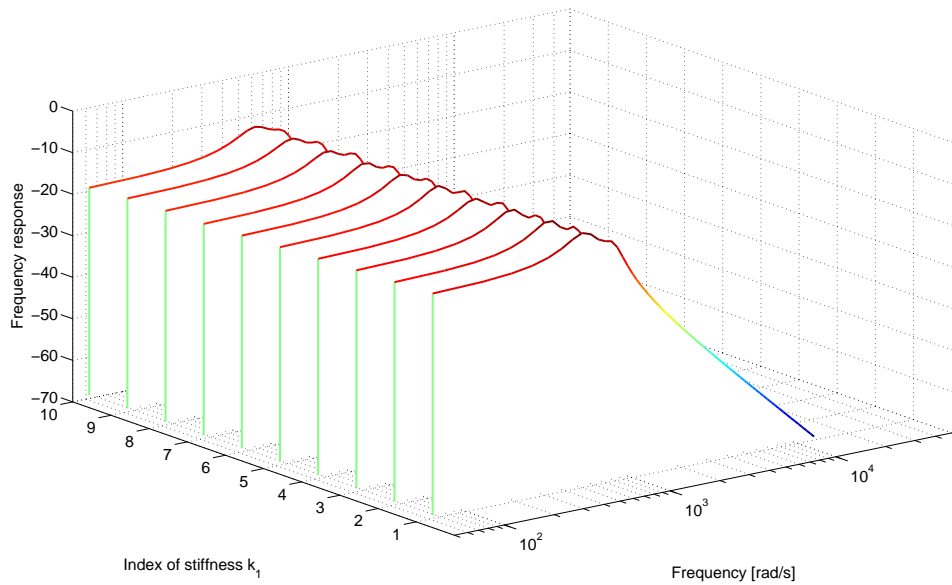


Figure 4.13: The fitted frequency response at different  $k_1$

Table 4.2: Estimated and FEM calculated natural frequencies of the AMB-rotor system

index	stiffness $k_1$ [ $N/m$ ]	$f_{n1}$ [Hz]	$f_{n2}$ [Hz]	$f_{cn1}$ [Hz]	$f_{cn2}$ [Hz]
1	$4.9273 \times 10^5$	84.7	121.7	85	117
2	$5.1845 \times 10^5$	89.3	121.7	87	120
3	$5.4417 \times 10^5$	90.0	124.1	89	123
4	$5.6989 \times 10^5$	92.1	126.6	92	125
5	$5.9561 \times 10^5$	94.3	129.2	94	128
6	$6.2133 \times 10^5$	96.3	133.4	96	131
7	$6.4705 \times 10^5$	98.1	136.1	98	134
8	$6.7277 \times 10^5$	99.1	137.8	99	136
9	$6.9850 \times 10^5$	103.3	143.8	101	139
10	$7.2422 \times 10^5$	104.1	149.5	103	141

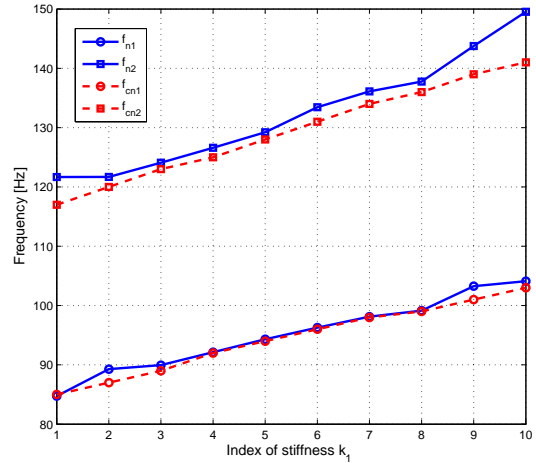


Figure 4.14: Results of identification and calculation at different  $k_1$

### Driving frequency varying

In most situations, the FRF measurements are carried out when rotor is stand still. A series of FRF measurements have been taken with different rotor driving frequencies to study the influence caused by driving frequency to the natural frequencies of AMB-rotor system.

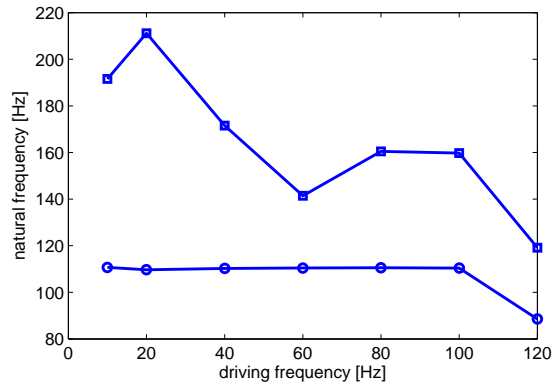


Figure 4.15: Results of identification during rotating

The range of speed reached from 10 to 120Hz. The results from the identification

FRF measurements at different rotor driving frequencies are shown in figure 4.15. The plot shows the first two natural frequencies at each driving frequency. The line with circles are the first natural frequencies and line with squares are the second natural frequencies at different rotor driving frequencies.

From figure 4.15, it can be seen that the first natural frequencies do not show obvious change, which agrees with the theoretical FE calculation results as shown in figure 4.4. But the second natural frequencies show a slight decline versus the driving frequency. It can be because of that, when the FRF measurements is carried out during rotor rotating, the measurements contain excessive noise or distortion, another reason may be that the measurements lack sufficient frequency resolution.

Through experimental measurements and identification in both time domain and frequency domain, the conclusion can be drawn that these two parameter identification methods presented here are sufficiently fast and accurate. The identification results and FE theoretical results are in fairly good agreement with each other, which can reveal that the experimental rotor in this study can be modeled as rigid rotor with two modes, rigid cylindrical mode and rigid conical mode, and without gyroscopic effect.

### 4.3 Experiments and Results Analysis

Generally speaking, the experiments have been carried out in this work can be divided into two types according to different purposes. One is designed to identify the system important parameters for the verification of theoretical calculated results and numerical simulations. The other type experiments are proposed to study parameters or factors of the AMB-rotor system with auxiliary bearings.

All sensor measurement data are stored in PC by data acquisition systems. The sample frequency is 5000 Hz. Succeeding analysis of experimental data can be carried out with MATLAB.

### 4.3.1 Parameter identification experiments

These experiments carried out in this work for important system parameters identification both in time domain and frequency domain. In time domain parameter identification experiments, the displacements, and the output of system are measured by creating step input force on the rotor. The sweep sine method is applied to the frequency response function measurements with different controller algorithm and rotor driving frequency. The both identification results are coincided with the theoretical results. These parameters will be used in numerical simulation later.

### 4.3.2 Parameter study experiments

The emphasis of this type experiments is placed on the influence of various factors or parameters on the rotor dynamic behavior and performance during its interaction with auxiliary bearings. The factors or parameters including the equivalent stiffness and damping provided by active magnetic bearing, contact stiffness and damping provided by interaction, supporting stiffness and damping provided by housing or support component components, driving frequency, unbalance harmonic force, the coefficient of friction, transient overload disturbances and initial conditions have been studied and verified in the test rig.

Some modifications and extensions of the hardware and software of the test rig have been conducted for these kinds of parameter study experiments. Different auxiliary bearing settings, including bronze plain bearing, new or worn ball bearing, with or without tolerance ring and adjustable ring have been designed to study stiffness, damping of bearing and the coefficient of friction. Through setting different controller algorithms of active magnetic bearing, the stiffness and damping of the AMB-rotor system are studied.

Under some specific designed cases, it is found that the AMB-rotor-auxiliary bearing system undergoes complicated motion behavior. The experiment results will be presented and analyzed.

### 4.3.3 Experimental results analysis and rotor motion behaviors

The results of the measurements will be shown together with an analysis. The behavior of the rotor, during interaction with its auxiliary bearings, changes with different types of auxiliary bearing setting and operation conditions.

The dynamic interaction behavior between a rotor and its auxiliary bearings presents different types of motion. These motion types are dependent on various factors or parameters such as the rotor driving frequency, coefficient of friction, stiffness and damping of auxiliary bearing and randomly occurring initial conditions and parameters.

#### Spring motion of rotor and Oscillatory motion of rotor

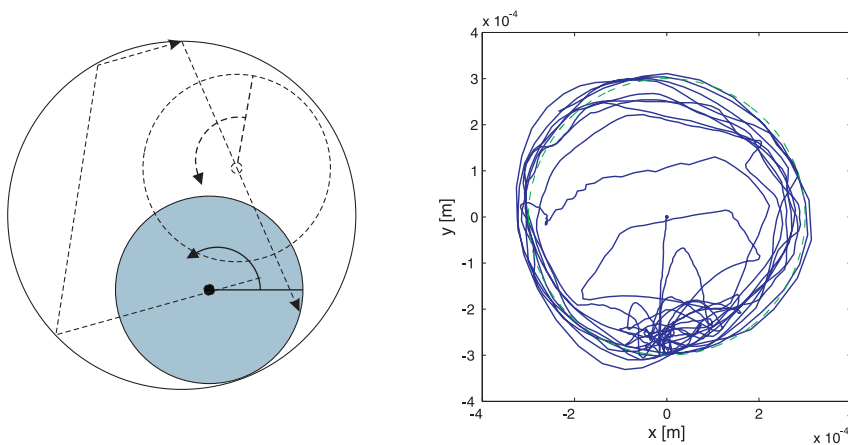


Figure 4.16: Spring motion of rotor

After a desired power failure of a magnetic bearing or transient overload acting on rotor in the test rig, the rotor enters into a transient series of impacts, and then it occasionally springs inside the auxiliary bearings and does not maintain contact with auxiliary bearings continuously. As shown in figure 4.16, this is an example of spring motion of rotor. Usually it is not too dangerous to the integrity of the machine.

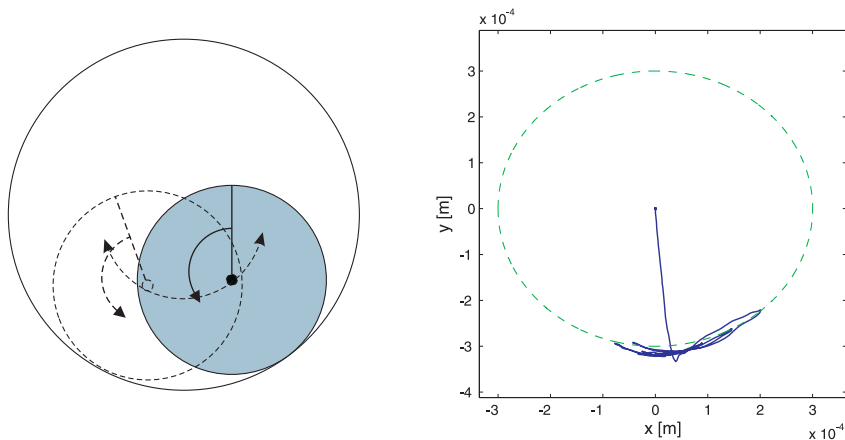


Figure 4.17: Oscillation motion of rotor

When rotor driving frequency is in a relatively low range, one possibility of rotor motions, oscillation motion of rotor, has also been observed in the horizontally assembled test rig. From the orbit diagram of rotor in figure 4.17, it can be clearly seen that the rotor, with 40Hz initial driving frequency, oscillates at the bottom of the auxiliary bearing after touching it.

### Backward whirl motion of rotor

The interaction between rotor and auxiliary bearing causes the motion behavior of rotor to be very complicated. Under some specific designed cases, rotor can enter into the backward whirl after a few transient impacts with auxiliary bearing. The extra load, which is produced by backward whirl and acts on rotor and auxiliary bearing, can destroy the auxiliary bearing very soon. The analyzed experimental data in the example are extracted from steady state backward whirl motion of the rotor.

The following experimental results discussed here have been made with an initial driving frequency of 150Hz. Figure 4.18(a) shows the rotor center orbit. The radius of the rotor orbit is a little larger than the clearance. After a few quick springs inside of the auxiliary bearings, rotor enters to backward whirl and it maintains contact with the auxiliary bearing continuously or almost continuously. Figure 4.18(b) shows the spectra of displacement of rotor in horizontal direction. The spectrum

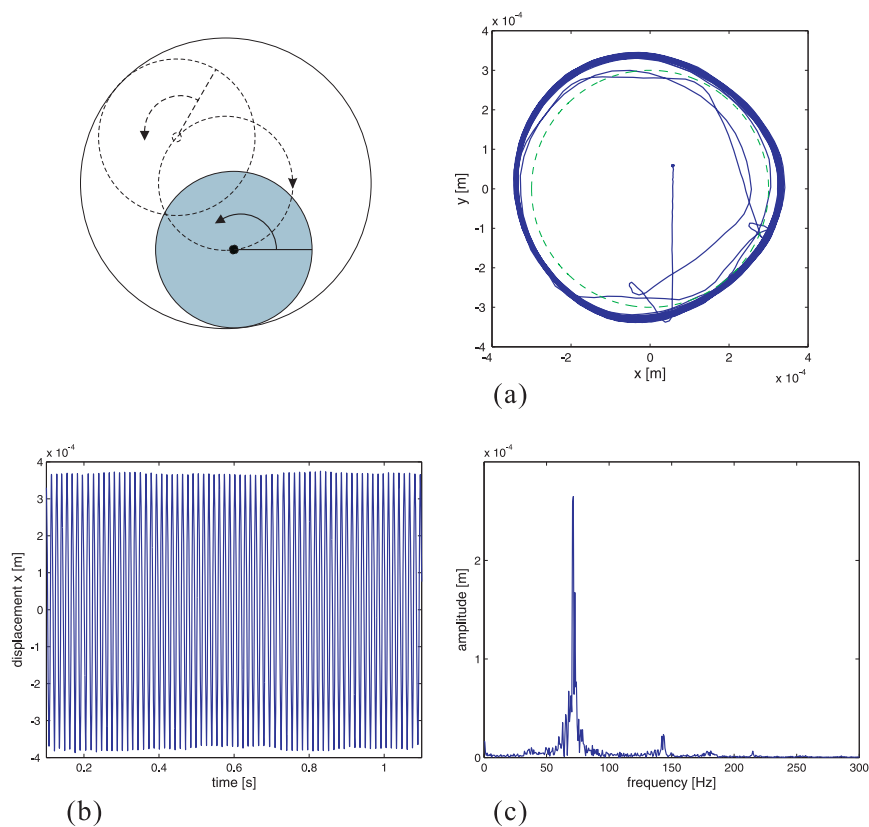


Figure 4.18: Backward whirl motion of rotor ( (a) is rotor orbit diagram, (b) is spectrum diagram of displacement when rotor in steady state backward whirl, (c) time history of the rotor )

indicates that rotor radial vibration with driving frequency  $150Hz$  and  $1/2$  fractional driving frequency round  $75Hz$  are very apparent and the amplitude of radial vibration of rotor at half driving frequency is much larger than the amplitude at driving frequency. From the spectrum, the components of  $3/2$  multiple of driving frequency about  $220Hz$  is small but clear to see. Figure 4.18(c) is a part of the time history of the rotor horizontal vibration.

It is found that in most experiments, when the backward whirl happens, besides the multiple harmonic components such as  $2\times$ ,  $3\times$ , etc. The fractional harmonic components such as  $1/2\times$ ,  $3/2\times$ , etc. can be observed as well. Chaotic vibration motion can be found under some circumstances. In other words, the measurement data show diverse motion behaviors. The possible reasons for this phenomenon are that the initial conditions and the parameters of real test rig could not be given exactly the same and the system is very complication due its nonlinearity [52].

## 5 Numerical Simulation of Interaction between Rotor and Auxiliary Bearing

The interaction between high rotating rotor and auxiliary bearing could cause a very serious instable motion, backwards whirl. It may lead to the destruction of the machine. Therefore, it is important to build a detailed model of the system to study the dynamic behavior of the rotor, explore which factors or parameters are essential to system performance, and then find an appropriate optimized design to prevent it.

In this chapter, the detailed models of the AMBs supported rotor interacting with auxiliary bearing system are introduced, which consider discontinuous stiffness caused by bearing clearance effects, nonlinear Hertzian contact and Coulomb friction forces. The auxiliary bearings can be fixed and compliant mounted in machine housing. The rotor is assumed rigid mass or rigid beam in the operation range. Several groups of differential equations are presented and used for the analysis and numerical simulation in this chapter.

The basic model is the AMBs supported rigid rotor with fixed mounted auxiliary bearing and the linear contact stiffness. The friction force follows Coulomb friction law. There are many studies based on piecewise linear equation of motions with constant coefficients.

The extended models of the system are introduced as well, which include rigid beam rotor interacting with rigid mounting auxiliary bearing model and rigid rotor interacting with flexible mounting auxiliary bearing model. For the nonlinear equations of motion of these models, there is no known method exists to derive general analytic solutions. Hence, numerical simulation is the main tool in the analysis.

Numerical investigations as time history, orbit diagram, Poincaré section diagram are proposed to study the complex dynamic response of the system. The numerical

investigation of the system is implemented in commercial software MATLAB.

### 5.1 Basic model of the system

When the auxiliary bearings are mounted directly on housing, the contact and supporting stiffness are in series, the supporting stiffness is much higher than the contact stiffness, therefore, the supporting stiffness and damping could be ignored. The system model is shown in figure 5.1.

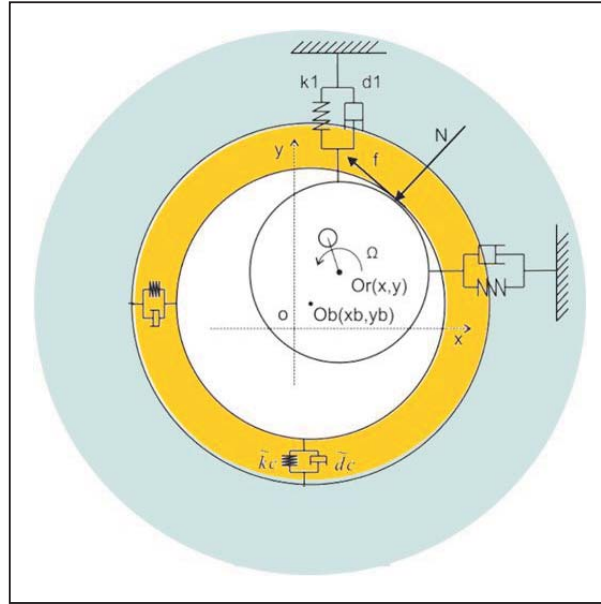


Figure 5.1: Basic model of the interaction between rotor and auxiliary bearing

Rotor is assumed as a rigid mass here. The gyroscopic effect can be neglected. The unbalance force of the rotor provides the harmonic excitation with different driving frequency. AMBs provide electromagnetic force on the rotor, it can be modeled as spring force and damping force, the equivalent stiffness and damping are respectively  $k_1$  and  $d_1$ . They depend on the control parameters, rotor position and coil currents. When rotor interacts with auxiliary bearing, then additional contact force and friction force are generated. The contact force is also modeled as a spring and damping force. Here,  $\tilde{k}c$  and  $\tilde{d}c$  are contact stiffness and damping

respectively. The discontinuous stiffness of the system model is caused by clearance between rotor and auxiliary bearing, linear contact, coulomb friction force, variable rotor driving frequency and fixed mounted auxiliary bearing.

### 5.1.1 The Equations of motion

As shown in Figure 5.2, the absolute coordinate system is  $OXY$ ; the displacement of the rotor center  $Or$  in horizontal direction and vertical direction are denoted as  $x$  and  $y$ ; the center of the auxiliary bearing  $Os$  is at position  $[x_s, y_s]$ , which are not equal to zero when the auxiliary bearing is misaligned with the absolute coordinate system. The clearance between rotor and auxiliary bearing is  $C_s$ .

In this basic model, when rotor contacts with the auxiliary bearing, the contact force  $N$  can be assumed as linear contact force  $N = \tilde{k}_c \delta$ . The friction force  $f$  between two contact surfaces follows the Coulomb law  $f = \mu N$ , where  $\mu$  is the friction coefficient between rotor and auxiliary bearing.

The second order equations of motion for this type of model can be described in two states, one is without interaction (State 1) and the other is with the interaction (State 2).

The Equations of motion of AMBs supported rotor with fixed mounted auxiliary bearing is given in the following [52]:

**State 1:**

$$\begin{aligned} m\ddot{x}(t) + d_1\dot{x}(t) + k_1x(t) &= \Omega^2 me \cos(\Omega t + \theta_0), \\ m\ddot{y}(t) + d_1\dot{y}(t) + k_1y(t) &= \Omega^2 me \sin(\Omega t + \theta_0), \end{aligned} \quad (5.1)$$

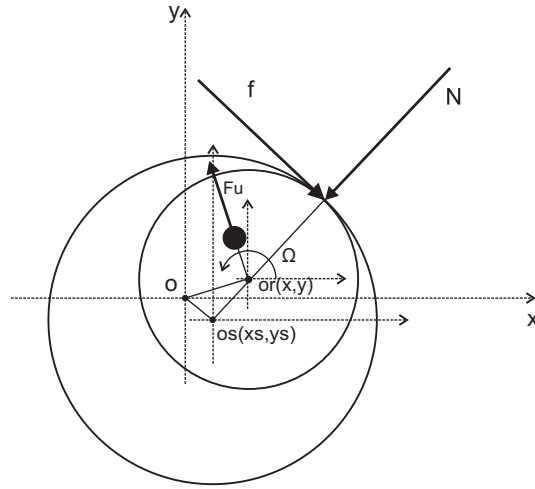


Figure 5.2: Geometrical representation of basic model

State 2:

$$\begin{aligned} m\ddot{x}(t) + d_1\dot{x}(t) + k_1x(t) &= \Omega^2me \cos(\Omega t + \theta_0) + N_x + f_x, \\ m\ddot{y}(t) + d_1\dot{y}(t) + k_1y(t) &= \Omega^2me \sin(\Omega t + \theta_0) + N_y + f_y, \end{aligned} \quad (5.2)$$

where,  $m$  is mass of the rotor.  $\Omega$  is rotor driving frequency.  $\Omega^2me$  is unbalance force.  $N_x$  and  $N_y$  are normal contact force in  $x$  and  $y$  directions respectively.  $f_x$  and  $f_y$  are tangential friction force in  $x$  and  $y$  directions respectively.

### 5.1.2 Nondimensionalised equations

In order to compare and discuss numerical simulation results conveniently, the equations of motion are nondimensionalized. The time  $t$  is nondimensionalized by using natural frequency of the rotor system. The displacements  $x$ ,  $y$  are nondimensionalized by employing the clearance  $C_s$ . On this premise the following dimensionless equations can be defined:

$$\tau = w_n t, \quad \hat{x} = \frac{x}{C_s}, \quad \hat{y} = \frac{y}{C_s}. \quad (5.3)$$

It is assumed that  $\alpha$  is the ratio between linear contact stiffness  $k_c$  and rotor stiffness  $k_1$ ,  $k_c = \alpha k_1$ . The non-negative radial penetration  $\delta = \sqrt{(x - x_s)^2 + (y - y_s)^2} - C_s$  can be written in the following form in terms of the dimensionless quantities,

$$\hat{\delta} = \sqrt{(\hat{x} - \hat{x}_s)^2 + (\hat{y} - \hat{y}_s)^2} - 1. \quad (5.4)$$

Thus, in terms of dimensionless variables, equations 5.1 and 5.2 can be nondimensionalised and written as follows, where, for a freely rotating rotor, the equations of motion are given in this form,

$$\begin{aligned} \ddot{\hat{x}} + \hat{d}_1\dot{\hat{x}} + \hat{x} &= \eta^2\hat{e} \cos(\eta\tau + \theta_0), \\ \ddot{\hat{y}} + \hat{d}_1\dot{\hat{y}} + \hat{y} &= \eta^2\hat{e} \sin(\eta\tau + \theta_0). \end{aligned} \quad (5.5)$$

For a rotor in contact with auxiliary bearing  $\hat{\delta} > 0$  the equations are defined as following:

$$\begin{aligned} \ddot{\hat{x}} + \hat{d}_1\dot{\hat{x}} + \hat{x} &= \eta^2\hat{e} \cos(\eta\tau + \theta_0) + \hat{N}_x + \hat{f}_x, \\ \ddot{\hat{y}} + \hat{d}_1\dot{\hat{y}} + \hat{y} &= \eta^2\hat{e} \sin(\eta\tau + \theta_0) + \hat{N}_y + \hat{f}_y, \end{aligned} \quad (5.6)$$

where,  $\hat{d}_1 = \frac{d_1}{mw_n}$ ,  $\eta = \frac{\Omega}{w_n}$ ,  $\hat{e} = \frac{e}{C_S}$ ,  $\hat{N}_x$ ,  $\hat{N}_y$  are dimensionless normal contact force in  $x$  and  $y$  directions respectively.  $\hat{f}_x$ ,  $\hat{f}_y$  are tangential friction force in  $x$  and  $y$  directions respectively.

### 5.1.3 Steady state harmonic response analysis

From the equations of motion (5.5 and 5.6) for the basic model, the unbalance force of the rotor provides the harmonic excitation with different driving frequency  $\Omega$ . When the rotor does not contact with auxiliary bearings, such rotor system is linear and the steady state response of the system shows purely harmonic rotor synchronous vibrations, which can be solved analytically. Due to the clearance between rotor and auxiliary bearings, when rotor interacts with auxiliary bearing, the system is nonlinear. The solutions of the equations of motion of this basic are dependent on two possible analytical solutions: synchronous vibration, as response to the rotor unbalance force and non-synchronous vibration, which is caused by the contact constraint and friction.

The analytical method will be presented here that has been originally proposed by Black [22], with refinements provided by Zhang in [65] and Jiang in [66]. The extensive studies on analytical determination of the rotor synchronous steady state motions of multi-disk rotors and continuous rotors in retainer bearings were carried out by Wegener, Ehehalt and Markert in [25, 24, 26]. The techniques for analytically calculating the nonlinear steady state behavior are presented. The full annular rubbing interaction between rotor and seal, including synchronous or reverse (backward) precessions, has been experimentally and analytically discussed by Bently and Yu in [6, 7, 64]. The authors demonstrate the synchronous and nonsynchronous motions of the rotor. In [12], the authors discuss the results of different unbalance conditions when the rotor is run up, then down through the speed range. Specifically, synchronous components are extracted from a measurement signal over the  $k$ th period according to where the phase is referred to a fixed point on the shaft.

The steady state synchronous ( $1\times$ ) response of the rotor to the unbalance force represents the forced solution of equations 5.5 as follows:

$$q = Ae^{j(\Omega t + \beta)}, \quad (5.7)$$

where  $A$ ,  $\beta$  are measurable amplitude and phase of the rotor synchronous response, often called a fundamental response of the rotor. Note that the adjective synchronous related to the frequency of excitation equal to rotor rotation.

For the case when the rotor does not contact the auxiliary bearing (equations 5.5), the response amplitude  $A$  and phase  $\beta$  are:

$$A = \frac{me\Omega^2}{\sqrt{k_1 - m\Omega^2 + (d_1\Omega)^2}}, \quad (5.8)$$

$$\beta = \theta_0 - \arctan\left(\frac{d_1\Omega}{k_1 - m\Omega^2}\right). \quad (5.9)$$

For the rotor continuously contact (with sliding) the auxiliary bearing (equations 5.6), the response amplitude  $A$  and phase  $\beta$  can be calculated from a nonlinear complex number relationship algebraic equation [64]. However, though observing the experimental and numerical simulation results of AMB-rotor with interaction with auxiliary bearings system, it can be found that the rotor motion behavior is very complex, besides continuous contacting with auxiliary bearing, it may discontinuously interacts with auxiliary bearing, loose contact. Moreover, the pure analytical steady state solution analysis can not be applied to the experimental measurement results analysis. Therefore, a method is introduced in this work based on Fourier analysis experimental and numerical simulation results.

Assuming that displacement signal  $q(t)$ , which includes  $x(t)$  and  $y(t)$  of the nonlinear system, is periodic with frequency  $\Omega$ , there will be a Fourier series representation:

$$q(t) = \frac{U_0}{2} + \sum_{k=1}^{\infty} (U_k \cos(k\Omega t) + V_k \sin(k\Omega t)), \quad (5.10)$$

where  $k$  represents the rank of the harmonics ( $k = 1$  corresponds to the fundamental component).  $U_k$  and  $V_k$  are defined by:

$$U_k = \frac{2}{T} + \int_{t-T}^t u(t) \cos(k\Omega t) dt, \quad (5.11)$$

$$V_k = \frac{2}{T} + \int_{t-T}^t u(t) \sin(k\Omega t) dt. \quad (5.12)$$

The magnitude and phase of the selected harmonic component are calculated by:

$$A_k = \sqrt{U_k^2 + V_k^2}, \quad (5.13)$$

$$\beta_k = \arctan 2 \left( \frac{U_k}{V_k} \right). \quad (5.14)$$

The Fourier coefficients corresponding to the fundamental harmonic are given by:

$$U_1 = \frac{2}{T} + \int_{t-T}^t u(t) \cos(\Omega t) dt, \quad (5.15)$$

$$V_1 = \frac{2}{T} + \int_{t-T}^t u(t) \sin(\Omega t) dt. \quad (5.16)$$

We now consider the approximation:

$$q(t) \approx U_1 \cos(kwt) + V_1 \sin(kwt). \quad (5.17)$$

The magnitude and phase of the synchronous harmonic component are calculated by:

$$A = \sqrt{U_1^2 + V_1^2}, \quad (5.18)$$

$$\beta = \arctan 2 \left( \frac{U_1}{V_1} \right). \quad (5.19)$$

The synchronous harmonic response are extracted from steady state measurement or simulation displacement signal over a running window of one or several cycle of the unbalance harmonic excitation. It can also be programmed to calculate the magnitude and phase of any harmonic component of the signal.

Figure 5.3 shows the steady state synchronous harmonic response. It is an example of steady state synchronous harmonic response of rotor in  $x$  direction without contact with auxiliary bearing during the driving frequency starting  $\Omega$  from 75Hz to 200Hz. Several cycles steady state simulation displacement signal is extracted to be calculated. In this figure, the driving frequency  $\Omega$  is nondimensionalized by using natural frequency of the rotor system, the displacements  $x$  are nondimensionalized by employing the clearance  $C_s$ . The amplitude of the rotor increases during the rotor run-up. When rotor driving frequency enters the range of the original natural

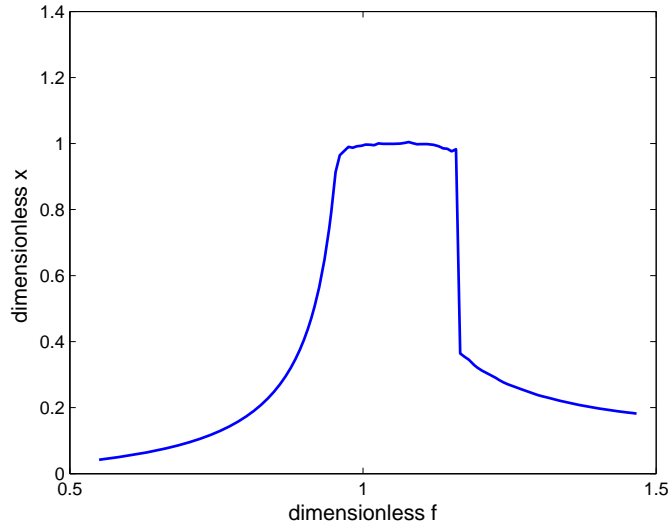


Figure 5.3: Steady state synchronous harmonic response

frequency, the clearance is exceeded, and then the rotor interacts with the auxiliary bearing. Due to the additional contact stiffness providing by auxiliary bearing, the response amplitudes is reduced by an amount depending on the clearance. The response changes when the interaction between rotor and auxiliary bearing is involved. At high driving frequency the rotor runs in the overcritical state, the conditions change from intermittent or continuous contact to non-contact, the amplitude jumps (discontinuities) occur. But the jump of amplitude takes place at a different rotor speed. Compared with the steady state synchronous harmonic response without contacting with the auxiliary bearing, the steady state harmonic response amplitude jumps occur, which is discontinuous as shown in figure 5.3. With the rotor driving frequency increasing or decreasing, the rotor conditions change from no-contact to intermittent contact, then to no-contact again.

### 5.1.4 Stability discussion

The basic model is the simplest case, without nonlinear contact stiffness and damping. When the unbalance force is ignored in equation 5.6, the analytical solution of this ordinary differential equations(ODE) for the basic model has been found. It is

important to investigate the stability of these solutions. By applying Routh-Hurwitz Stability Criterion, the stability criterion for this basic model has been obtained by authors in [64]:

$$\mu < \frac{2\zeta}{\alpha\sqrt{1+\alpha}}, \quad (5.20)$$

where rotor damping factor  $\zeta = \frac{d_1}{2\sqrt{mk_1}}$ ,  $\mu$  is friction coefficient and  $\alpha$  is the ratio between linear contact stiffness  $k_c$  and rotor stiffness  $k_1$ .

The inequality 5.20 clearly shows which parameters are mainly responsible for the rotor instability. They are the friction coefficient and the stiffness ratio. The stabilizing factors are the rotor modal damping and the high rotor-to-stationary part stiffness ratio. For the stability of the rotor synchronous response, the friction to damping ratio has to be smaller than the value depending on a function of the stiffness ratio. This function is a decreasing function of the stiffness ratio. On the contrary case,  $\mu > \frac{2\zeta}{\alpha\sqrt{1+\alpha}}$  indicates rotor may interact with auxiliary bearing, the synchronous response can become unstable and then lead to backward whirl for above certain amount of mass unbalance.

### 5.2 Extended models of the system

In last section, the basic model of the AMBs supported rotor interacting with auxiliary bearing system is introduced in detail, which considers discontinuous stiffness caused by bearing clearance effects, linear contact and Coulomb friction forces. The auxiliary bearings are mounted in machine housing rigidly. The rotor is assumed rigid mass in the operation range. Several groups of differential equations are presented and used for the analysis.

The extended models of the system are introduced as well, which include rigid beam rotor interacting with rigid mounting auxiliary bearing model and rigid rotor interacting with flexible mounting auxiliary bearing model. In order to get more actual physical contact model, Hertzian nonlinear contact model is used as well. That means during the rotor contacting the auxiliary bearing, the contact force

is continually changing with time and it varies at different penetration, which is different with linear contact.

For the nonlinear equations of motion of these models, there is no known method exists to derive general analytic solutions. Hence, numerical simulation is the main tool in the analysis. State space representation of the second order ordinary differential equations are introduced for the numerical simulation. the parameters of the rotor models are assumed as constant values. But in actual condition, it can not be simplified as constant. It is a variable depending on many factors. Therefore, The simulation method is developed for both second-order time-invariant parameter ODEs of the system and time-varying parameter ODEs.

### 5.2.1 Rigid beam rotor with rigid mounting auxiliary bearing model

Since the maximal driving frequency of the test rig is up to 500 Hz (30000 rpm), the first two natural frequencies, which are the rigid cylindrical and conical mode frequency, about 94 Hz, and 128 Hz respectively, are in the operation range. As a consequence, it is interesting to study the rigid beam rotor interacting with rigid mounting auxiliary bearing model.

From the discussion of the test rig used in this work in chapter 3, it is known that the gyroscopic effect is neglected. It is assumed that the coupling of axial and radial dynamics motion and the coupling of two radial perpendicular planes dynamics motion are negligible. As a result, it is sufficient to analyze the motion in one plane. As an example, figure 5.4 shows the rigid beam rotor in one plane  $YOZ$ .

The radial rotor motion in plane  $YOZ$  can be completely described by rigid beam model.  $y$  is the radial displacement of the rotor's center of gravity  $S$  and  $\varphi$  is the rotation of the rotor about an axis through  $S$ .

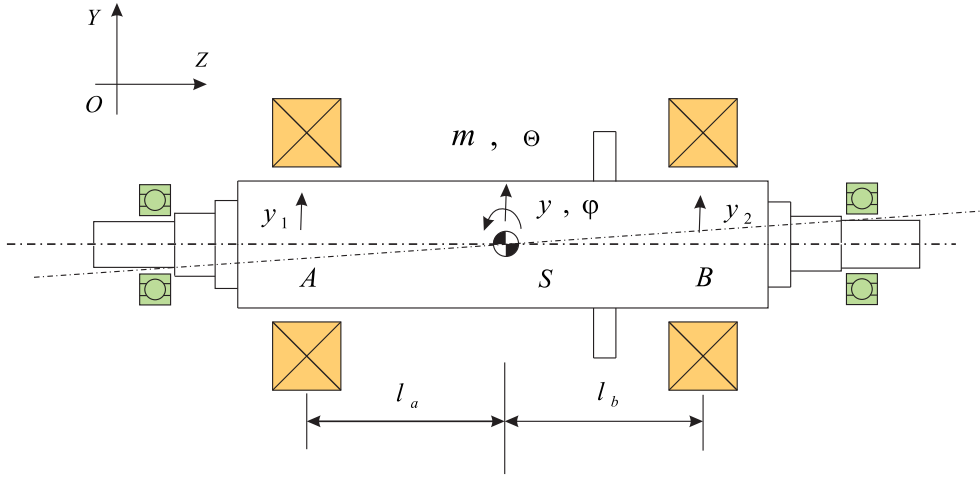


Figure 5.4: The rigid beam rotor with rigid mounting auxiliary bearing model

### Equations of motion

In general, the dynamics of the rigid beam rotor supported by AMBs can be described in one plane by:

$$\begin{bmatrix} m & 0 \\ 0 & \Theta \end{bmatrix} \begin{bmatrix} \ddot{y} \\ \ddot{\varphi} \end{bmatrix} = \begin{bmatrix} F_s \\ M_s \end{bmatrix}, \quad (5.21)$$

where,  $m$  is the rotor total mass.  $\Theta$  is its transverse moment of inertia.  $\ddot{y}$  is the second derivative of radial displacement  $y$  respect to time.  $\ddot{\varphi}$  is the second derivative of rotation displacement  $\varphi$  with respect to time.  $F_s$  is the the net force acting upon rotor and  $M_s$  is the moment with respect to the axis that goes through the point  $S$ . They consist of magnetic force provided by AMB, gravity force and radial unbalance force (assumed that there in no couple unbalance). Moreover, when the rotor interacts with auxiliary bearing, contact force is generated. Therefore, the equation of motion for this type rotor model can also be described in two states due to clearance between rotor and auxiliary bearing. The  $F_s$  and  $M_s$  are different in the two states.

By introducing the transformation matrix  $T_1$ , the forces generated by the AMB bearings  $F_{amb}$  and auxiliary bearings  $F_b$  are transfered to gravity point  $S$ , given by following:

$$T_1 = \begin{bmatrix} 1 & 1 \\ -l_a & l_b \end{bmatrix}, \quad (5.22)$$

$$\begin{bmatrix} F_s \\ M_s \end{bmatrix}_{amb} = T_1 \begin{bmatrix} k_1 & 0 \\ 0 & k_1 \end{bmatrix} \begin{bmatrix} y_1 \\ y_2 \end{bmatrix} + T_1 \begin{bmatrix} d_1 & 0 \\ 0 & d_1 \end{bmatrix} \begin{bmatrix} \dot{y}_1 \\ \dot{y}_2 \end{bmatrix}, \quad (5.23)$$

$$\begin{bmatrix} F_s \\ M_s \end{bmatrix}_b = T_1 \begin{bmatrix} F_b^{y_1} \\ F_b^{y_2} \end{bmatrix}, \quad (5.24)$$

where,  $F_b^{y_1}$  and  $F_b^{y_2}$  is the vertical component of the interaction force during contact in  $A$  and  $B$  side respectively.

When rotor works normally and does not contact with auxiliary bearing, and the gravity of rotor is neglected, the equation of motion for the rigid beam rotor model is given by:

$$\begin{bmatrix} m & 0 \\ 0 & \Theta \end{bmatrix} \begin{bmatrix} \ddot{y} \\ \ddot{\varphi} \end{bmatrix} = \begin{bmatrix} F_s \\ M_s \end{bmatrix}_{amb} + \begin{bmatrix} F_u^y \\ 0 \end{bmatrix} \quad (5.25)$$

When rotor contacts with auxiliary bearing in case of overload, and the gravity of rotor is neglected:

$$\begin{bmatrix} m & 0 \\ 0 & \Theta \end{bmatrix} \begin{bmatrix} \ddot{y} \\ \ddot{\varphi} \end{bmatrix} = \begin{bmatrix} F_s \\ M_s \end{bmatrix}_{amb} + \begin{bmatrix} F_u^y \\ 0 \end{bmatrix} + \begin{bmatrix} F_s \\ M_s \end{bmatrix}_b \quad (5.26)$$

where,  $F_u^y$  is the unbalance force in vertical direction. By defining transformation matrix  $T_2$ , the displacement vector  $\begin{bmatrix} y & \varphi \end{bmatrix}^T$  at gravity point  $S$  can be transformed to  $A$  and  $B$  section as shown in figure 5.4. It is given by,

$$T_2 = \frac{1}{l_a + l_b} \begin{bmatrix} l_b & l_a \\ -1 & 1 \end{bmatrix}. \quad (5.27)$$

Then, the equations of motion (eqations 5.25 and 5.26) for the rigid beam rotor model can be transformed as following:

$$\begin{bmatrix} ml_b & ml_a \\ -\Theta & \Theta \end{bmatrix} \begin{bmatrix} \ddot{y}_1 \\ \ddot{y}_2 \end{bmatrix} = \begin{bmatrix} F_s \\ M_s \end{bmatrix}_{amb} + \begin{bmatrix} F_u^y \\ 0 \end{bmatrix}, \quad (5.28)$$

$$\begin{bmatrix} ml_b & ml_a \\ -\Theta & \Theta \end{bmatrix} \begin{bmatrix} \ddot{y}_1 \\ \ddot{y}_2 \end{bmatrix} = \begin{bmatrix} F_s \\ M_s \end{bmatrix}_{amb} + \begin{bmatrix} F_u^y \\ 0 \end{bmatrix} + \begin{bmatrix} F_s \\ M_s \end{bmatrix}_b. \quad (5.29)$$

### 5.2.2 Rigid rotor with flexible mounting auxiliary bearing model

When the auxiliary bearings are mounted directly with the machine housing, it could be assumed as fixed mounted auxiliary bearings. Since the supporting stiffness is much higher than the contact stiffness, the supporting stiffness and damping could be ignored. Otherwise, when the auxiliary bearings are compliantly mounted on the machine housing, the supporting stiffness and damping must be taken into account in the mathematical model of system.

In this work, the model of rigid mass rotor interaction with flexible mounting auxiliary bearing as one of the extended models is also introduced. Rotor can be considered as a rigid rotor and the gyroscopic effect is neglected. The equivalent stiffness of active magnetic bearing is dependent on controller parameters, rotor position and coil currents. Under some special conditions such as active magnetic bearing failures or high transient overloads etc., rotor interacts with auxiliary bearing, and then additional contact force and friction force are generated between rotor and auxiliary bearing. The unbalance of the rotor provides the harmonic excitation with varying driving frequencies.

A model of rigid rotor interaction with flexible mounting auxiliary bearing is shown in figure 5.5. The absolute coordinate system is  $OXY$ ; the displacements of the center rotor  $O_r$  in horizontal direction and vertical direction are denoted as  $x$  and  $y$ . The center of the auxiliary bearing  $O_b$  is at position  $[x_b, y_b]$ , which are not equal to zero when the auxiliary bearing is misaligned with absolute coordinate system. The clearance between rotor and auxiliary bearing is  $C_s$ . AMBs provide spring force and damping force, whose stiffness and damping are respectively  $k_1$  and  $d_1$ .  $k_2$  and  $d_2$  are supporting stiffness and damping of the auxiliary bearing respectively, which are provide by machine housing or support component.  $\tilde{k}_c$  and  $\tilde{d}_c$  are respectively contact stiffness and damping which could be linear contact stiffness or nonlinear Hertzian contact stiffness.

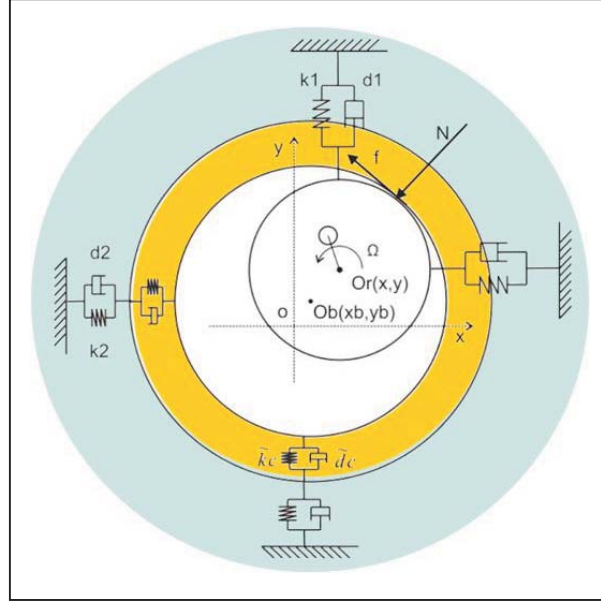


Figure 5.5: The model of rigid mass rotor interaction with flexible mounting auxiliary bearing

### Equations of motion

The second order equations of motion for this type rotor model can be described in two states due to clearance between rotor and auxiliary bearing, one is without interaction (State 1) between rotor and auxiliary bearings, and the other is with the interaction between rotor and auxiliary bearings (State 2).

#### State 1:

$$m\ddot{x}(t) + d_1\dot{x}(t) + k_1x(t) = \Omega^2 me \cos(\Omega t + \theta_0), \quad (5.30)$$

$$m\ddot{y}(t) + d_1\dot{y}(t) + k_1y(t) = \Omega^2 me \sin(\Omega t + \theta_0), \quad (5.31)$$

$$m_b\ddot{x}_b(t) + d_1\dot{x}_b(t) + k_1x_b(t) = 0, \quad (5.32)$$

$$m_b\ddot{y}_b(t) + d_1\dot{y}_b(t) + k_1y_b(t) = 0, \quad (5.33)$$

#### State 2:

$$m\ddot{x}(t) + d_1\dot{x}(t) + k_1x(t) = \Omega^2 me \cos(\Omega t + \theta_0) + N_x + f_x, \quad (5.34)$$

$$m\ddot{y}(t) + d_1\dot{y}(t) + k_1y(t) = \Omega^2 me \sin(\Omega t + \theta_0) + N_y + f_y, \quad (5.35)$$

$$m_b\ddot{x}_b(t) + d_1\dot{x}_b(t) + k_1x_b(t) = -N_x - f_x, \quad (5.36)$$

$$m_b \ddot{y}_b(t) + d_1 \dot{y}_b(t) + k_1 y_b(t) = -N_y - f_y, \quad (5.37)$$

where,  $m$  is mass of the rotor.  $m_b$  is mass of the auxiliary bearing.  $\Omega$  is rotor driving frequency. In many studies, the rotor driving frequency  $\Omega$  is assumed as a constant value. But in actual condition, it can not be simplified as a constant, it is a variable which depends on many factors. In [58], authors introduced experimental formulas for the deceleration of the driving speed due to the aerodynamic torque in the case of power failure. In this work, the rotor driving frequency could be modeled as a time variable parameter.  $me$  is unbalance of the rotor. Unbalance force can be modeled as  $F = \Omega^2 me$ .  $N_x$  and  $N_y$  are normal contact force components in horizontal and vertical directions respectively.  $f_x$  and  $f_y$  are tangential friction force components in horizontal and vertical directions respectively. The contact force between rotor and auxiliary bearing can be calculated by ideal linear contact force model or nonlinear Hertzian contact model. The penetration of rotor can be obtained by calculating the displacement between the center of rotor  $[x, y]$  and auxiliary bearing  $[x_b, y_b]$ . The friction force between two contact surfaces follows Coulomb law.

### 5.3 Numerical computing method

In last section, according to different situations and study purposes, several kinds of model of AMB-rotor system with interaction auxiliary bearing have been presented, and the corresponding equations of motion have been derived as well, which are a series of ordinary differential equations (ODEs). Due to the basic physical properties of mechanical systems, these equations are second order ODEs. In order to properly represent the systems behavior, these differential equations could be linear or nonlinear, time-invariant or time-variant.

As we know, many differential equations cannot be solved analytically, in which case we have to satisfy ourselves with an approximation to the solution. There are a wide variety of numerical solvers (algorithms) for computing the numerical solutions of ODEs [68]. These solvers can be classified according to the number of already calculated points of the solution they use to calculate the next solution step, i.e. single step algorithms, multi step algorithms. According to whether the value to be calculated appears in the calculation algorithm itself or not, i.e. implicit algorithms,

explicit algorithms.

The simplest numerical method for the solution of initial value problems is Euler's method. It uses a fixed step size  $h$  and generates the approximate solution. Tiny steps are needed to get even a few digits of accuracy. But the biggest defect of Euler's method is that it does not provide an error estimate. There is no automatic way to determine what step size is needed to achieve a specified accuracy. The classical Runge Kutta method (also named as Fourth-order Runge-Kutta method) was widely used for hand computation before the invention of digital computers and is still popular today. It uses four function evaluations per step. It does not provide an error estimate either [67]. But we now know that there exist more efficient methods for numerical integration with development of computers. Since the commercial software MATLAB has several different functions for the numerical solution of ordinary differential equations and the results can be displayed graphically, the numerical computing is carried out in MATLAB computing environment in this work.

### 5.3.1 State space representation

In Matlab, all solvers solve systems of equations in the form  $y' = \mathbb{F}(t, y)$  or problems that involve a mass matrix  $\mathbb{M}(t, y)y' = \mathbb{F}(t, y)$  [69].

According to the equations of motion of different kinds models of a rotor-AMB with auxiliary bearings, the most common second order ordinary differential equation is given:

$$\mathbf{M}\ddot{q}(t) + \mathbf{D}\dot{q}(t) + \mathbf{K}q(t) = \mathbf{F}(t, q), \quad (5.38)$$

where  $q(t)$  is a vector of displacement coordinates which can include all the displacement vectors  $x, y, x_b, y_b$ .  $\dot{q}(t)$  is a vector of velocities,  $\ddot{q}(t)$  is a vector of accelerations.  $\mathbf{M}$ ,  $\mathbf{D}$  and  $\mathbf{K}$  are matrices of mass, damping, stiffness respectively.  $\mathbf{F}(t, q)$  is an applied force.

Defining state vector is  $\mathbf{x}(t) = \begin{bmatrix} q \\ \dot{q} \end{bmatrix}$ , output vector is  $\mathbf{y}(t) = \begin{bmatrix} q \\ \dot{q} \\ \ddot{q} \end{bmatrix}$

A state space representation is a mathematical model of a physical system as a set of

input, output and state variables related by first order differential equations. If the inverse of the mass matrix exists, the second order differential equation of the AMB-rotor with auxiliary bearing model can be transformed into first order differential equation by some simple matrix manipulations with reference to the state space representation [34].

The state space representation of the AMB-rotor with auxiliary bearings system could be expressed as following:

$$\dot{\mathbf{x}}(t) = A\mathbf{x}(t) + B\mathbf{F}, \quad (5.39)$$

$$\mathbf{y}(t) = C\mathbf{x}(t) + D\mathbf{F}, \quad (5.40)$$

where matrix  $A$  is the state matrix,  $B$  is the input matrix,  $C$  is the output matrix, and  $D$  is the feedthrough (or feedforward) matrix. Notice that in this general formulation all matrices are supposed to be time-variant, i.e. some or all their elements can depend on time. They are defined in the following forms:

$$A = \begin{bmatrix} 0 & I \\ -M^{-1}K & -M^{-1}D \end{bmatrix}, \quad B = \begin{bmatrix} 0 \\ M^{-1} \end{bmatrix},$$

$$C = \begin{bmatrix} I & 0 \\ 0 & I \\ -M^{-1}K & -M^{-1}D \end{bmatrix}, \quad D = \begin{bmatrix} 0 \\ 0 \\ -M^{-1} \end{bmatrix}. \quad (5.41)$$

After transferring the derived equations of motion of different model into a set of first-order differential equations, the well-known Runge-Kutta method is applied to solve these equations in MATLAB computing environment.

### 5.3.2 Numerical simulation of a nonlinear time variant system

As discussed above, it is known that the ordinary differential equations of the system model have time-dependent and nonlinear terms. The stiffness of rotor depends on

the rotor position and the coil currents controller design parameters. The rotor driving frequency is varying during the rotor interacting with auxiliary bearings. As a result the unbalance force is also changed during contact. Moreover, there are some uncertain excitation forces adding on the rotor which can be commonly modeled as time function. The nonlinear term is mainly caused by the clearance between rotor and auxiliary bearing. In order to get more actual physical contact model, Hertzian nonlinear contact model is used to calculate the contact force. The friction between rotor and auxiliary bearing is one of nonlinear terms in the model as well. As a result, the state equation 5.39 and output equation 5.40 can be rewritten as the following form:

$$\dot{\mathbf{x}}(t) = A(t, q)\mathbf{x}(t) + B\mathbf{F}(t, q), \quad (5.42)$$

$$\mathbf{y}(t) = C(t, q)\mathbf{x}(t) + D\mathbf{F}(t, q). \quad (5.43)$$

The ODE solver in Matlab can solve an ordinary differential equation with time-dependent terms. Firstly, according to the real physical model, the time dependent parameters are defined. In this work,  $A(t, q)$  and  $\mathbf{F}(t, q)$  might be time dependent parameters. The reasonable initial conditions are given. Then, the derivative function is called with the solver function specifying time as the first input argument in MATLAB .

*Events* are used to describe sudden changes in model behavior [69]. In these rotor AMB with interaction auxiliary bearing models, the contact force and friction force are generated when penetration  $\delta$  is larger than zero. This condition uses a combination of relational and logical operators, which can be used to build a trigger expression. The different kinds of contact and friction force models can be defined in the Event functions, and parameters can be defined conveniently in the Event function. When the Trigger becomes true during calling the derivative function within the MATLAB solver function, the event is executed, i.e., the contact and friction force are taking effect on the rotor.

### 5.4 Simulation results and analysis

The detailed models of the AMB-Rotor-Auxiliary bearing system have considered important system parameters such as clearance effect, unbalance of rotor, driving frequency, stiffness and damping of contact, etc. Since the driving frequency is one of the most convenient parameters to be controlled in the build up test rig, it has been chosen as one of study parameters in this work both in experimental method and numerical method. The important parameters of the detailed model are obtained from test rig which have been introduced in the above chapters and listed in Table 5.1.

Moreover, for numerical solution, the initial conditions are very important for successive and economic computational solution. Particularly for nonlinear systems, different initial conditions mean totally different solutions. In the following simulation results, they are calculated with same initial conditions and the data were analyzed after many cycles to ensure that a steady state solution had been achieved.

The equations of motion derived in above section are nondimensionalized in order to compare and discuss numerical simulation results with different control parameters conveniently. The time is nondimensionalized by using natural frequency of the rotor system; the displacements, such as horizontal and vertical displacements of rotor center, are nondimensionalized by employing the clearance between rotor and auxiliary bearing.

#### 5.4.1 Case 1: variant of driving frequency with linear contact model

The simulation results of the basic model show the period one, period two, period four and chaotic motion, etc. Figures 5.6, 5.7, 5.8 and 5.9 show the Poincaré section diagrams, the rotor orbits, the rotor time histories in dimensionless coordinate at different driving frequency of 0.55, 0.10, 1.25 and 1.28 respectively. Contact force of the system is modeled as piecewise ideal elastic linear contact when rotor interacts with fixed mounted auxiliary bearing in this case [53].

When the dimensionless driving frequency is 0.55, the motion is regular and periodic

Table 5.1: Main parameters of the test rig for numerical simulation

<b>Rotor</b>	
Mass of the rotor	3.36 kg
Length of the rotor	0.326 m
Center of gravity(from left side)	0.160 m
Polar moment of inertia of rotor	0.001kgm <sup>2</sup>
Transverse moment of inertia of rotor	0.017kgm <sup>2</sup>
Unbalance eccentricity	0.0292 mm
Maximum driving frequency	500 Hz
Clearance between rotor and auxiliary bearing	0.3 mm
<b>AMB</b>	
Stiffness parameter of coil current	19 N/A
Stiffness parameter of displacement	39.7 N/mm
Radial equivalent stiffness	$2.47 \times 10^6$ N/m
Radial equivalent damping coefficient	100 N <sub>s</sub> /m
<b>Auxiliary bearing</b>	
Mass of the auxiliary bearing	0.069 kg
Coefficient of Coulomb friction	0.015
stiffness parameter of linear contact	$3.38 \times 10^7$ N/m
Local stiffness parameter of Hertzian contact	$2.4 \times 10^9$ N/m <sup>3/2</sup>
Damping coefficient of Hertzian contact	5
Tolerance ring support stiffness paramter	$2.00 \times 10^6$ N/m

one. The orbit map and time history of this prierod one motion are shown in figure 5.6(right) and figure 5.6(down) respectively. There are many points clustered into one point in the Poincaré section diagram in figure 5.6(left). The system response presents a period one motion.

When the dimensionless driving frequency is 1.10, the motion is regular and periodic two as shown the orbit map in figure 5.7 (right) and time history in figure 5.7 (down). There are many points clustered into two points in the Poincaré section diagram in figure 5.7(left). The system response presents a period two motion.

As shown in figure 5.8, the dimensionless driving frequency is about 1.25, there are

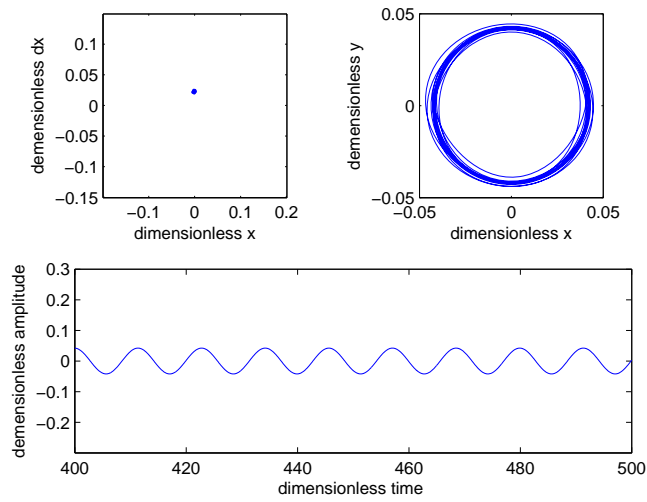


Figure 5.6: Poincaré section diagram, rotor orbit, rotor time history in dimensionless coordinates at dimensionless driving frequency 0.55 (piecewise linear contact model)

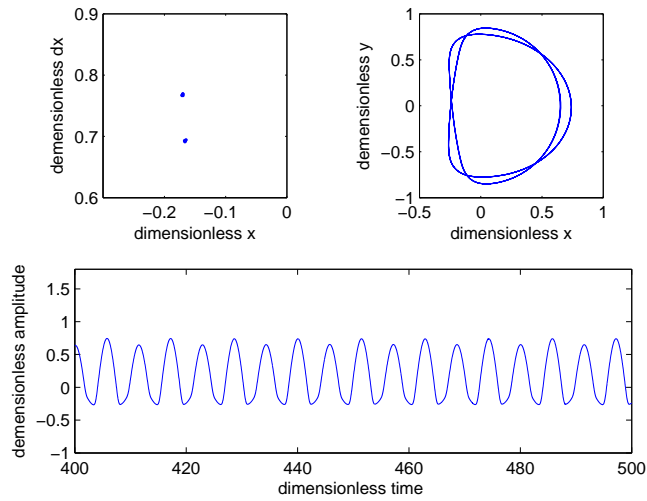


Figure 5.7: Poincaré section diagram, rotor orbit, rotor time history in dimensionless coordinates at dimensionless driving frequency 1.10 (piecewise linear contact model)

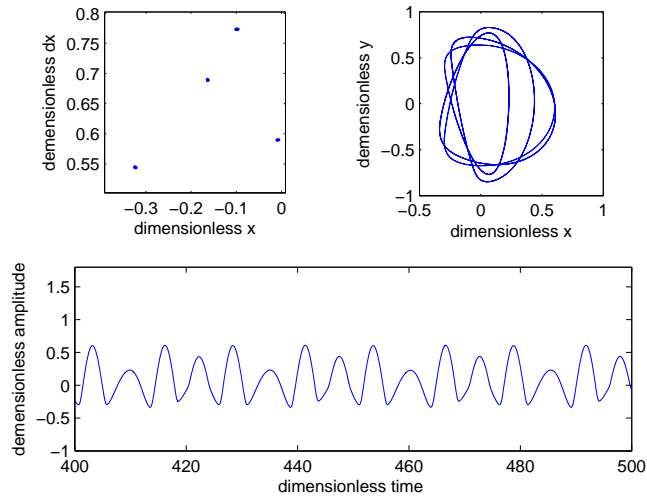


Figure 5.8: Poincaré section diagram, rotor orbit, rotor time history in dimensionless coordinates at dimensionless driving frequency 1.25 (piecewise linear contact model)

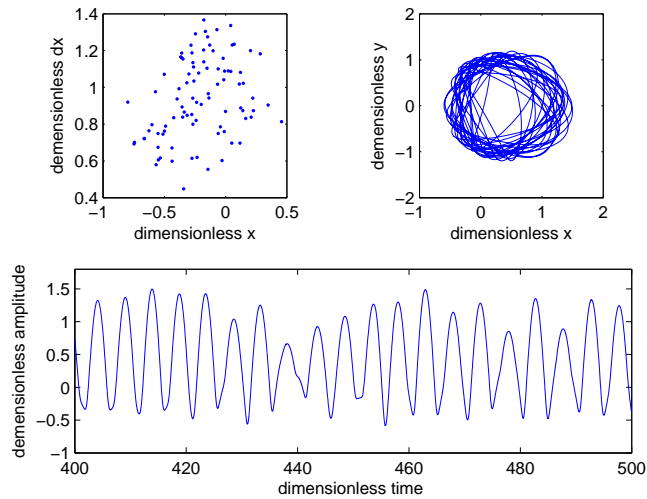


Figure 5.9: Poincaré section diagram, rotor orbit, rotor time history in dimensionless coordinates at dimensionless driving frequency 1.28 (piecewise linear contact model)

four isolated points in the Poincaré section diagram and the rotor orbit shows a regular periodic motion. The time history of the dimensionless rotor displacement also shows the motion to be quasi periodic.

When the dimensionless driving frequency is about 1.28, figure 5.9 shows chaotic motion of the study model. The rotor orbit and time history is obviously chaotic, Poincaré section diagram shows a geometrically fractal like structure.

### 5.4.2 Case 2: variant driving frequency with Hertzian nonlinear contact model

In this case, figures 5.10, 5.11 and 5.12 show the Poincaré section diagrams, the rotor orbits, the rotor time histories in dimensionless coordinate at different driving frequency of 0.55, 0.10 and 1.28 respectively. Contact force of the system is modeled as Hertzian nonlinear contact. Except the contact force model, the other parameters are same with the models discussed in the above case.

As shown in figure 5.10, the dimensionless driving frequency is also about 0.55. From Poincaré section diagrams in figure 5.10 (left) and the time history of the dimensionless rotor displacement in figure 5.10 (down), motion of the study model is chaotic. From the orbit map, we can see that rotor is continuously contacted with auxiliary bearing. It can be confirmed in the contact force results in next section. However, the simulation results show obvious difference with the results in figure 5.6 with the linear contact model. It is period one motion from the poincaré section diagram. From the orbit map of figure 5.6, it can be seen that the rotor does not interact with auxiliary bearing.

When the dimensionless driving frequency is about 1.10, figure 5.11 shows chaotic motion of the study model. The time history is obviously chaotic, and the Poincaré section diagram shows a geometrically fractal like structure. It can be seen that the rotor contacts with auxiliary bearing partially as shown in rotor orbit map in figure 5.11. The results shown in figure 5.7 are of the model whose contact force is modeled as ideal linear contact. Although the dimensionless driving frequency is also 1.10, that is periodic two motion and the rotor dose not contact with auxiliary bearing.

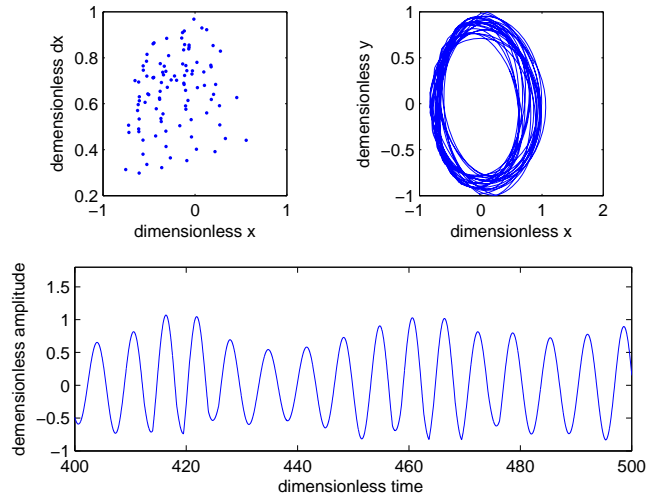


Figure 5.10: Poincaré section diagram, rotor orbit, rotor time history in dimensionless coordinates at dimensionless driving frequency 0.55 (Hertzian non-linear contact model)

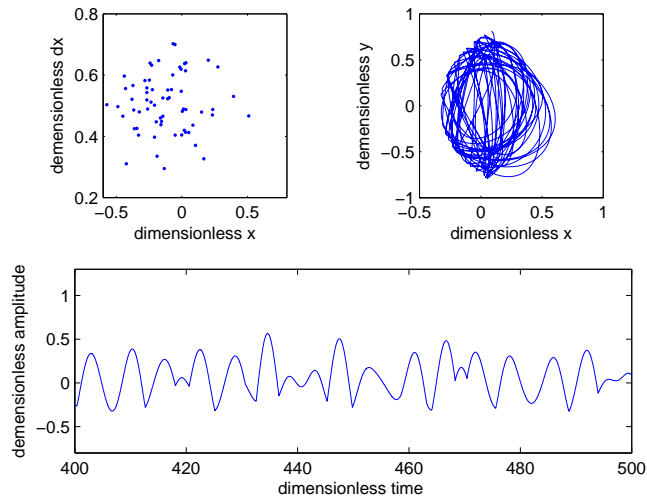


Figure 5.11: Poincaré section diagram, rotor orbit, rotor time history in dimensionless coordinates at dimensionless driving frequency 1.10 (Hertzian non-linear contact model)

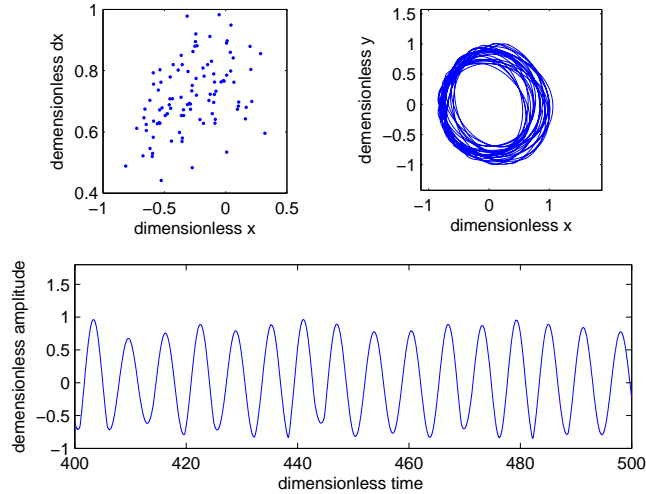


Figure 5.12: Poincaré section diagram, rotor orbit, rotor time history in dimensionless coordinates at dimensionless driving frequency 1.28 (Hertzian nonlinear contact model)

Figure 5.9 and figure 5.12 show simulation results at 1.28 dimensionless driving frequencies of the piecewise linear contact system model and hertzian nonlinear contact system model respectively. Figure 5.9 and figure 5.12 both show chaotic motion. The rotor orbits and time histories are obviously chaotic, the Poincaré section diagrams show geometrically fractal like structures. However, there exists difference between orbit maps in these two figures. The rotor is continuously interacting with auxiliary bearing from the orbit map in the figure 5.12. But we could see that the rotor springs inside the auxiliary bearing clearly from figure 5.9(right), and the contact force simulation result can approve this spring phenomenon, because sometimes it is equal to zero.

Based on all the figures 5.6 - 5.12, one can say that the detailed nonlinear AMB-rotor-auxiliary bearing system represents the complex dynamic characters at different driving frequencies obviously. But it is worth mentioning that the other parameters of the model and model type are also very important terms, which may be related to the stability of rotor motion.

## 5.4.3 Case 3: contact force with different contact model

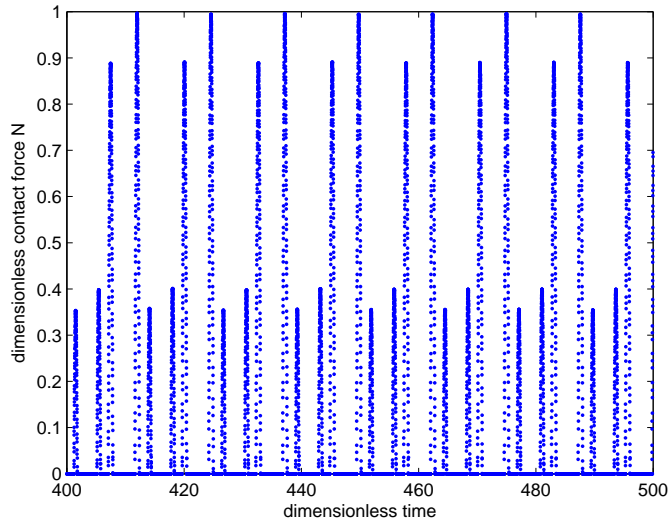


Figure 5.13: Dimensionless contact force simulation result (linear contact model, dimensionless driving frequency 1.28, stiffness ratio  $\alpha = 13$ )

The contact forces are calculated both with ideal linear contact and nonlinear Hertzian contact in case the rotor interacting with the auxiliary bearing.

Figure 5.13, 5.14 and 5.15 present the simulated dimensionless contact force of the piecewise linear contact model and nonlinear Hertzian contact model respectively. Both figure 5.13 and figure 5.14 use dimensionless piecewise linear contact force model, and are calculated with the dimensionless rotor driving frequency 1.28. The only difference is that the contact stiffness. Comparing these two results, it can be seen that the higher contact stiffness has higher contact force magnitude. From figure 5.13 and 5.14 it can be seen that rotor dose not continuously contact with auxiliary bearing, when there is no interaction between rotor and auxiliary bearing, the non negative contact force is equal to zero from dimesionless time 400 to 500. The piecewise contact force at this situation is quasi-period as shown in figure 5.13.

Figure 5.15 is dimensionless hertzian contact force which is simulated with dimensionless rotor driving frequency of 0.55. It can be clearly seen that the rotor continuously contacts with auxiliary bearing from dimensionless time 400 to 500, and it is quite chaotic. It may be that the hertzian contact force is more complicated

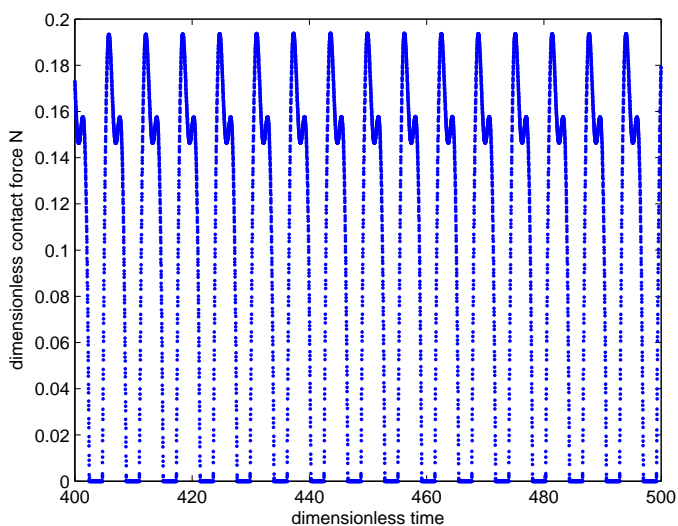


Figure 5.14: Dimensionless contact force simulation result (linear contact model, dimensionless driving frequency 1.28, stiffness ratio  $\alpha = 1.3$ )

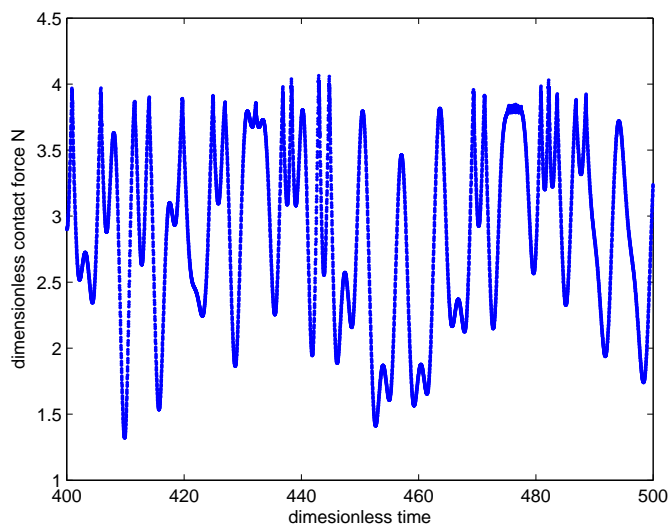


Figure 5.15: Dimensionless contact force simulation result (Hertzian nonlinear contact model, dimensionless driving frequency 0.55)

than the piecewise linear contact which only depends on the contact stiffness and the value of penetration; but the hertzian nonlinear contact is not only depend on some system parameters, local stiffness parameter and damping parameter, but also on the penetration and its derivative with respect to time.

5.4.4 Case 4: waterfall spectrum analysis

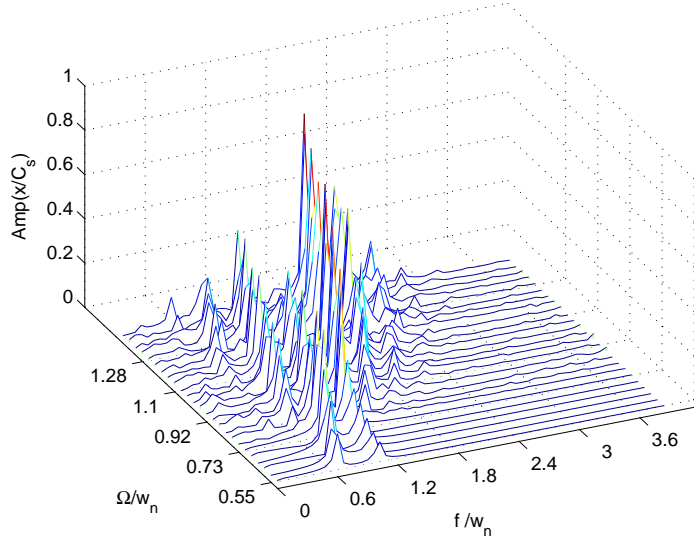


Figure 5.16: Waterfall spectrum diagram ( $\alpha = 13$ , linear contact model)

Waterfall spectrum diagrams present the spectrum versus rotor driving frequency changing as shown in figure 5.16 and figure 5.17. The amplitude ( $z$  axis) in both figures is dimensionless displacement of rotor in horizontal direction by dividing the clearance.  $y$  axis is dimensionless driving frequency, which is changing in range  $[0.55, 1.47]$ , and the  $x$  axis is dimensionless frequency. Both frequency terms are nondimensionlised by applying natural frequency of the system.

Figure 5.16 shows the waterfall spectrum with harder contact stiffness ratio ( $\alpha = 13$ ). In the low driving frequency range, the rotor may not contact with auxiliary bearing in this case. The waterfall spectrum diagram indicates that rotor radial vibration contained mainly  $1\times$  and  $2\times$  of the driving frequency components. With the driving frequency speeding up, the rotor may interact with auxiliary bearing, the fractional

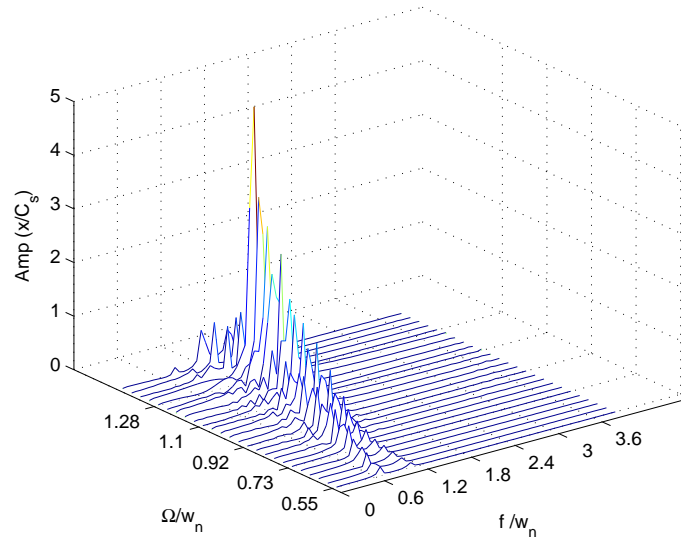


Figure 5.17: Waterfall spectrum digram ( $\alpha = 1.3$ , linear contact model)

driving frequency round  $1/2\times$  are very apparent and the other components  $1\times$ ,  $3/2\times$  and  $2\times$ , etc. can be observed as well from the waterfall spectrum diagram. Chaotic vibration motion can be found under some conditions.

Figure 5.17 shows the waterfall spectrum with softer contact stiffness ratio ( $\alpha = 1.3$ ). It is found that, in this condition, regardless the high or low driving frequency of the rotor, and regardless the appearance of backward whirl, there are mainly two harmonic components at  $1\times$ ,  $2\times$  in the spectrum. The rotor displacement shows the quasi-period motion.

# 6 Bifurcation Analysis of Rotor System Parameters

Since the most equations of motion derived in last chapter cannot be solved analytically, the most analysis is done numerically in this work. This chapter provides a brief overview of dynamical systems theory including Poincaré surfaces of section, bifurcation analysis. Bifurcation analysis is a very effective method to reflect the motion changed by changing control parameter. The parameter study through bifurcation analysis of rotor system parameters will be presented in this chapter. Some possible crucial system parameters such as driving frequency, support stiffness and damping, contact stiffness and damping will be used as a control parameter in the bifurcation analysis respectively.

## 6.1 Theory introduction

### 6.1.1 Dynamic system

A dynamical system is any system that evolves in time. Dynamical systems whose behaviors change continuously in time are mathematically described by a coupled set of first-order autonomous ordinary differential equations [71]:

$$\dot{\mathbf{x}} = \mathbf{f}(\mathbf{x}, \boldsymbol{\mu}), \quad \mathbf{f} : \mathbb{R}^n \times \mathbb{R} \rightarrow \mathbb{R}^n. \quad (6.1)$$

The components of the vector  $\mathbf{x}$  are the dynamical variables of the system, the components of the vector  $\boldsymbol{\mu}$  are parameters, and the components of the vector field  $\mathbf{f}$  are the dynamical rules governing the behavior of the dynamical variables. There is no loss of generality in the restriction to autonomous systems, where  $\mathbf{f}$  is not an

explicit function of  $t$ , since a *non autonomous* system in  $\mathbb{R}^n$  can be transformed into an autonomous system in  $\mathbb{R}^{n+1}$ . If the vector field is *affine*, i.e.,

$$\mathbf{f}(\mathbf{x}, \boldsymbol{\mu}) = \underline{\mathbf{A}}\mathbf{x} + \underline{\mathbf{b}}\boldsymbol{\mu} \quad (6.2)$$

for some constant matrix  $\underline{\mathbf{A}}$  and vector  $\underline{\mathbf{b}}$ , then the dynamical system is said to be linear. Otherwise it is nonlinear.

### 6.1.2 Poincaré section diagram

As shown in figure 6.1, Poincaré section is a carefully chosen plane in the phase space that is crossed by almost all orbits. It is a tool developed for a visualization of the flow in a phase space of more than two dimensions [72].

In [70], the author give a description of Poincaré section. For  $n$  dimension dynamic system,  $\mathbf{f}(\mathbf{x}, \boldsymbol{\mu})$ , the Poincaré section has one dimension less than the phase space. Let  $S$  be an  $n - 1$  dimensional *surface of section* as shown in figure 6.1.  $S$  is required to be transverse to the orbit, i.e., all trajectories starting on  $S$  flow through it, not parallel to it.

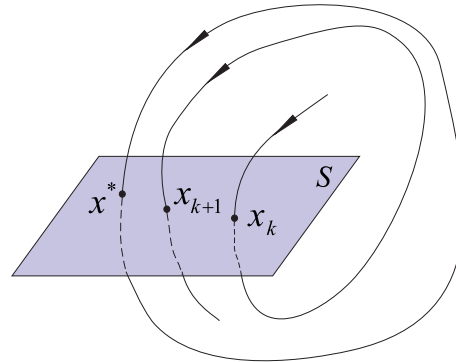


Figure 6.1: Poincaré section

The Poincaré section diagram maps the points of the Poincaré section onto itself.

It relates two consecutive intersection points. Note that only those intersection points count which come from the same side of the plane. A Poincaré section diagram turns a continuous dynamical system into a discrete one. If the Poincaré section is carefully chosen, no information is lost concerning the qualitative behavior of the dynamics. When it comes to the determination of the motion type, the Poincaré section diagram is a strong tool [72].

### 6.1.3 Bifurcation diagram

In mathematics, particularly in dynamical systems, a bifurcation diagram shows the possible long-term values (fixed points or periodic orbits) of a system as a function of a bifurcation parameter in the system. It is usual to represent stable solutions with a solid line and unstable solutions with a dotted line [77]. A bifurcation occurs when a small smooth change made to the parameter values (the bifurcation parameters or control parameter) of a system causes a sudden *qualitative* change in its behavior. Therefore, the bifurcation diagram represents an idealized version of how a system can become chaotic, quasi-periodic, periodic by varying control parameters.

## 6.2 Parameter study of the dynamic system

The detailed model of the AMB-Rotor-Auxiliary bearing system has considered important system parameters such as unbalance of rotor, driving frequency, stiffness and damping of contact, clearance etc. The nonlinear terms in the detailed model have considered discontinuous stiffness caused by bearing clearance effects, nonlinear Hertzian contact stiffness and Coulomb friction forces. In [74], [75] and [76], the authors have studied the parameter of rotor damping and stiffness, etc.. However they both used the simulation results based on linear contact model. In this work, the bifurcation analysis used detailed dynamic system model with linear contact and nonlinear contact model.

Moreover, for numerical solution, the initial conditions are very important for successive and economic computational solution. Particularly for nonlinear systems, different initial conditions mean totally different solutions. The control parameter was increased in small steps, each step starting with same initial conditions, and plenty cycles were allowed before data was analyzed to ensure that a steady state solution had been achieved.

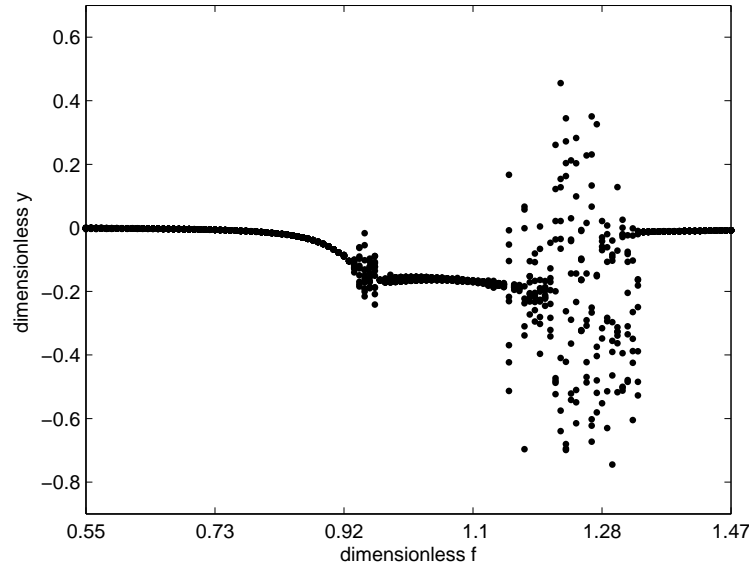


Figure 6.2: Bifurcation diagram of the driving frequency

### 6.2.1 Driving frequency

Since the driving frequency is one of the most convenient parameters to be controlled in the build up test rig, it has been chosen as a parameter of study in this work. The other parameters of the detailed model are obtained from test rig which have been introduced and listed in Table 5.1.

A bifurcation diagram is a very effective method to reflect the motion change by the control of parameter change. In order to compute a bifurcation diagram, a control parameter dimensionless driving frequency is varied from 0.55 to 1.5 at a constant step size 0.0073.

As figure 6.2 shows, the numerical simulation results obtained from the study system model represent complex behaviors with different dimensionless driving frequencies. In the low dimensionless driving frequency range from 0.55 to 0.91, period one motion is observed. At around 0.92 it flips to period three motion, then after a slender range period one motion, it shows a possible band of chaotic motion between 0.94 and 0.96. Period two motion is observed in the region [0.971.17]. With increase of the control parameter, the motion of the system model becomes more complicated.

From 1.17 to 1.33, chaotic motion was predominant, but period two motion, period four motion are observed at some specific values of the control parameter as well. If the dimensionless driving frequency is beyond 1.34, the bifurcation diagram shows a transition from chaotic motion into period one motion obviously.

### 6.2.2 Support stiffness

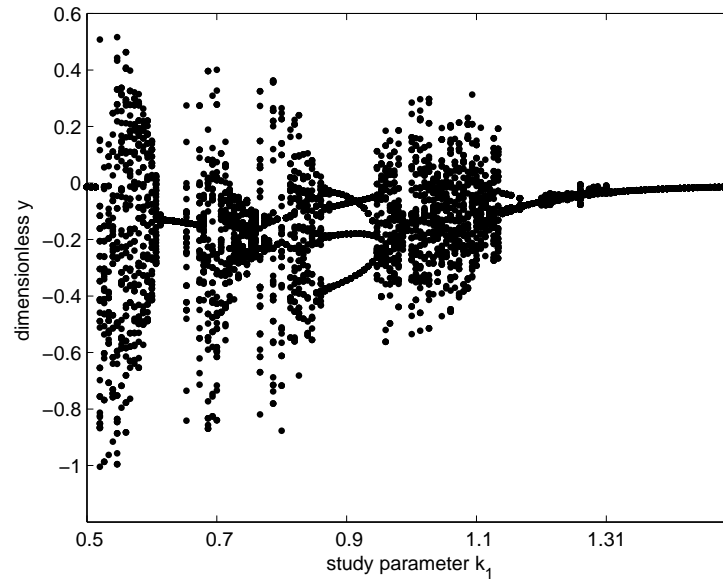


Figure 6.3: Bifurcation diagram of the support stiffness

Support stiffness  $k_1$  is one of the most important parameters for the AMB-rotor system design. It can be adjudged in test rig through changing controller parameters. Commonly speaking the support stiffness provided by AMB can be varied from 80% -120% of the original value. For the bifurcation analysis of the support stiffness, a control parameter is dimensionless ratio of the original support stiffness, which is varied from 0.50 to 1.5 at a constant small step size.

The bifurcation diagram of the support stiffness is shown in figure 6.3. With changing the ratio of the support stiffness, it presents the complex behaviors of rotor. The numerical simulation results are obtained from the detailed system model with nonlinear Hertzian contact. From starting where is round the half of the original

support stiffness, the period one motion is observed. Shortly, with the increase of the study parameter, rotor shows a possible band of chaotic motion between 0.52 and 0.61. Then, the rotor enters the period one motion again. In the region [0.68 0.87], the motion of the system model becomes more complicated. Chaotic motion is predominant, but period two motion and period eight motion are observed at some specific values of the control parameter as well. From 0.87 to 0.96, the rotor changes to period four motion from chaotic. In the range [1.15 1.50], period one and period two motion of rotor are obviously observed.

### 6.2.3 Contact stiffness

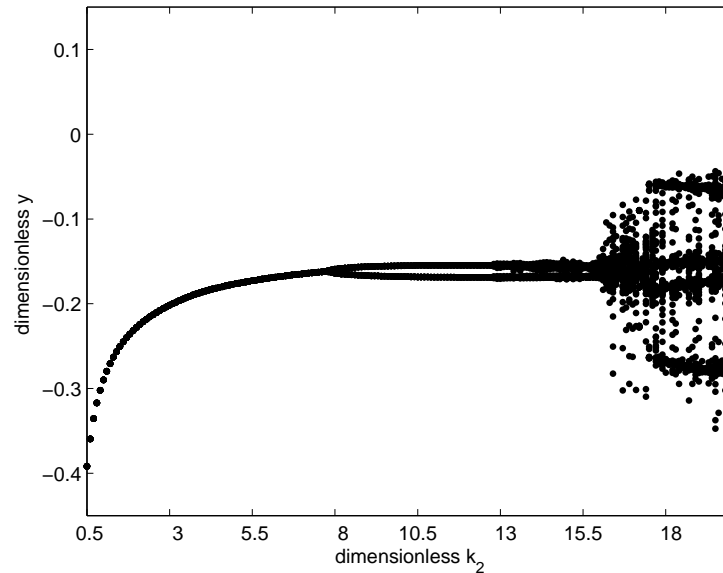


Figure 6.4: Bifurcation diagram of the contact stiffness

Figure 6.4 shows bifurcation diagrams of the contact stiffness. The ratio between contact stiffness and rotor support stiffness  $\alpha$  is taken as a control parameter. It is defined to vary from 0.50 to 20 at a constant small step size. All remaining parameters are kept constant. From 0.5 to 0.72, the rotor clearly shows period one motion. When the stiffness ration reaches around 0.72, the rotor flips to period two motion. Then in the range [13.4, 15,6], the period four motion is mainly observed.

When the stiffness ratio  $\alpha$  increases beyond 15.6, the complicated motion can occur. Rotor flips to period eight motion and more. Through analysis the bifurcation diagram, It found that rotor shows the changing sign in bifurcation points between periodic and chaotic or quasi periodic motion at  $\alpha = 15.6$ . With high values of  $\alpha$ , the occurrence of chaotic whirling motion is possible [73]. Therefore, when designing the AMB-rotor-auxiliary bearing system with consideration of significant nonlinearities such as contact and friction, it is usually desirable to avoid chaotic motion. To avoid chaos in the system shown in figure 6.4, the design parameter  $\alpha$  should be less than about 15.3 to prevent this destructive failure, backward whirl.

## 7 Conclusion and Outlook

In this work, we investigate the interaction between rotor and auxiliary bearing by both numerical and experimental methods. The overview of the basic mathematical models for the AMB supported rotor with auxiliary bearing system is provided. The theoretical method for estimation equivalent stiffness and damping of the AMB is developed in this work. The dynamic equivalent stiffness and damping of the AMB are calculated from the knowledge of frequency response of the digital controlled AMB.

Plenty experiments have been made to explore which factors or parameters are essential to system performance. Some modifications and extensions of the hardware and software of the test rig have been conducted, which has more facilities to make experimental investigation. The rotor driving frequency is measured by optical sensor and the deceleration relationship is found. Several impotent parameters of system such as stiffness and damping have been estimated through frequency domain and time domain methods by analyzing the experimental results. These parameters have been used in numerical simulations. Under some specific designed cases, it is found that the AMB-rotor-auxiliary bearing system undergoes complicated motion behavior, backward whirl. The experiment results have been presented and analyzed.

The interaction between high rotating rotor and auxiliary bearing could cause a very serious instable motion, backwards whirl. It may lead to the destruction of the machine. So it is important to build a detailed model of the system to study the dynamic behavior of the rotor. The detailed models of the AMB supported rotor interacting with auxiliary bearing system are introduced, which consider discontinuous stiffness caused by bearing clearance effects, nonlinear Hertzian contact and Coulomb friction forces. Furthermore, according to the real test rig, the auxiliary bearings could be modeled as fixed and compliant mounted. The rotor is modeled as rigid mass or rigid beam by paying regard to its operation range. Several groups

of differential equations are presented and the numerical simulation method is developed for the nonlinear time variant ODEs based on event function in Matlab. Numerical investigations such as time history, orbit diagram, Poincaré section diagram and waterfall spectrum diagram are proposed to study the complex dynamic response of the system. It is found that the AMB-rotor-auxiliary bearing system undergoes complicated motion behavior including chaotic response.

The bifurcation analysis is presented, to explore which factors or parameters are essential to system performance then find an appropriate optimized design to prevent it. The important parameters studies on rotor driving frequency and support and contact stiffness are carried out through bifurcation analysis. The complicated motions of rotor are observed by changing the control parameters. These parameter studies can be used to optimize the design and operation of AMB-rotor-auxiliary bearing system.

For future research, a new measurement technique need be developed to fully record backward whirl of rotor including the sliding and rolling motion of rotor. It is interesting to discover the energy transferring of the rotor, and estimate the whirl velocity. For the future development of auxiliary bearings, it would be important to optimize the design of auxiliary bearing, which can dissipate the energy and avoid instable motion of rotor.

# Bibliography

- [1] R. Nordmann. Use of mechatronic components in rotating machinery. In *Proceeding of the 7th Conference on Vibration Problems*, Istanbul, 2005.
- [2] M. Orth and R. Nordmann. Aneas - a modeling tool for nonlinear analysis of active magnetic bearing systems. In *Proceeding of Mechatronic 2002 conference*, Berkeley, California, Dec. 2002.
- [3] M. Helfert, M. Ernst, R. Nordmann, and B. Aeschlimann. High-speed video analysis of rotor-retainer bearing contacts due to failure of active magnetic bearings. In *Proceeding of 10th International Symposium on Magnetic Bearings*, Martigny, Switzerland, Aug. 2006.
- [4] F. F. Ehrich and J. J. Oconnor. Stator whirl with rotors in bearing clearance. *ASME Journal of engineering for Industry*, 89(3):381–390, Aug. 1967.
- [5] F. F. Ehrich. High-order subharmonic response of high-speed rotors in bearing clearance. *ASME Journal of Vibration Acoustics and Reliability in Design*, 110(1):9–16, Jan. 1988.
- [6] D. E. Bently, J. Yu, P. Goldman, and A. Muszynska. Full annular rub in mechanical seals part I: experimental results. *International Journal of Rotating Machinery*, 8(5):319–328, Aug. 2002.
- [7] D. E. Bently, P. Goldman, and J. Yu. Full annular rub in mechanical seals part II: Analytical study. *International Journal of Rotating Machinery*, 8(5):329–336, Aug. 2002.
- [8] F. K. Choy and J. Padovan. Non-linear transient analysis of rotor-casing rub events. *Journal of sound and vibration*, 113(3):529–545, 1987.
- [9] E. V. Karpenko, M. Wiercigroch, and M. P. Cartmell. Regular and chaotic

- dynamics of a discontinuously nonlinear rotor system. *Chaos, Solitons and Fractals*, 13:1231–1242, Aug. 2002.
- [10] F. Chu. and W. Lu. Experimental observation of nonlinear vibrations in a rub-impact rotor system. *Journal of Sound and Vibration*, 283:621–643, 2005.
- [11] R. G. Kirk. Evaluation of amb turbomachinery auxiliary bearings. *ASME Journal of Vibration and Acoustics*, 121:156–161, 1999.
- [12] P. S. Keogh and M. O. T. Cole. Contact dynamic response with misalignment in a flexible rotor/ magnetic bearing system. *Journal of Applied Mechanics*, 128:362–369, 2006.
- [13] M. Orth, R. Erb, and R. Nordmann. Investigations of the behavior of a magnetically suspended rotor during contact with its retainer bearings. In *the proceeding of 7th International Symposium on Magnetic Bearings*, Zurich, Switzerland, 2000.
- [14] R. Gasch, R. Nordmann, and H. Pfützner. *Rotordynamik*. Springer Verlag, 2002.
- [15] K.H. Hunt and F.R. Crossley. Coefficient of restitution interpreted as damping in vibroimpact. *ASME Journal of Vibration and Acoustics*, 121:156–161, 2000.
- [16] M. A. Fumagalli. *Modelling and measurement analysis of the contact interaction between a high speed rotor and its stator*. PhD thesis, ETH Zürich, 1997.
- [17] M. Orth. *Fanglagerkontakt magnetgelagerter Rotoren: nichtlineare Modellierung sowie Systemanalyse nach einem Magnetlagerausfall*. PhD thesis, TU darmstadt, 2007.
- [18] E. H. Maslen. *Course notes on Magnetic Bearings*. 1999.
- [19] M. Schlotter. *Robust Control and Contact Recovery of Rotor/Magnetic Bearing Systems*. PhD thesis, University of Bath, 2007.
- [20] G. Schweitzer. Safety and reliability aspects for active magnetic bearing applications - a survey. *Proceedings of the Institution of Mechanical Engineers, Part I: Journal of Systems and Control Engineering*, 219(6), 2005.

- [21] A. R. Bartha. *Dry Friction Backward Whirl of Rotors*. PhD thesis, ETH Zürich, 2000.
- [22] H. F. Black. Interaction of a whirling rotor with a vibrating stator across a clearance annulus. *Journal Mechanical Engineering Science*, 10(1-12):88–89, 1968.
- [23] J. Jiang and H. Ulbrich. Stability analysis of full annular rub in rotor-to-stator systems. *Proceedings in Applied Mathematics and Mechanics*, 2:88–89, 2003.
- [24] G. Wegener, R. Markert, and K. Pothmann. Steady state analysis of a multidisk or continuous rotor with one retainer bearing. In *Proceedings of IFToMM Fifth International Conference on Rotor Dynamics*, Darmstadt, 1998.
- [25] G. Wegener. *Elastische Fanglager zur Amplitudenbegrenzung elastischer Rotoren*. PhD thesis, TU darmstadt, 2000.
- [26] U. Eehalt. *Bewegungsformen elastischer Rotoren bei Statorkontakt*. PhD thesis, TU darmstadt, 2008.
- [27] A. Muszynska. Whirl and whip–rotor/ bearing stability problems. *Journal of Sound and Vibration*, 110(3):443–462, 1986.
- [28] A. Muszynska. Stability of whirl and whip in rotor/ bearing systems. *Journal of Sound and Vibration*, 127(1):49–64, 1988.
- [29] A. Muszynska. Vibrational diagnostics of rotating machinery malfunctions. *International Journal of Rotating Machinery*, 1(3-4):237–266, 1995.
- [30] Y. A. Amer, M. H. Eissa, U. H. Hegazy, and A. S. Sabbah. Dynamic behavior of an amb/supported rotor subject to parametric excitation. *Journal of Vibration and Acoustics*, 128:646–652, Oct. 2006.
- [31] P. S. Keogh and W. Y. Yong. Thermal assessment of dynamic rotor/auxiliary bearing contact events. *Journal of Tribology by ASME*, 129:143–152, Jan. 2007.
- [32] A. Muszynska. *Rotordynamics*. CRC, 2005.
- [33] T. Yamamoto and Y. Ishida. *Linear and Nonlinear Rotordynamics: A Modern Treatment with Applications*. Wiley-Interscience, 2001.

- [34] R. Nordmann. *Mechatronische Systeme im Maschinenbau I*. Shaker Verlag, 2005.
- [35] G. Genta. *Vibration of Structures and Machines : practical aspects*. Springer, 1998.
- [36] K. J. Bathe. *Finite Element Procedures*. Prentice Hall, 1996.
- [37] D. Thorby. *Structural Dynamics and Vibration in Practice: An Engineering Handbook*. Butterworth-Heinemann, 2008.
- [38] R. Gasch. *Strukturdynamik*. Springer, 1987.
- [39] N. L. Pedersen. On the formulation of flexible multibody systems with constant mass matrix. *Multibody System Dynamics*, 1(3):323–337, Sep. 1997.
- [40] J. V. Vance. *Rotordynamics of Turbomachinery*. Wiley-Interscience, 1988.
- [41] Y. A. Khulief and M. A. Mohiuddin. On the dynamic analysis of rotors using modal reduction. *Finite Elements in Analysis and Design*, 26(1):41–55, May 1997.
- [42] Zu-Qing Qu. *Model order reduction techniques : with applications in finite element analysis*. Springer, 2004.
- [43] C. Kenney and G. Hewer. Necessary and sufficient conditions for balancing unstable systems. *IEEE Transactions on Automatic Control*, 32(2):157– 160, Feb 1987.
- [44] P. Koutsovasilis and M. Beitelschmidt. Comparison of model reduction techniques for large mechanical systems. *Journal Multibody System Dynamics*, 20(2):111–128, Sep. 2008.
- [45] G. Schweitzer, A. Traxler, and H. Bleuler. *Magnetlager: Grundlagen, Eigenschaften und Anwendungen Berührungsfreier, Elektromagnetischer Lager*. Springer Verlag, 1993.
- [46] A. Chiba, T. Fukao, and O. Ichikawa. *Magnetic Bearings and Bearingless Drives*. CIMA Publishing, 2005.
- [47] The technical support documents of MECOS.

- [48] <http://www.rencol.co.uk/en/technical.html>.
- [49] <http://sine.ni.com/nips/cds/view/p/lang/en/nid/14605>.
- [50] J. W. Smith. Tolerance rings: motor-overload protection]. *Industry Applications Magazine, IEEE*, 8(5):74 – 82, Sep/Oct 2002.
- [51] M. Gao, G. Yang, Y. Xu, L. Zhao, and S. Yu. Auxiliary bearing design and rotor dynamics analysis of blower fan for htr-10. In *18th International Conference on Structural Mechanics in Reactor Technology (SMiRT 18)*, Beijing, China, Aug. 2005.
- [52] L. Xie, M. Helfert, and R. Nordmann. Numerical and experimental investigation of an amb supported rotor system with auxiliary bearings. In *The proceeding of 9th International Conference on Vibrations in Rotating Machinery*, Exeter, UK, Sep. 2008.
- [53] L. Xie, R. Nordmann, and B. Aeschlimann. Numerical investigation of amb supported rotor interaction with auxiliary bearings. In *The proceeding of 11th International Symposium on Magnetic Bearings*, Nara, Japan, Aug. 2008.
- [54] <http://www.skf.com/portal/skf/home?lang=en& site=COM>.
- [55] T. A. Harris and M. N. Kotzalas. *Essential Concepts of Bearing Technology (Rolling Bearing Analysis, Fifth Edition)*. CRC, 2006.
- [56] H. M. Chen, J. Walton, and H. Heshmat. Zero clearance auxiliary bearings for magnetic bearing systems. In *Proceedings of 42nd International Gas Turbine and Aeroengine Congress and Exposition*, Orlando, USA., June 1997.
- [57] L. Ginzinger and H. Ulbrich. Control of a rubbing rotor using and active auxiliary bearing. In *Proceedings of the 8th International Conference on Motion and Vibration Control (MOVIC)*, Daejeon, Korea, Aug. 2006.
- [58] J. Schmied and J. C. Pradetto. Behaviour of a one ton rotor being dropped into auxiliary bearings. In *Proceeding of the 3rd International Symposium on Magnetic Bearings*, pages 145–156, Alexandria, USA.,.
- [59] S. Andersson, A. Soederberg, and S. Bjoerklund. Friction models for sliding dry, boundary and mixed lubricated contacts. *Tribology International*, 40(4):580–587, April 2007.

- [60] R. Micheletti. Dynamic parameter estimation of a second-order system to a step function. *Instrumentation and Measurement, IEEE Transactions*, 39(5):790 – 792, Oct. 1990.
- [61] G. F. Franklin, J. D. Powell, and M. L. Workman. *Digital Control of Dynamic Systems*. Addison Wesley, 1998.
- [62] M. Aenis, E. Knopf, and R. Nordmann. Active magnetic bearings for the identification and fault diagnosis in turbomachinery. *Mechatronics*, 12(8):1011–1021, Oct. 2002.
- [63] G. Gloth and M. Sinapius. Analysis of swept-sine runs during modal identification. *Mechanical Systems and Signal Processing*, 18(6):1421–1441, Nov. 2004.
- [64] J. J. Yu, P. Goldman, D. E. Bently, and A. Muzynska. Rotor/ seal experimental and analytical study on full annular rub. *Journal of Engineering for Gas Turbines and Power*, 124:340–350, April 2002.
- [65] W. Zhang. Dynamic instability of multi-degree-of-freedom flexible rotor systems due to full annular rub. In *IMEchE C252/88*, pages 305–308, 1988.
- [66] J. Jiang, H. Ulbrich, and A. Chavez. Improvement of rotor performance under rubbing conditions through active auxiliary bearings. *International Journal of Non-Linear Mechanics*, 41(8):949–957, October 2006.
- [67] C. B. Moler. *Numerical Computing with Matlab*. Society for Industrial Mathematics, 2004.
- [68] L. G. Kelly. *Handbook of Numerical Methods and Applications*. ADDISON-WESLEY, 1967.
- [69] <http://www.mathworks.com>.
- [70] S. H. Strogatz. *Nonlinear Dynamics And Chaos: With Applications To Physics, Biology, Chemistry, And Engineering*. Westview Press, 2001.
- [71] A. Katok and B. Hasselblatt. *Introduction to the modern theory of dynamical systems*. Cambridge University Press, 1996.
- [72] <http://monet.physik.unibas.ch/elmer/pendulum/bterm.htm>.

- [73] Y. B. Kim and S. T. Noah. Bifurcation analysis for a modified jeffcott rotor with bearing clearances. *Nonlinear Dynamics*, 1(6):221–241, Nov. 1990.
- [74] A. R. Guido and G. Adiletta. Dynamics of a rigid unbalanced rotor with nonlinear elastic restoring forces. part i: Theoretical analysis. *Nonlinear Dynamics*, 19(4):359–385, Aug. 1999.
- [75] M. Karlberg and J. O. Aidanpää. Numerical investigation of an unbalanced rotor system with bearing clearance. *Chaos, Solitons and Fractals*, 18(14):653–664, Nov. 1999.
- [76] J. Huaa, S. Swaddiwudhipong, Z. S. Liu, and Q. Y. Xu. Numerical analysis of nonlinear rotor-seal system. *Journal of Sound and Vibration*, 283(3-5):525–542, 2005.
- [77] [http://en.wikipedia.org/wiki/Bifurcation\\_theory](http://en.wikipedia.org/wiki/Bifurcation_theory).

# Lebenslauf

## Persönliche Daten

Name: Lei Xie  
Geburtsdatum: 06. 08. 1978  
Geburtsort: Henan, VR China  
Staatsangehörigkeit: Chinesisch

## Ausbildung und Beruf

1985-1990 Grundschule, Henan Province Shiyan primary school in Zhengzhou  
1990-1991 Grundschule, Pingdingshan Wutiaolu primary school in Pingdingshan  
1991-1994 Gymnasium, Pingdingshan Nr. 6 middle school in Pingdingshan  
1994-1997 Gymnasium, Pingdingshan Nr. 1 middle school in Pingdingshan  
1997-2001 Studium Mechatronik an Universität, Zhengzhou Anti-Aircraft Academy of P.L.A. in Zhengzhou mit Abschluß Bachelor  
2001-2002 als Ingenieurin bei Shenzhen Epochi Technology Co.,ltd in Beijing.  
2002-2005 Studium Mechatronik an Universität, China Petroleum University in Beijing mit Abschluß Master  
2006-2009 als Doktorandin am Fachgebiet Mechatronik im Maschinenbau, TU Darmstadt